

RETURNING MATERIALS:
Place in book drop to remove this checkout from your record. FINES will be charged if book is returned after the date stamped below.

LAMINAR FLOW OVER A SPINNING PROJECTILE AT AN ANGLE OF ATTACK

BY

Fouad Ahmed Youssef

A DISSERTATION

Michigan State university
in partial fulfilment of the requirements
for the degree of

submitted to

DOCTOR OF PHILOSOPHY

Department of Mechanical Engineering
1987

ABSTRACT

LAMINAR FLOW OVER A SPINNING PROJECTILE AT AN ANGLE OF ATTACK

By

Fouad Ahmed Youssef

The study of forces and moments on a spinning pointed body at an angle of attack is extremely important in ballistics. Previous work has been mostly experimental. This is because the governing Navier-Stokes equations are nonlinear and fully three dimensional, making analysis impossible and direct numerical solutions impractical.

The most promising theoretical technique is the unsteady cross flow analogy. Considering the axial direction as timelike, the pressure and the flow field can be obtained from the impulsive starting of a two-dimensional cylinder. Although the analogy is heuristic, the results do correlate well with experimental data on slender bodies for subsonic through supersonic free stream speeds.

In this study we investigate the impulsive starting of expanding, rotating cylinders. The results are used to calculate the force and moment coefficients for projectiles by means of the unsteady cross-flow analogy. We solve the unsteady Navier-Stokes equations using matched asympototic inner-outer perturbation method and comparing these results with the solution obtained using numerical methods. Excellent agreement between the two methods has been established in the region where both solutions are valid.

The results obtained are consistent with existing experimental work.

For example, a pair of secondary recirculating zones has been predicted,

in addition to the well-known primary pair for high Reynolds numbers. The numerical scheme used showed stability and robustness in the integration of the full Navier-Stokes equations.

ACKNOWLEDGMENTS

The author wishes to express his indebtedness to his dissertation committee chairman, professor C.Y. Wang who has given encouragement and guidance throughout the course of this research.

The author would like to thank professor M.Potter, guidance committee member, who carried out the advising responsibility during Professor Wang's sabbatical leave during the year 1984-1985, and has been of great help to the author.

Thanks are also due to Professor D. Yen for his kind discussion from time to time, Professor D. Wiggert for his kind guidance and support, and Professor I. Wichman who agreed to join the guidance committee during the last stage due to Professor Potter's temporary illness.

The author is also grateful to the valuable help from the members of the Albert Case Center for Computer Aided Design, without which the present work could never have been completed.

Finally the author is indebted to the government of Egypt, which provided the fellowship support necessary for completion of this thesis.

TABLE OF CONTENTS

Chapter No					
No.					
	NOMEN	CLATURE	vi		
	I	INTRODUCTION	1		
		1-1 Scope and Objective	. 1		
		1-2 Literature Survey	. 2		
	II	PROBLEM FORMULATION	. 7		
		2-1 The Cross Flow Analogy	. 7		
		2-2 The Governing Equations	. 8		
	III	ANALYTICAL SOLUTION	. 14		
		3-1 Formulation	. 14		
		3-2 First-Order Solution	. 17		
		3-2-1 First-Order Outer Solution	. 17		
		3-2-2 First-Order Inner Solution	. 18		
		3-3 Second-Order Solution	. 20		
		3-3-1 Second-Order Outer Solution	. 20		
		3-3-2 Second-Order Inner Solution	. 21		

	3-4 Composite Solution	28
	3-5 Vorticity Distribution On The Surface of	
	The Cylinder	30
	3-6 Pressure Distribution On The Cylinder	32
	3-7 Drag, Lift and Moment	33
	3-8 Results	36
	3-8-1 Stream Lines	37
	3-8-2 Pressure Coefficient	37
	3-8-3 Drag	38
	3-8-4 Lift	38
	3-8-5 Moment	38
	3-8-6 Surface Vorticity	39
	3-8-7 Separation Progression	39
IV	NUMERICAL SOLUTION	51
	4-1 Grid Structure	52
	4-2 Formulation	52
	4-2-1 Finite Difference Scheme for	
	the Vorticity Equation	54
	4-2-2 Finite Difference Scheme for	
	Poisson Equation	58
	4-2-3 Numerical Boundary and Initial Conditions	63
	4-2-3a Boundary Conditions	63

4-2-3b	o Initial Conditions and Flow Initialization	
		. 63
4-2-4	Scheme and Flow Initialization Implementation	
		. 65
4-3 Pr	ressure and the Pressure Coefficient	. 66
	rag, Lift and Moment	
	esults ·	
4-5-1	Stream lines	69
4-5-2	Pressure Coefficient	70
4-5-3	Drag	71
4-5-4	Lift	71
4-5-5	Moment	71
4-5-6	Surface Vorticity	71
4-5-7	Effect of Outer Numerical Boundary	72
4-6	Transforming to steady State Three Dimensional	
	Problem	72
CONCL	USION AND DISCUSSION	100
REFERI	ENCES	105

V

NOMENCLATURE

- a Cylinder radius
- C Coefficients
- d Diameter
- f Function of θ ; t is an integration constant
- G Function of η , defined by equation (3.61)
- p Pressure
- u = Velocity in the r, ξ -direction
- v Velocity in the θ , ζ -direction
- r Radial coordinate
- R Stretched radial coordinate, Reynolds number and half the Reynolds number, depending on the subscript
- t,T- Time
- z Axial direction in cylinderical system of coordinate
- α Angle of attack
- β Half-cone angle
- $\gamma = \tan(\beta)/\tan(\alpha)$
- δ = Gauge function in ϵ
- Δ Laplacian

- ε Small number
- ς Transformed meridian coordinate θ
- η Stretched radial coordinate
- θ Meridian coordinate, angle
- κ Wave number
- λ Function of ϵ
- ν Viscosity
- ξ Radial transformed coordinate
- $\pi = 3.14159262....$
- ρ Density
- τ Shear stress
- ϕ Transformed stream function
- ψ Stream function
- ω Vorticity
- Ω Angular velocity
- ∇ Difference operator

Subscript

- d Distinguishes Reynolds number (R_d) from half Reynolds number (R_a)
- i Numerical index in the ξ -direction
- j Numerical index in the ζ -direction
- r = In the r-direction
- ° Degree, initial, surface

- ∞ Free-stream
- θ In the θ -direction

Superscripts

- i Inner solution
- n Numerical index for time
- ⁰ Outer solution

CHAPTER I

INTRODUCTION

1-1 Scope and Objective

In 1951 Allen and Perkins ^[1] (see[2]) remarked upon a certain analogy between the cross flow at various stations along a cylindrical body of revolution and the development with time of the flow about a circular cylinder starting from rest. They considered conditions in a plane of fluid which is perpendicular to the body axis and moving with the free stream velocity V_{∞} times $\cos(\alpha)$ (α is the angle of attack). The trace of the body is a circle, whose size expand and contract as the plane moves along the body. They proposed that the change of the cross sectional area be ignored for slender bodies, because the cross-flow is only aware of the circle suddenly appearing in it, and is thus similar to a flow that would be observed for a fixed-diameter circular cylinder suddenly introduced in a stream with velocity V_{∞} $\sin(\alpha)$.

Although the problem of impulsively-started cylinder has attracted the attention of many investigators, the analogy established by Allen and Perkins (now known as cross-flow analogy) did accelerate research on the important problem of projectiles at various angles of attack. The approximation of the three-dimensional steady state problem by its equivalent cross-flow problem (two-dimensional time-dependent) has certain advantages. The characteristics of the equations that govern problems in the two-dimensional unsteady state are easier to handle, using analytical or numerical integration techniques, than the original three dimensional problem.

The reduction in the number of space variables directly decreases the number of assigned memory locations required. It also reduces programing complexity and run time. Although it is possible theoretically to derive solutions for the three dimensional problems, there are few computers available that are able to carry out the numerical experiment with the same number of grid points in each space direction; memory limitations quickly become significant.

In the present study we investigate the flow field surrounding a cylindrical body of revolution at an angle of attack. Different projectile shapes are investigated. Using the cross-flow analogy hypothesis, our objective is to go one step further than previous studies, by taking into consideration the effect of diameter change and rotation in the cross-flow plane.

1-2 Literature Survey

There are many research articles in the open literature dealing with this problem. These can be categorized as analytical or theoretical work, numerical work and laboratory or experimental work, and are briefly reviewed here.

Previous theoretical investigations of the initial flow field over an impulsively-started circular cylinder may be separated into three different approaches, namely

- 1- Boundary-layer solutions,
- 2- Matched-asymptotic expansion of the time-dependent Navier-Stokes equations, and
- 3- Potential flow models.

The growth of the boundary layer on a circular cylinder started impulsively from rest was first studied by Blasius [3] (1908). Tollmien [4] (1924) studied the impulsively started rotating cylinder. Goldstein and Rosenhead [5] (1936) extended the Blasius solution to third order. Gortler^[6,7] (1936) and Watson^[8] (1955) conducted further investigations of the series expansions, but no more terms were added. Shuh [9] (1953) studied this problem using the momentum integral method. Wundt [10] (1955) carried out a detailed study, and showed that Goldstein and Rosenhead's [5] solution is in error; he gave the solution in terms of tabulated coefficients. Wang [11, 12] (1966, 1967) was the first to employ the method of matched-asympototic expansions to solve the time dependent Navier-Stokes equations to second order. He carried out a successful attempt to extend the boundary-layer theory for large Reynolds numbers. His solution was the first to be valid even after separation occurred. Wang [13] (1968) then extended the validity of his solution to include small Reynolds numbers.

Collins and Dennis^[14] (1973a) extended Wang's analysis by expanding the stream function and vorticity in powers of time. They improved their results later ^[15](1973b). By expressing the stream function and vorticity in boundary-layer coordinates, and using unsteady boundary-layer theory to obtain solution for small time, they were able to push the solution further in time by continuing the integration numerically, using the implicit Crank-Nicolson numerical integration scheme. However they did not match with the "Outer Solution" which means that the entire solution is of the boundary layer kind.

Bar-Lev and Bar-Lev and Yang [16,17] (1974,1975) improved Wang's solution by extending it to third order, using the method of matched asymptotic expansions. Chien [18] (1977) carried out a study including both numerical and analytical solutions. His analytical solution agrees with that of Bar-Lev and Yang. He used what is known as the Hopscotch method [19] for the solution of the vorticity equation, and the method of successive overrelaxation for Poisson equation.

Thom^[20] (1933) carried out the first successful attempt to integrate the equations of motion numerically for a viscous fluid.

Later Kawaguti^[21] (1953) obtained a solution for Reynolds number of 40.

Payne [22] (1958) was the first to use the electronic computer to obtain a solution for the problem. He used an explicit time difference formula for the vorticity equation. Proudman and Johnson [23] (1962) solved the Navier-Stokes equations in the neighborhood of the rear stagnation point of an impulsively started circular cylinder. Kawaguti and Jain [24] (1966) considered the same problem and extended the solution previously obtained by Kawaguti [21] to include other Reynolds numbers. Ingham [25] (1968) improved Payne's work by using a finer grid, enlarging the computational domain and extending the computation to longer time. Thoman and Szewczyk [26] used a hybrid mesh cell structure in the vicinity of the cylinder surface and computed the non-linear convection term by a directional differential scheme. Jain and Rao [27] (1969) obtained the steady state solution up to a Reynolds number of 60 and found that for higher Reynolds numbers the drag coefficient

decreases monotonically with time. Son and Hanratty $^{[28]}$ (1969) attempted unsuccessfully to arrive a steady state solution for larger Reynolds numbers by integrating the time-dependent Navier-Stokes equations from rest. Nevertheless, aside from the primary separation bubble pair, they found a secondary bubble near separation for $R_d = 500$.

Chorin^[29] (1973) used computer-generated pseudo-random numbers to solve the two dimensional time dependent Navier-Stokes equations at high Reynolds numbers and studied the case R_d=1000. Loc^[30] (1980), using a compact fourth-order accurate scheme, utilized the A.D.I. method to solve the problem. His results agree with the previously known results. Loc claims that his solution is fourth order accurate although he uses a second-order formula for the surface vorticity.

The most recently published work is that of Ece and Walker [31] (1985) for the impulsive start of a rotating and translating cylinder. They used two different methods to solve the problem. Their results are obtained either by an expansion of the solution in a power series in time, or by a fully numerical technique.

Hill^[32] (1954), and Bryson^[33] (1959) and others have used an **inviscid** mathematical model with point vortices for longer times. However, their results do not agree with the available experimental work, probably because the separation phenomenon is primarily viscous.

Although theoretical and numerical techniques have been used extensively to investigate this problem, experimental work on the same problem is scarce. Schwabe [34](1935) measured the variation from

vortex pictures and computed the pressure distribution. Sarpkaya^[35] (1966) measured the cross-flow drag and normal-force coefficient as a function of relative displacement of the fluid in a time-dependent and two-dimensional flow. Honji and Taneda^[36] (1969) determined the variation of the length of vortices with time photographically. They also found the second bubble at the upstream side of the main bubble at Reynolds numbers greater than 550. Lamont and Hunt^[37] (1976) measured the out-of-plane force (i.e., the "Magnus" side force if the body is at incidence). The experimental model consisted of an extensively pressure-tapped cylinder to which four different noses were fitted. The general nature of the out-of-plane force is found to be consistent with the cross-flow analogy. The Reynolds number was found to have an important influence at inclinations above 55 degree. However, it was also found that the range of Reynolds numbers over which this effect occurs can depend on the scale of the model.

The present work is concerned with the study of the flow field, forces and moment for a projectile at an angle of attack. We intend to use the cross-flow analogy as a practical means to study the problem. Analytically, we use the method of matched inner-outer expansions to obtain the progressive events of the flow field and the forms necessary to evaluate the forces and moments in a closed form to second order. Numerically, we use the forward-in-time centered-space explicit scheme to solve the vorticity equation in plane-polar coordinates. We also use the Fast Fourier Transform to solve Poisson equation for the same purpose stated above. Comparison of solutions obtained by the numerical and analytical methods shows excellent agreement in the overlaping region of validity.

CHAPTER II

PROBLEM FORMULATION

2-1 The Cross-Flow Analogy

The obvious need for accurate information about the forces and moments acting on lifting bodies moving at an angle of attack in the subsonic to supersonic-velocity range is reflected in the fluid mechanics literature. Extensive discussion exists concerning the normal- force distribution and the wake-vortex characteristics of bodies of revolution and the cross-flow analogy. Thirty five years ago a method for calculating the flow over cylindrical bodies at large angles of attack was proposed^[1]. The method bypasses the difficulties arising in three-dimensional problems, which are usually unsolvable analytically. However, even to solve such a problem numerically is at the present time beyond most computers capabilities because of the excess memory required.

The proposed method attempts to approximate the difficult three dimensional steady state problem by a two-dimensional unsteady flow (see Refs. [1] to [38]). The model (Figure II-1) employs an observer in a plane perpendicular to the direction of motion of the body and recording the development of flow as the body moves in space, crossing the fixed plane of the observer. A furthur simplification, used by previous authors, is to neglect the variation in the diameter of the body as it moves in the fixed plane. The flow is thus assumed to be that of an impulsively started circular cylinder. This is known as the cross-flow analogy.

In the present study we attempt to investigate the unsteady twodimensional flow field of an incompressible fluid, with constant properties, arising from the sudden appearance of an expanding, rotating cylinder. The main objective is to take into consideration the effect of the previously neglected diameter change by using cross-flow analogy.

2-2 The Governing Equations

We seek to determine the flow field and to predict the forces and the moment on a three-dimensional projectile in a steady uniform flow with velocity ∇ , at an angle of attack α . The component of the free-stream velocity, V, in the cross-flow plane is

$$U_{m} = V \sin(\alpha) \tag{2.1}$$

which defines the cross-flow upstream velocity, and

$$V_{m} = V \cos(\alpha) \tag{2.2}$$

is the component of the free-stream velocity in a direction parallel to the projectile axis (relative velocity between the body and the fixed observer plane).

Hence

$$V_{\infty} = U_{\infty} \cot(\alpha) \tag{2.3}$$

The body shape is given by the radial distribution r_0 as a function of the axial distance z (in cylinderical coordinates) from the body tip (see Figure II-1). Thus the relation between the cross-sectional radius and the axial distance for a pointed cone is

$$\mathbf{r_0} = \mathbf{z} \, \tan(\beta) \tag{2.4}$$

where β is the half cone angle, and, for a truncated cone

$$\mathbf{r}_0 = \mathbf{a}_0 + \mathbf{z} \, \tan(\beta) \tag{2.5}$$

where a_0 is the initial radius (radius at z = 0). Lastly, for a paraboloidal body we have

$$r_0 - a z (2.6)$$

where a is a constant.

The essence of the cross-flow analogy becomes clear when we introduce the transformation

$$(r, \theta, z) = (r, \theta, z_0 + V_n t)$$
 (2.7)

and consider the plane where $z_0 = 0$ (observer plane). In that plane the flow field is that induced by a circular cylinder of varying radius $r_0(z) = r_0(\sqrt{y})$. Information available from the relatively simpler two-dimensional unsteady flow can now be applied to the three-dimensional steady flow field.

Thus, since
$$z = t V_{\infty}$$
, one finds
$$r_0 = t U_{\infty} \gamma \tag{2.8}$$

For a pointed right cone. Here

$$\gamma = \tan(\beta) / \tan(\alpha) \tag{2.9}$$

For a truncated right cone, one finds

$$r_0 = a_0 + t U_{\infty} \gamma$$
 , (2.10)

and for a paraboloidal body,

$$r_0 = \left[a t U_{\infty} \cot(\alpha) \right]^{1/2} . \qquad (2.11)$$

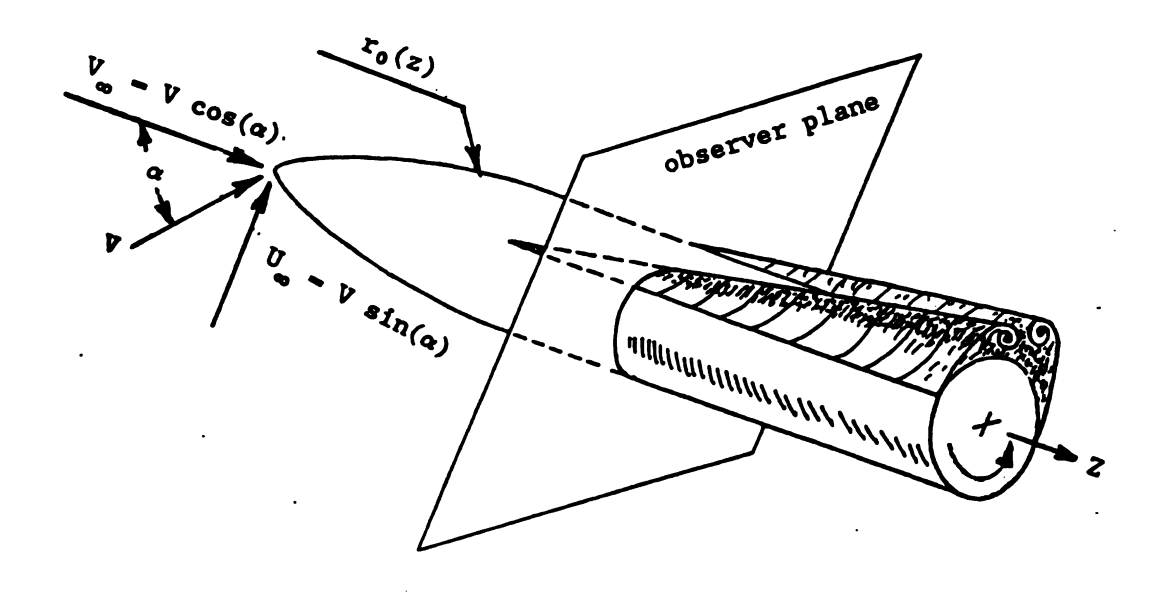


Figure II-1 The Spinning Projectile at an Angle of Attack
is Studied Through the Impulsive Start of
Expanding, Rotating Circular Cylinder

The following formulation was used for the case of a <u>truncated right</u>

cone. Similar relations for other cases can be easily derived. The

continuity equation is satisfied identically if^[2]

$$\vec{\nabla} = \nabla \times \vec{\Psi} \tag{2.12}$$

where $\vec{\Psi}$ is a vector function of position. In two-dimensional flow, two components of $\vec{\Psi}$ may be taken to be zero; therefor, $\vec{\Psi}$ reduces to the scaler function

$$\vec{\Psi} = (0, 0, \psi),$$
 (2.13)

where ψ is the scaler stream function. Also,

$$\vec{\mathbf{V}} = (\mathbf{v}_r, \mathbf{v}_\theta, \mathbf{v}_z), \tag{2.14}$$

where \vec{V} is the velocity vector, v_r is the radial velocity, and v_θ is the meridian velocity in polar coordinates. However since we are working in plane polar coordinates $v_z = 0$. The above relationships imply

$$v_r(r,\theta,t) = -\frac{1}{r} \frac{\partial \psi(r,\theta,t)}{\partial \theta},$$
 (2.15)

and

$$v_{\theta}(r,\theta,t) = \frac{\partial \psi(r,\theta,t)}{\partial r}$$
 (2.16)

We now define the vorticity vector $\overrightarrow{\omega}$ as

$$\vec{\omega} = (0, 0, \omega) = - \nabla \times \vec{v}, \qquad (2.17)$$

where ω is the scaler vorticity function.

From (2.10) it is obvious that the following relationship holds at the cylinder surface, where $\mathbf{r}=\mathbf{r}_0$,

$$\frac{d\mathbf{r}_0}{dt} = \mathbf{U}_{\infty} \ \gamma = \mathbf{v}_{\mathbf{r}}(\mathbf{r}_0, \theta, t) = -\frac{1}{\mathbf{r}_0} \ \frac{\partial \psi}{\partial \theta}(\mathbf{r}_0, \theta, t) \ . \tag{2.18}$$

Integration of equation (2.18) with respect to θ , implies

$$\psi(r_0,\theta,t) = -r_0U_{m}\gamma\theta + f_1(t).$$

Since ψ cannot be uniquely determined and can only be obtained to within a constant, we take $f_1(t)$ to be zero, whereby

$$\psi(\mathbf{r}_0,\theta,\mathbf{t}) = -\mathbf{r}_0 \mathbf{U}_{\alpha} \gamma \theta = -\mathbf{U}_{\alpha} \gamma \theta (\mathbf{a}_0 + \mathbf{U}_{\alpha} \gamma \mathbf{t}). \tag{2.19}$$

The (upstream) stream function, before the appearance of the cylinder, is that due to the uniform flow, viz.,

$$\psi(r,\theta,t) = r \sin(\theta) , t < 0 . \qquad (2.20)$$

By superposition, conservation of mass requires

$$\psi = r \sin(\theta) - U_{\infty} \gamma \theta (a_0 + U_{\infty} \gamma t)$$
 , $r \rightarrow \infty$. (2.21)

On the surface of the cylinder

$$v_{\theta}(r_0, \theta, t) = \frac{\partial \psi(r_0, \theta, t)}{\partial r} = \Omega r_0 = \Omega(a_0 + U_{\infty} \gamma t),$$
 (2.22)

where Ω is the angular velocity. By Normalizing the variables as

$$\hat{\psi} = \psi / U_{\infty} a_{0} , \hat{t} = t U_{\infty} / a_{0}$$

$$\hat{r} = r / a_{0} , \hat{\Omega} = \Omega a_{0}$$

$$\hat{\omega} = \omega a_{0} / U_{\infty}$$

and then dropping the superscripts, the Navier-Stokes equation in conservative form become

$$\frac{\partial \omega}{\partial t} - \frac{1}{r} \left\{ \frac{\partial}{\partial r} \left[\omega \frac{\partial \psi}{\partial \theta} \right] - \frac{\partial}{\partial \theta} \left[\omega \frac{\partial \psi}{\partial r} \right] \right\} - \frac{1}{R_e} \nabla^2 \omega, \qquad (2.23)$$

where $R_d = 2 \times R_e = \frac{2 a_0 U_\infty}{\nu}$ is the initial Reynolds number based on the initial diameter. Also by (2.12) and (2.16) we have

$$\nabla^2 \psi \stackrel{\text{def}}{=} \omega \tag{2.24}$$

where

$$\nabla^2 = \frac{\partial}{\partial r}^2 + \frac{1}{r} \frac{\partial}{\partial r} + \frac{1}{r} \frac{\partial^2}{\partial \theta^2}$$

Equations (2.22) and (2.23) are to be solved subject to the following initial conditions:

$$\psi(r,\theta,0^+) - r \sin(\theta) - \gamma\theta$$
 , $r \neq r_o$, (2.25)

$$\psi(\mathbf{r},\theta,0^{-}) = \mathbf{r} \sin(\theta), \qquad (2.25b)$$

$$\omega(r,\theta,0^{+}) = 0$$
 , $r \neq r_{0}$, (2.26)

and the boundary conditions

$$\psi(\mathbf{r}_0, \theta, \mathbf{t}) = -\gamma \theta(1 + \gamma \mathbf{t}), \qquad (2.27)$$

$$\psi_{\mathbf{r}}(\mathbf{r}_0, \theta, \mathbf{t}) = \Omega(1 + \gamma \mathbf{t}), \qquad (2.28)$$

where for a truncated right cone,

$$r_0$$
 (t) = 1 + γ t, (2.29)

and

$$\psi = r \sin(\theta) - \gamma \theta (1+\gamma t)$$
 as $r \to \infty$, (2.30)

$$\omega = 0$$
 as $r \to \infty$. (2.31)

CHAPTER III

ANALYTICAL SOLUTION

The available theory for the analytical solution of non-linear partial differential equations is inadequate for the exact analytical solution of such equations. Perturbation methods have been used frequently to obtain approximate solutions with a high degree of accuracy. Among these is the method of matched asymptotic expansions, which can be systematically used for such problems provided a perturbation parameter exists. The main difficulty of the method lies in the complexity one faces as he proceeds to higher order solutions. In this thesis the method of matched asymptotic expansions is employed to solve the Navier-Stokes equations in order to obtain the fluid behavior in the initial stages of motion.

3-1 Formulation

The governing equations, initial and boundary conditions are (2.23) - (2.30). By substituting ψ for ω (from Eq. (2.24) into (2.33)) we find

$$\left\{ \frac{\partial}{\partial t} + \frac{1}{r} \left[\frac{\partial \psi}{\partial r} \frac{\partial}{\partial \theta} - \frac{\partial \psi}{\partial \theta} \frac{\partial}{\partial r} \right] - \frac{1}{R_{\rho}} \nabla^{2} \right\} \nabla^{2} \psi = 0. \quad (3.1)$$

The initial conditions are

$$\psi(r,\theta,0^{+}) = r \sin(\theta) - \gamma\theta , \qquad (3.2)$$

(3.3)

and $\omega(r,\theta,0^+) = 0$, $r \neq r_0$.

The boundary conditions are

$$\psi(\mathbf{r}_0, \theta, \mathbf{t}) = -\gamma \theta (1 + \gamma \mathbf{t}), \qquad (3.4)$$

and
$$\frac{\partial \psi(\mathbf{r}_0, \theta, t)}{\partial \mathbf{r}} = \Omega (1 + \gamma t).$$
 (3.5)

where,

$$r_0 = 1 + \gamma t$$

and

$$\psi = r \sin(\theta) - \gamma \theta (1+\gamma t) \qquad \text{as } r \to \infty, \quad (3.6)$$

$$\omega = 0 \qquad \text{as } r \to \infty. \quad (3.7)$$

The boundary condition (3.4) and (3.6) imply that the solution is **not periodic** in θ . This is because of the expansion of the surface, which acts as a source located at the origin. In order to simplify the manipulation, it is advantageous to subtract this nonperiodicity a priori. Therefore we redefine ψ as

$$\psi(\mathbf{r},\theta,\mathbf{t}) = -\gamma\theta(1+\gamma\mathbf{t}) + \Omega(1+\gamma\mathbf{t})^{2}\ln[\mathbf{r}/(1+\gamma\mathbf{t})] + \dot{\psi}(\mathbf{r},\theta,\mathbf{t}). \tag{3.8}$$

Substituting in equation (3.1) to (3.7), and dropping the astrisk yields

$$\left\{\frac{\partial}{\partial t} + \frac{1}{r} \left(\left[\frac{\Omega(1+\gamma t)^{2}}{r} + \frac{\partial \psi}{\partial r} \right] \frac{\partial}{\partial \theta} - \left[-\gamma(1+\gamma t) + \frac{\partial \psi}{\partial \theta} \right] \frac{\partial}{\partial r} \right\}$$

$$-\frac{1}{R_{\rho}}\nabla^{2}\nabla^{2}\psi = 0, \qquad (3.9)$$

subjected to

$$\psi(r,\theta,0) = r \sin(\theta) - \Omega \ln(r), \qquad (3.10)$$

$$\omega(r, \theta, 0) = 0$$
 , $r \neq r_0 = 1 + \gamma t$, (3.11)

$$\psi(1+\gamma t, \theta, t) = 0, \tag{3.12}$$

$$\frac{\partial \psi(1+\gamma t, \theta, t)}{\partial r} = 0, \qquad (3.13)$$

$$\psi = r \sin(\theta) - \Omega(1+\gamma t)^{2} \ln[r/(1+\gamma t)] \qquad \text{as } r \to \infty, \qquad (3.14)$$

$$\omega = 0 \qquad \text{as } r \to \infty. \tag{3.15}$$

Note that the initial condition (3.10) is now periodic in θ , replacing (3.2), which is not periodic.

To obtain the viscous layer growth for the initial flow, we employ the following transformation [12];

or

$$\epsilon \stackrel{\text{def}}{=} \frac{T_0 U_{\infty}}{a_0} \ll 1. \tag{3.17}$$

Here T_0 is a reference time representing the time for the cylinder to travel a small fraction of its radius, and ϵ is the ratio of the two times t and \mathring{t} .

Because we shall focus our attention on small times, we assume the Reynolds number is large, viz.,

$$R_{e} \stackrel{\text{def}}{=} \frac{U_{\infty} a_{0}}{\nu} - \frac{1}{\epsilon \alpha} , \qquad (3.18)$$

where α is a nondimensional constant of order unity.

The Navier-Stokes equations become, after dropping the astrisk on t,

$$\left\{ \frac{\partial}{\partial t} + \frac{\epsilon}{r} \left[\left[\frac{\Omega(1+\epsilon\gamma t)^2}{r} + \frac{\partial \psi}{\partial r} \right] \frac{\partial}{\partial \theta} - \left[-\gamma(1+\epsilon\gamma t) + \frac{\partial \psi}{\partial \theta} \right] \frac{\partial}{\partial r} \right] \right\}$$

$$-\alpha \epsilon^2 \nabla^2 \right\} \nabla^2 \psi = 0, \qquad (3.19)$$

subjected to the initial conditions

$$\psi(r,\theta,0^{\dagger}) = r \sin(\theta) - \Omega \ln(r), \qquad (3.20)$$

$$\omega(r,\theta,0^{+}) = 0$$
 $r \neq r_{0}$, (3.21)

$$\psi(1+\epsilon\gamma t,\theta,t) = 0, \qquad (3.22)$$

$$\frac{\partial \psi(1+\epsilon\gamma t,\theta,t)}{\partial r} = 0, \qquad (3.23)$$

$$\psi = r \sin(\theta) - \Omega(1+\epsilon\gamma t)^2 \ln[r/(1+\epsilon\gamma t)], \quad \text{as } r \to \infty, \quad (3.24)$$

$$\omega = 0$$
 as $r \to \infty$. (3.25)

3-2 First Order Solution

3-2-1 First-Order Outer Solution

Assume an expansion of the form

$$\psi = \sum_{n=1}^{\infty} \delta_n(\epsilon) \psi_n^0(r, \theta, t), \qquad (3.26)$$

where $\delta_{n}(\epsilon)$ are gauge functions in ϵ . The boundary conditions as $r \to \infty \text{ imply that}$

$$\delta_1(\epsilon) = 1$$

Thus, upon substituting the outer expansion in Eq.(3.19) and equating like powers of ϵ , we obtain

$$\frac{\partial \nabla^2 \psi_n^0}{\partial t} = 0, \qquad , n = 1, 2, 3, \dots$$

which imply

$$\nabla^2 \psi_n^0$$
 = constant ,n = 1,2,3,....

However, since the flow is initially irrotational at infinity, by Kelvin's theorem it will remain irrotational, whereby

$$\nabla^2 \psi_n^0 = 0$$
 , $n = 1, 2, 3$. (3.27)

For n = 1 we have, expanding (3.22) and (3.24),

$$\psi_1^0(1,\theta,t) = 0,$$
 (3.28)

$$\psi_1^0 = r \sin(\theta) - \Omega \ln(r) \quad \text{as } r \to \infty. \tag{3.29}$$

The solution is for potential flow over a cylinder, plus a vortex, viz.,

$$\psi_1^0(r,\theta,t) = (r - \frac{1}{r}) \sin(\theta) - \Omega \ln(r)$$
 (3.30)

3-2-2 First-Order Inner Solution

For the inner expansion we stretch the radial variable as

$$R = \frac{r - (1 + \epsilon \gamma t)}{\lambda(\epsilon)}, \qquad (3.31)$$

where $\lambda(\epsilon)$ is to be determined. We assume an inner expansion of the form

$$\psi = \sum_{m=1}^{\infty} \Delta_{m}(\epsilon) \psi_{m}^{i}(R,\theta,t). \qquad (3.32)$$

Since the tangential velocity at the edge of the boundary layer is to be matched, i.e.,

$$\frac{\partial \psi}{\partial r} - \frac{\partial \psi_1^0}{\partial r} - \frac{\Delta_1(\epsilon)}{\lambda(\epsilon)} \frac{\partial \psi_1^{\dot{1}}}{\partial R} , \qquad (3.33)$$

we find

$$\Delta_1(\epsilon) = \lambda(\epsilon). \tag{3.34}$$

By substituting the inner expansion into the vorticity equation and letting ϵ vanish, keeping in mind that we need to retain the highest power of ϵ , one obtains

$$\psi_{1RRt}^{i} - \lim_{\epsilon \to 0} \left(\frac{\epsilon^{2} \alpha}{\Delta_{1}(\epsilon)} \right) \psi_{1RRRR}^{i} = 0,$$

which implies that

$$\Delta_1(\epsilon) = \epsilon \tag{3.35}$$

By substituting transformation (3.31) in (3.19), Eq.(3.19) becomes

$$\left\{ \frac{\partial}{\partial t} - \gamma \frac{\partial}{\partial R} + \frac{\epsilon}{R_1} \left[\left[\frac{\Omega(1 + \epsilon \gamma t)^2}{R_1} + \frac{1}{\epsilon} \frac{\partial \psi}{\partial R} \right] \frac{\partial}{\partial \theta} - \left[-\gamma(1 + \epsilon \gamma t) + \frac{\partial \psi}{\partial \theta} \right] \frac{1}{\epsilon} \frac{\partial}{\partial R} \right] - \alpha \epsilon^2 \nabla_1^2 \right\} \nabla_1^2 \psi = 0 , \quad (3.36)$$

where

$$R_1 = 1 + \epsilon (R + \gamma t),$$

and

$$\nabla_1^2 = \frac{1}{\epsilon} \frac{\partial^2}{\partial R} + \frac{1}{\epsilon} \frac{\partial}{R_1} + \frac{1}{2} \frac{\partial^2}{\partial \theta}.$$

The equation governing the first order inner expansion is now

$$\psi_{1RRt}^{i} - \alpha \psi_{1RRRR}^{i} = 0.$$
 (3.37)

Integrating once with respect to R yields

$$\psi_{1RR}^{i} - \alpha \psi_{1RRR}^{i} = f(\theta, t).$$
 (3.38)

The no-slip boundary conditions are, from (3.22) and (3.23)

$$\psi_1^{\mathbf{i}}(0,\theta,t) = 0$$
, (3.39)

$$\psi_{1R}^{i}(0,\theta,t) = 0.$$
 (3.40)

The matching condition is that the tangential velocity at the edge of the the inner region $(R \to \infty)$ approaches that in the outer region as $r \to 1$. Employing the asympototic matching principle [38], we obtain

$$\psi_{1R}^{i}(\infty,\theta,t) - \psi_{1r}^{0}(1,\theta,t) - 2\sin(\theta) - \Omega.$$
 (3.41)

Applying the matching condition (3.41) to equation (3.38) we obtain

$$f(\theta,t) = \psi_{1rt}^{0}(1,\theta,t) - \alpha \epsilon^{2} \psi_{1rrr}^{0}(1,\theta,t) = 0.$$
 (3.42)

The problem is now equivalent to what is widely known as the Rayleigh problem for impulsive start of a flat plate [39]. The solution is thus,

$$\psi_{1R}^{i} = (2 \sin(\theta) - \Omega) \operatorname{erf}(\eta), \qquad (3.43)$$

or, after carrying one more integration,

$$\psi_1^{\hat{1}} = 2\sqrt{\alpha t} \left[\eta \operatorname{erf}(\eta) + \frac{1}{\sqrt{\pi}} \left(e^{-\eta^2} - 1 \right) \right] \left[2 \sin(\theta) - \Omega \right], \quad (3.44)$$

where

$$\eta = \frac{R}{2\sqrt{\alpha t}} . \tag{3.45}$$

Formulas (3.30) and (3.44) are available in the literature [11,12,16,17,18], without the omega term. The quantity η is defined in a way that accounts for the expanding boundary.

3-3 Second-Order Solution

3-3-1 Second-Order Outer Solution

Applying the asymptotic matching principle [38] again, with m = 1 in (3.32), n = 2 in (3.26) and matching ψ itself, we obtain

$$\delta_2(\epsilon) = \epsilon,$$
 (3.46)

and

$$\psi_2^0(1,\theta,t) = -\left(2\sin(\theta) - \Omega\right)\left(\gamma t + 2\left[\frac{\alpha - t}{\pi}\right]^{1/2}\right). \tag{3.47}$$

we also have from (3.24)

$$\psi_2^0 = \Omega \gamma t \left[1 - 2 \ln(r) \right] \qquad \text{as } r \to \infty . \tag{3.48}$$

Now, since

$$\nabla^2 \psi_2^0 = 0 , \qquad (3.49)$$

the solution is

$$\psi_{2}^{0}(\mathbf{r},\theta,t) = -\frac{2\sin(\theta)}{r} \left(\gamma t + 2 \left[\frac{\alpha t}{\pi} \right]^{1/2} \right) + \Omega \left(\gamma t + 2 \left[\frac{\alpha t}{\pi} \right]^{1/2} \right)$$

$$-2\Omega \gamma t \ln(r). \tag{3.50}$$

3-3-2 Second-Order Inner Solution

To obtain the second-order inner solution, we first match the meridian velocity (ψ_r). Thus we set m = 2 in (3.32) and n = 2 in (3.26), with ψ_2^0 given by (3.50), to obtain

$$\Delta_2(\epsilon) = \epsilon^2 , \qquad (3.51)$$

and

$$\psi_{2R}^{i}(\infty,\theta,t) = 2\left(2\left[\frac{\alpha-t}{\pi}\right]^{1/2} - R\right)\sin(\theta) + \Omega\left(R - \gamma t\right). \quad (3.52)$$

Substituting (3.32) into (3.36) yield the second order inner expansion equation, viz.,

$$\psi_{2RRt}^{i} - \alpha \psi_{2RRRR}^{i} = \left[\alpha + \gamma R + \psi_{1\theta}^{i} \right] \psi_{1RRR}^{i} - \left[\Omega + \psi_{1R}^{i} \right] \psi_{1RR\theta}^{i}$$

$$= \left\{ \alpha + 2 \gamma \sqrt{\alpha t} \eta + 4 \sqrt{\alpha t} \cos(\theta) \left[\eta \operatorname{erf}(\eta) \right] + \frac{1}{\sqrt{\pi}} \left(e^{-\eta^{2}} - 1 \right) \right\} \left\{ \frac{1}{\sqrt{\pi} \alpha t} \left(\Omega - 2 \sin(\theta) \right) \eta e^{-\eta^{2}} \right\}$$

$$- \left[\Omega + \left(2 \sin(\theta) - \Omega \right) \operatorname{erf}(\eta) \right] \left(\frac{2}{\sqrt{\pi c t}} \cos(\theta) e^{-\eta^{2}} \right). \quad (3.53)$$

The no slip boundary conditions are

$$\psi_2^{\mathbf{i}}(0,\theta,t) = 0$$
 , (3.54)

$$\psi_{2R}^{i}(0,\theta,t) = 0$$
 (3.55)

Integrating (3.53) once with respect to R, we find

$$\psi_{2Rt}^{i} - \alpha \psi_{2RRR}^{i} = \Omega \left[\gamma \operatorname{erf}(\eta) - \frac{2}{\sqrt{\pi}} \gamma \eta e^{-\eta^{2}} - \left[\frac{\alpha}{\pi t} \right]^{1/2} e^{-\eta^{2}} \right]$$

$$- 2 \sin(\theta) \left[\gamma \operatorname{erf}(\eta) - \frac{2}{\sqrt{\pi}} \gamma \eta e^{-\eta^{2}} - \left[\frac{\alpha}{\pi t} \right]^{1/2} e^{-\eta^{2}} \right]$$

$$+ 2 \Omega \cos(\theta) \left[\operatorname{erf}(\eta) - \operatorname{erf}(\eta) + \frac{2}{\pi} \left[e^{-\eta^{2}} - e^{-2\eta^{2}} \right] - \frac{2}{\sqrt{\pi}} \eta \operatorname{erf}(\eta) e^{-\eta^{2}} \right]$$

$$- 4 \sin(\theta) \cos(\theta) \left[\operatorname{erf}(\eta) - \frac{2}{\sqrt{\pi}} \eta \operatorname{erf}(\eta) e^{-\eta^{2}} + \frac{2}{\pi} \left[e^{-\eta^{2}} - e^{-2\eta^{2}} \right] \right]$$

$$+ f_{1}(\theta, t) . \tag{3.56}$$

To evaluate $f_1(\theta,t)$, we make use of the matching condition (3.52) which implies

$$\psi_{2Rt}^{i}(\infty,\theta,t) = 2 \left[\frac{\alpha}{\pi t}\right]^{1/2} \sin(\theta) - \Omega \gamma , \qquad (3.57)$$

also,

$$\psi_{2RRR}^{\mathbf{i}}(\infty,\theta,t) = 0 . \qquad (3.58)$$

Substituting in (3.56) we find

$$f_1(\theta,t) = 2\left(\gamma + \left[\frac{\alpha}{\pi t}\right]^{1/2}\right) \sin(\theta) + 4\sin(\theta)\cos(\theta) - 2\Omega\gamma . (3.59)$$

Thus

$$\psi_{2Rt}^{1} - \alpha \psi_{2RRR}^{1} = \Omega \left(\gamma \operatorname{erf}(\eta) - \frac{2}{\sqrt{\pi}} \gamma \eta e^{-\eta^{2}} - \left[\frac{\alpha}{\pi t} \right]^{1/2} e^{-\eta^{2}} - 2 \gamma \right)$$

$$+ 2 \sin(\theta) \left(\gamma \operatorname{erfc}(\eta) + \frac{2}{\sqrt{\pi}} \gamma \eta e^{-\eta^{2}} + \left[\frac{\alpha}{\pi t} \right]^{1/2} \left[1 + e^{-\eta^{2}} \right] \right)$$

$$+ 2 \Omega \cos(\theta) \left(\frac{2}{\pi} \left[e^{-\eta^{2}} - e^{-2\eta^{2}} \right] - \operatorname{erfc}(\eta) \operatorname{erf}(\eta) - \frac{2}{\sqrt{\pi}} \eta e^{-\eta^{2}} \operatorname{erf}(\eta) \right)$$

$$-4 \sin(\theta) \cos(\theta) \left(\operatorname{erf}(\eta) - 1 - \frac{2}{\sqrt{\pi}} \eta e^{-\eta^{2}} \operatorname{erf}(\eta) + \frac{2}{\pi} \left[e^{-\eta^{2}} - e^{-2\eta^{2}} \right] \right) .$$

To solve this equation we make use of the linearity of ψ_2^i . For this purpose, we assume a solution of the form

$$\psi_{2R}^{i} = t G_{1}(\eta) + t^{1/2}G_{2}(\eta) + t G_{3}(\eta) \sin(\theta) + t^{1/2}G_{4}(\eta) \sin(\theta) + t G_{5}(\eta) \cos(\theta) + t G_{6}(\eta) \sin(\theta) \cos(\theta).$$
(3.61)

By comparing the right hand side of equation (3.60) with (3.61), we recognize that

$$G_1(\eta) - \frac{\eta}{2} \frac{dG_1(\eta)}{d\eta} - \frac{1}{4} \frac{d^2G_1(\eta)}{d\eta^2} - \Omega \gamma \left[erf(\eta) - \frac{2}{\sqrt{\pi}} \eta e^{-\eta^2} - 2 \right], (3.62)$$

$$\frac{1}{2} G_2(\eta) - \frac{1}{2} \eta \frac{dG_2}{d\eta} - \frac{1}{4} \frac{d^2 G_2(\eta)}{d\eta^2} - \Omega \left[\frac{\alpha}{\pi} \right]^{1/2} e^{-\eta^2}, \qquad (3.63)$$

$$G_3(\eta) - \frac{1}{2} \eta \frac{dG_3(\eta)}{d\eta} - \frac{1}{4} \frac{d^2G_3(\eta)}{d\eta^2} - 2\gamma \left(\operatorname{erfc}(\eta) + \frac{2}{\sqrt{\pi}} \eta e^{-\eta^2} \right), (3.64)$$

$$\frac{1}{2} G_4(\eta) - \frac{1}{2} \eta \frac{dG_4(\eta)}{d\eta} - \frac{1}{4} \frac{d^2 G_4(\eta)}{d\eta^2} - 2 \left[\frac{\alpha}{\pi} \right]^{1/2} \left(1 + e^{-\eta^2} \right), (3.65)$$

$$G_5(\eta) - \frac{1}{2} \eta \frac{d^2 G_5(\eta)}{d \eta} - \frac{1}{4} \frac{d^2 G_5(\eta)}{d \eta^2} - 2 \Omega \left[\frac{2}{\pi} \left[e^{-\eta^2} - e^{-2\eta^2} \right] \right]$$

-
$$\operatorname{erf}(\eta) \operatorname{erfc}(\eta) - \frac{2}{\sqrt{\pi}} \eta e^{-\eta^2} \operatorname{erf}(\eta)$$
, (3.66)

$$G_{6}(\eta) - \frac{1}{2} \eta \frac{d G_{6}(\eta)}{d \eta} - \frac{1}{4} \frac{d^{2}G_{6}(\eta)}{d \eta^{2}} = -4 \left[erf_{(\eta)}^{2} - 1 - \frac{2}{\sqrt{\pi}} \eta e^{-\eta^{2}} erf_{(\eta)} \right]$$

$$+\frac{2}{\pi}\left[e^{-\eta^2}-e^{-2\eta^2}\right]$$
. (3.67)

The boundary conditions, (3.52) and (3.55), imply that

$$G_1(0) - G_2(0) - G_3(0) - G_4(0) - G_5(0) - G_6(0) - 0,$$
 (3.68)

$$G_1(\infty) = - \gamma \Omega, \qquad (3.69a)$$

$$G_2(\infty) = 2 \sqrt{\alpha} \Omega \eta, \qquad (3.69b)$$

$$G_{\mathbf{S}}(\mathbf{x}) = 0, \tag{3.69c}$$

$$G_4(\infty) = 4 \sqrt{\alpha} \left[\frac{1}{\sqrt{\pi}} - \eta \right], \qquad (3.69d)$$

$$G_{\delta}(\infty) = 0, \tag{3.69e}$$

$$G_{\mathbf{g}}(\mathbf{x}) = 0. \tag{3.69f}$$

The homogeneous part of the equations are clearly of the general form

$$\xi''(\eta) + 2 \eta \xi'(\eta) - 2 n \xi(\eta) = 0,$$
 (3.70)

where the prime indicate differentiation with respect to η , and n is an integer.

In general the solutions are expressible in terms of error functions and Hermite polynomials [40]. The solution is thus

$$\xi(\eta) = c_1 i^n \operatorname{erfc}(\eta) + c_2 H_n(\eta) , \qquad (3.71)$$

where $i^n \operatorname{erfc}(\eta)$ is the $n^{\frac{th}{n}}$ repeated integral of the complementary error function, defined [41] by

$$i^n \operatorname{erfc}(\eta) - \int_{\eta}^{\infty} i^{n-1} \operatorname{erfc}(\eta)$$
,

with

$$i^{0} \operatorname{erfc}(\eta) \stackrel{\text{def}}{=} \operatorname{erfc}(\eta)$$

and $H_n(\eta)$ is the Hermite polynomial, defined [41] by

$$H_n(\eta) = (-1)^n e^{\eta^2} \frac{d^n}{d\eta^n} e^{-\eta^2}$$
 (3.72)

In particular:

For n - 1 the solution is ;

$$\xi(\eta) = c_1 \eta + c_2 \operatorname{ierfc}(\eta)$$

$$-c_1 \eta + c_2 \left(\frac{1}{\sqrt{\pi}} e^{-\eta^2} - \eta \ \text{erfc}(\eta) \right), \qquad (3.73)$$

and for n = 2 we have

$$\xi(\eta) = A_1 \left(1 + 2 \eta^2 \right) + A_2 \left((1 + 2 \eta^2) \operatorname{erfc}(\eta) - \frac{2}{\sqrt{\pi}} \eta e^{-\eta^2} \right) (3.74)$$

using the boundary conditions, we obtain

$$G_1(\eta) = \Omega \gamma \left\{ \left[1 + 4 \eta^2 \right] \operatorname{erfc}(\eta) - \frac{5}{\sqrt{\pi}} \eta e^{-\eta^2} - 1 \right\},$$
 (3.75)

$$G_2(\eta) = \Omega \sqrt{\alpha} \left(2 - \operatorname{erfc}(\eta) \right) \eta , \qquad (3.76)$$

$$G_3(\eta) = 2 \gamma \left(\frac{3}{\sqrt{\pi}} \eta e^{-\eta^2} - 2 \eta^2 \operatorname{erfc}(\eta) \right),$$
 (3.77)

$$G_4(\eta) = 2 \sqrt{\alpha} \left(\frac{2}{\sqrt{\pi}} \left[1 - e^{-\eta^2} \right] + 3 \eta \operatorname{erfc}(\eta) - 2 \eta \right), \quad (3.78)$$

The solution of (3.66) and (3.67) is a slightly modified version for that obtained by Goldstein and Rosenhead [42] (page 184). Thus,

$$G_{5}(\eta) = \Omega \left\{ 2 \left[1 + \frac{4}{3\pi} \right] \eta^{2} \operatorname{erfc}(\eta) + \left[1 - 2 \eta^{2} \right] \operatorname{erfc}^{2}(\eta) \right.$$

$$\left. - \left[1 - \frac{4}{3\pi} \right] \operatorname{erfc}(\eta) - \frac{4}{\sqrt{\pi}} \left[1 + \frac{2}{3\pi} \right] \eta e^{-\eta^{2}} \right.$$

$$\left. + \frac{6}{\sqrt{\pi}} \eta e^{-\eta^{2}} \operatorname{erfc}(\eta) + \frac{8}{3\pi} e^{-\eta^{2}} - \frac{4}{\pi} e^{-2\eta^{2}} \right\}, (3.79)$$

$$G_{6}(\eta) = 4 \left\{ \left[\eta^{2} - \frac{1}{2} \right] \operatorname{erfc}^{2}(\eta) - \frac{3}{\sqrt{\pi}} \eta e^{-\eta^{2}} \operatorname{erfc}(\eta) \right.$$

$$\left. + \left[\left(\frac{1}{2} - \frac{2}{3\pi} \right) - \left(3 + \frac{4}{3\pi} \right) \eta^{2} \right] \operatorname{erfc}(\eta) \right.$$

$$\left. + \frac{4}{\sqrt{\pi}} \left[1 + \frac{1}{3\pi} \right] \eta e^{-\eta^{2}} - \frac{4}{3\pi} e^{-\eta^{2}} + \frac{2}{\pi} e^{-2\eta^{2}} \right\}, (3.80)$$

The total solution is therefore

$$\begin{split} \psi_{2R}^{1} &= \Omega \ \gamma \ t \ \left\{ \left[\ 1 + 4 \ \eta^{2} \ \right] \ \operatorname{erfc}(\eta) \ - \frac{5}{\sqrt{\pi}} \ \eta \ \operatorname{e}^{-\eta^{2}} \ - \ 1 \ \right\} \\ &+ \Omega \ \sqrt{\alpha} \ t \ \left\{ \ 2 - \operatorname{erfc}(\eta) \ \right\} \ \eta \\ &+ 2 \ \gamma \ t \ \left\{ \frac{3}{\sqrt{\pi}} \ \eta \ \operatorname{e}^{-\eta^{2}} \ - \ 2 \ \eta^{2} \ \operatorname{erfc}(\eta) \ \right\} \ \sin(\theta) \\ &+ 2 \ \sqrt{\alpha} \ t \ \left\{ \ \frac{2}{\sqrt{\pi}} \ (1 - \operatorname{e}^{-\eta^{2}}) + 3 \ \eta \ \operatorname{erfc}(\eta) \ - \ 2 \ \eta \ \right\} \ \sin(\theta) \\ &+ \Omega \ t \ \left\{ \ 2 \ \left[\ 1 + \frac{4}{3\pi} \ \right] \ \eta^{2} \ \operatorname{erfc}(\eta) \ + \left[\ 1 - 2 \ \eta^{2} \ \right] \ \operatorname{erfc}^{2}(\eta) \\ &- \left[\ 1 - \frac{4}{3\pi} \ \right] \ \operatorname{erfc}(\eta) \ - \frac{4}{\sqrt{\pi}} \left[\ 1 + \frac{2}{3\pi} \ \right] \ \eta \ \operatorname{e}^{-\eta^{2}} \\ &+ \frac{6}{\sqrt{\pi}} \ \eta \ \operatorname{e}^{-\eta^{2}} \ \operatorname{erfc}(\eta) \ + \frac{8}{3\pi} \ \operatorname{e}^{-\eta^{2}} \ - \frac{4}{\pi} \ \operatorname{e}^{-2\eta^{2}} \ \right\} \cos(\theta) \\ &+ 4 \ t \ \left\{ \ (\ \eta^{2} \ - \frac{1}{2} \) \ \operatorname{erfc}^{2}(\eta) \ - \frac{3}{\sqrt{\pi}} \ \eta \ \operatorname{e}^{-\eta^{2}} \ \operatorname{erfc}(\eta) \\ &+ \left[(\ \frac{1}{2} \ - \frac{2}{3\pi} \) \ - \ (\ 3 + \frac{4}{3\pi} \) \ \eta^{2} \ \right] \ \operatorname{erfc}(\eta) \\ &+ \frac{4}{\sqrt{\pi}} \ (\ 1 + \frac{1}{3\pi} \) \ \eta \ \operatorname{e}^{-\eta^{2}} \ - \frac{4}{3\pi} \ \operatorname{e}^{-\eta^{2}} \ + \frac{2}{\pi} \ \operatorname{e}^{-2\eta^{2}} \ \right] \ \sin(\theta) \ \cos(\theta) \ , \end{split}$$

Integrating once more, we find

$$\begin{split} \psi_{2}^{1} &= 2 \sqrt{\alpha t} \int_{0}^{\eta} \psi_{2R}^{1} d\eta \\ &= 2 \gamma \Omega \left[\alpha t^{3} \right]^{1/2} \left\{ \left(1 + \frac{4}{3} \eta^{2} \right) \eta \operatorname{erfc}(\eta) + \frac{1}{6 \sqrt{\pi}} \left(e^{-\eta^{2}} - 1 \right) \right. \\ &\left. - \eta - \frac{4}{3 \sqrt{\pi}} \eta^{2} e^{-\eta^{2}} \right\} + 2 \alpha \Omega t \left\{ \eta^{2} - \frac{1}{4} \left(2 \eta^{2} - 1 \right) \operatorname{erfc}(\eta) \right. \\ &\left. + \frac{1}{2\sqrt{\pi}} \eta e^{-\eta^{2}} - \frac{1}{4} \right\} + 4 \sqrt{\alpha} \gamma t^{\frac{3}{2}} \left\{ \frac{1}{6\sqrt{\pi}} \left(4 \eta^{2} - 5 \right) e^{-\eta^{2}} \right. \end{split}$$

$$-\frac{2}{3}\eta^{3} \operatorname{erfc}(\eta) + \frac{5}{6\sqrt{\pi}}\right) \sin(\theta)$$

$$+ 4\alpha t \left\{ \frac{2}{\sqrt{\pi}}\eta + \frac{3}{4}(2\eta^{2} + \frac{1}{3})\operatorname{erfc}(\eta) \cdot \frac{3}{2\sqrt{\pi}}\eta e^{-\eta^{2}} \cdot \eta^{2} \cdot \frac{1}{4} \right\} \sin(\theta)$$

$$+ 2\sqrt{\alpha} \operatorname{at}^{\frac{3}{2}} \left\{ \frac{2}{3} \left[1 + \frac{4}{3\pi} \right] \eta^{2} \operatorname{erfc}(\eta) \cdot \frac{2}{3\sqrt{\pi}} \left[1 + \frac{4}{3\pi} \right] \eta^{2} e^{-\eta^{2}} \right\}$$

$$+ \frac{1}{3\sqrt{\pi}} \left[7 \cdot \frac{8}{3\pi} \right] e^{-\eta^{2}} + \eta \operatorname{erfc}^{2}(\eta) \cdot \frac{11}{3\sqrt{\pi}} e^{-\eta^{2}} \operatorname{erfc}(\eta)$$

$$+ \frac{16}{3\sqrt{2\pi}} \operatorname{erfc}(\sqrt{2}\eta) \cdot \frac{2}{3}\eta^{3} \operatorname{erfc}^{2}(\eta) + \frac{4}{3\sqrt{\pi}}\eta^{2} e^{-\eta^{2}} \operatorname{erfc}(\eta)$$

$$- \frac{2}{3\pi}\eta e^{-2\eta^{2}} \cdot \left[1 \cdot \frac{4}{3\pi} \right] \eta \operatorname{erfc}(\eta) \cdot \frac{4}{3\sqrt{\pi}} \operatorname{erfc}(\eta)$$

$$+ \frac{8}{3\sqrt{\pi}} \left[1 + \frac{1}{3\pi} \cdot \sqrt{2} \right] \right\} \cos(\theta)$$

$$+ 8\sqrt{\alpha} t^{\frac{3}{2}} \left\{ \frac{11}{6\sqrt{\pi}} e^{-\eta^{2}} \operatorname{erfc}(\eta) \cdot \frac{8}{3\sqrt{2\pi}} \operatorname{erfc}(\sqrt{2}\eta) + \frac{1}{3}\eta^{3} \operatorname{erfc}^{2}(\eta)$$

$$- \frac{2}{3\sqrt{\pi}}\eta^{2} e^{-\eta^{2}} \operatorname{erfc}(\eta) + \frac{1}{3\pi}\eta e^{-2\eta^{2}} \cdot \frac{1}{2}\eta \operatorname{erfc}^{2}(\eta)$$

$$+ \frac{1}{\sqrt{\pi}} \left(\frac{4}{9\pi} - \frac{3}{2} \right) e^{-\eta^{2}} + \frac{1}{\sqrt{\pi}} \left(1 + \frac{4}{9\pi} \right) \eta^{2} e^{-\eta^{2}} \cdot \left(1 + \frac{4}{9\pi} \right) \eta^{3} \operatorname{erfc}(\eta)$$

$$+ \frac{2}{3\sqrt{\pi}} \operatorname{erfc}(\eta) + \left(\frac{1}{2} - \frac{2}{3\pi} \right) \eta \operatorname{erfc}(\eta)$$

$$+ \frac{1}{\sqrt{\pi}} \left(\frac{8}{3\sqrt{2}} - \frac{4}{9\pi} - 1 \right) \right\} \sin(\theta) \cos(\theta) . \tag{3.82}$$

3-4 Composite Solution

Until now we been developing two different solutions, each of which is valid in its separate time domain. Although the solutions are matched in an overlapping region, our goal now is to form a single uniformly-valid composite solution. We construct the composite solution by the method of additive composition^[38], i.e., by adding the inner solution to the outer solution, and then subtracting the common part. The common part is the matched quantity in each of the matching processes. Thus, we have,

Common part =
$$2 \left(\frac{T}{R_{e}}\right)^{1/2} \left(\eta - \frac{1}{\sqrt{\pi}}\right) \left(2 \sin(\theta) - \Omega\right)$$

 $- 2 \gamma \Omega \left[\frac{T^{3}}{R_{e}}\right]^{1/2} \left[\frac{1}{6\sqrt{\pi}} + \eta\right] + \frac{2 \Omega T}{R_{e}} \left[\eta^{2} - \frac{1}{4}\right]$
 $+ \frac{10}{3} \left[\frac{T^{3}}{\pi R_{e}}\right]^{1/2} \gamma \sin(\theta) + \frac{4 T}{R_{e}} \left[\frac{2}{\sqrt{\pi}} \eta - \eta^{2} - \frac{1}{4}\right] \sin(\theta)$
 $+ \frac{16}{3\sqrt{\pi}} \left[1 + \frac{1}{3\pi} - \sqrt{2}\right] \left[\frac{T^{3}}{R_{e}}\right]^{1/2} \Omega \cos(\theta)$
 $+ \frac{8}{\sqrt{\pi}} \left[\frac{8}{3\sqrt{2}} - \frac{4}{9\pi} - 1\right] \left[\frac{T^{3}}{R_{e}}\right]^{1/2} \sin(\theta) \cos(\theta)$, (3.83)

where $T = \epsilon t = U_{\infty} t / a_{\circ}$, and t is the dimensional time. Also,

$$\epsilon (\alpha t)^{1/2} = (T/R_e)^{1/2}$$
.

By using the inverse of transformation (3.8), the composite solution valid to second order is given by

$$\begin{split} \psi &= -\gamma (1 + \gamma T)\theta + \Omega (1 + \gamma T)^2 \ln(r/(1 + \gamma T)) + (r - \frac{1}{r}) \sin(\theta) \\ &- \Omega \ln(r) + \left(\Omega - \frac{2 \sin(\theta)}{r}\right) \left[\gamma T + 2\left[\frac{T}{\pi R_e}\right]^{1/2}\right] - 2\Omega \gamma T \ln(r) \\ &+ 2 \left(\frac{T}{R_e}\right)^{1/2} \left[\frac{1}{\sqrt{\pi}} e^{-\eta^2} - \operatorname{erfc}(\eta)\right] \left[2 \sin(\theta) - \Omega\right] \\ &+ 2 \gamma \Omega \left[\frac{T^3}{R_e}\right]^{1/2} \left\{(1 + \frac{4}{3} \eta^2) \eta \operatorname{erfc}(\eta) + \frac{1}{6\sqrt{\pi}} e^{-\eta^2} - \frac{4}{3\sqrt{\pi}} \eta^2 e^{-\eta^2}\right\} \\ &+ \frac{2 \Omega T}{R_e} \left[\frac{1}{4} (1 - 2 \eta^2) \operatorname{erfc}(\eta) + \frac{1}{2\sqrt{\pi}} \eta e^{-\eta^2}\right] \\ &+ 4 \gamma \left[\frac{T^3}{R_e}\right]^{1/2} \left\{\frac{1}{6\sqrt{\pi}} (4 \eta^2 - 5) e^{-\eta^2} - \frac{2}{3} \eta^3 \operatorname{erfc}(\eta)\right\} \sin(\theta) \\ &+ \frac{4}{4} T \left[\frac{1}{R_e}\right]^{1/2} \left\{\frac{2}{3} \left[1 + \frac{4}{3\pi}\right] \eta^2 \operatorname{erfc}(\eta) - \frac{2}{3\sqrt{\pi}} \left[1 + \frac{4}{3\pi}\right] \eta^2 e^{-\eta^2} + \frac{1}{3\sqrt{\pi}} \left[7 - \frac{8}{3\pi}\right] e^{-\eta^2} + \eta \operatorname{erfc}^2(\eta) - \frac{11}{3\sqrt{\pi}} e^{-\eta^2} \operatorname{erfc}(\eta) \\ &+ \frac{16}{3\sqrt{2\pi}} \operatorname{erfc}(\sqrt{2} \eta) - \frac{2}{3} \eta^3 \operatorname{erfc}^2(\eta) + \frac{4}{3\sqrt{\pi}} \eta^2 e^{-\eta^2} \operatorname{erfc}(\eta) \\ &- \frac{2}{3\pi} \eta e^{-2\eta^2} - \left[1 - \frac{4}{3\pi}\right] \eta \operatorname{erfc}(\eta) - \frac{8}{3\sqrt{2\pi}} \operatorname{erfc}(\eta) + \frac{1}{3} \eta^3 \operatorname{erfc}^2(\eta) \\ &- \frac{2}{3\sqrt{\pi}} \eta^2 e^{-\eta^2} \operatorname{erfc}(\eta) + \frac{1}{3\pi} \eta e^{-2\eta^2} - \frac{1}{2} \eta \operatorname{erfc}^2(\eta) \\ &- \frac{2}{3\sqrt{\pi}} \eta^2 e^{-\eta^2} \operatorname{erfc}(\eta) + \frac{1}{3\pi} \eta e^{-2\eta^2} - \frac{1}{2} \eta \operatorname{erfc}^2(\eta) \end{aligned}$$

$$+\frac{1}{\sqrt{\pi}}\left(\frac{4}{9\pi}-\frac{3}{2}\right)e^{-\eta^{2}}+\frac{1}{\sqrt{\pi}}\left(1+\frac{4}{9\pi}\right)\eta^{2}e^{-\eta^{2}}-\left(1+\frac{4}{9\pi}\right)\eta^{3}\operatorname{erfc}(\eta)$$

$$+\frac{2}{3\sqrt{\pi}}\operatorname{erfc}(\eta)+\left(\frac{1}{2}-\frac{2}{3\pi}\right)\eta\operatorname{erfc}(\eta)\right\}\sin(\theta)\cos(\theta)+{}^{0}(\epsilon^{2}), (3.84)$$

where η is now

$$\eta = \frac{(r-1-\gamma T)}{2} \left[\frac{R_e}{T}\right]^{1/2}$$
 (3.85)

3-5 Vorticity Distribution On The Cylinder

The vorticity is defined by equation (2.5). On the surface, the value of the vorticity is of major interest because it describes the development of the flow field as time advance. It also indicates, in most cases, the shear resistance to the motion, and the point at which separation is likely to occur. In our case, however, this is not true because of the moving boundary. The shear stress is given by

$$\tau_{r\theta} = \frac{1}{R_{\theta}} \left[\frac{\partial v_{\theta}}{\partial r} - \frac{v_{\theta}}{r} + \frac{1}{r} \frac{\partial v_{r}}{\partial \theta} \right] ,$$

which reduces on the cylinder surface to

$$\tau_{r\theta} = \frac{1}{R_e} \left[\frac{\partial v_{\theta}}{\partial r} - \frac{v_{\theta}}{r} \right] , \qquad (3.86)$$

where $\tau_{r\theta} = \overset{\star}{\tau}_{r\theta} / \rho U_{\infty}^2$, $\overset{\star}{\tau}_{r\theta}$ are the nondimensional and the dimensional shear stress in the r- θ plane. On the cylinder surface we have,

$$\omega = \frac{\partial^2 \psi}{\partial r} + \frac{1}{r} \frac{\partial \psi}{\partial r} - \frac{\partial v_{\theta}}{\partial r} + \frac{v_{\theta}}{r} . \tag{3.87}$$

Thus only when the meridian velocity is zero the two expressions for $au_{r heta}$ and ω are proportional.

By making use of (3.87), and substituting from (3.43) and (3.81), and performing the necessary manipulations we obtain

$$\omega \Big|_{\text{surface}} - \left(2 \left[\frac{R_e}{\pi T} \right]^{1/2} + 1 \right) \sin(\theta) + 4 \left(1 + \frac{4}{3\pi} \right) \left[\frac{T R_e}{\pi} \right]^{1/2} \sin(\theta) \cos(\theta)$$

$$+ \left(\frac{1}{2} - \left[\frac{R_e}{\pi T} \right]^{1/2} - \frac{7}{2} \gamma \left[\frac{T R_e}{\pi} \right]^{1/2} - \frac{8}{3\pi} \left[\frac{T R_e}{\pi} \right] \cos(\theta) \right) \Omega$$

$$+ 3\gamma \left[\frac{T R_e}{\pi} \right]^{1/2} \sin(\theta) , \qquad (3.88)$$

and

$$\tau_{r\theta}\Big|_{surface} = \frac{1}{R_e} \left\{ \left(2\left[\frac{R_e}{\pi T}\right]^{1/2} + 1 \right) \sin(\theta) + 4\left(1 + \frac{4}{3\pi}\right) \left[\frac{T R_e}{\pi}\right]^{1/2} \sin(\theta) \cos(\theta) \right\}$$

$$- \left(\frac{3}{2} + \left[\frac{R_e}{\pi T}\right]^{1/2} + \frac{7}{2} \gamma \left[\frac{T R_e}{\pi}\right]^{1/2} + \frac{8}{3\pi} \left[\frac{T R_e}{\pi}\right]^{1/2} \cos(\theta) \right) \Omega$$

$$+ 3\gamma \left[\frac{T R_e}{\pi}\right]^{1/2} \sin(\theta) \right\}. \quad (3.89)$$

It is clear that

$$\tau_{r\theta} \Big|_{surface} = \left(\omega \Big|_{surface} - 2 \Omega \right) / R_e$$

3-6 Pressure Distribution On The Cylinder

The pressure distribution on the cylinder surface is of principal interest. It provides the necessary information on the forces acting on the cylinder, i.e., the lift and the drag forces. The conventional way of expressing the pressure is by means of a dimensionless pressure coefficient, which is defined as

$$C_{p} = \frac{p - p_{o}}{\rho U_{m}^{2}}$$

Here, p. is a reference pressure, usually the pressure at a predefined location. For convenience, we take the value p. at the forward stagnation point, i.e., at $\theta = \eta = 0$.

The equation of motion (in cylindrical polar coordinates) in the meridian direction, for an incompressible fluid with constant properties, is given by

$$\frac{\partial \mathbf{v}_{\theta}}{\partial \mathbf{r}} + \mathbf{v}_{\mathbf{r}} \frac{\partial \mathbf{v}_{\theta}}{\partial \mathbf{r}} + \frac{\mathbf{v}_{\theta}}{\mathbf{r}} \frac{\partial \mathbf{v}_{\theta}}{\partial \theta} + \frac{\mathbf{v}_{\mathbf{r}} \mathbf{v}_{\theta}}{\mathbf{r}} - \frac{1}{\rho} \frac{\partial \mathbf{p}}{\partial \theta} + \nu \left[\nabla^{2} \mathbf{v}_{\theta} + \frac{2}{\mathbf{r}^{2}} \frac{\partial \mathbf{v}_{\mathbf{r}}}{\partial \theta} - \frac{\mathbf{v}_{\theta}}{\mathbf{r}^{2}} \right]$$

Nondimensionalizing, as before (chapter II), together with

$$p = \frac{p}{\rho U_{\infty}^2}$$

one obtain after dropping the bars

$$\frac{\partial \mathbf{v}_{\theta}}{\partial \mathbf{T}} + \mathbf{v}_{\mathbf{r}} \frac{\partial \mathbf{v}_{\theta}}{\partial \mathbf{r}} + \frac{\mathbf{v}_{\theta}}{\mathbf{r}} \frac{\partial \mathbf{v}_{\theta}}{\partial \theta} + \frac{\mathbf{v}_{\mathbf{r}} \mathbf{v}_{\theta}}{\mathbf{r}} =$$

$$-\frac{1}{r}\frac{\partial p}{\partial \theta} + \frac{1}{R}\left[\nabla^2 v_{\theta} + \frac{2}{r^2}\frac{\partial v_{r}}{\partial \theta} - \frac{v_{\theta}}{r^2}\right] \quad (3.90)$$

By integrating this equation on the cylinder surface from $\theta = 0$ to $\theta = \theta$, the needed pressure coefficient is obtained, viz.,

$$C_{p} = (1 + \gamma T) \int_{0}^{\theta} \left[-2\gamma \Omega + \frac{1}{R_{p}} \frac{\partial \omega}{\partial r} \right] d\theta . \qquad (3.91)$$

substituting and after some work

$$C_{p} = \left(2\gamma \left(1+\gamma T\right) + \gamma \left[\frac{T R_{e}}{\pi}\right]^{\frac{1}{2}} + \frac{2}{\sqrt{\pi T R_{e}}} - \frac{1}{R_{e}}\right] \left(\cos(\theta) - 1\right)$$

$$+ \left(1 + \gamma T - \left[1 + \frac{4}{3\pi}\right] \left[\frac{T R_{e}}{\pi}\right]^{1/2}\right) \left(\cos(2\theta) - 1\right)$$

$$+ \left(\frac{1}{2R_{e}} - \frac{5}{2} \left[\frac{T R_{e}}{\pi}\right]^{1/2}\right) \Omega \theta$$

$$- \frac{8}{3\pi} \left[\frac{T R_{e}}{\pi}\right]^{1/2} \Omega \sin(\theta) . \qquad (3.92)$$

3-7 Drag, Lift and Moment

The drag on the cylinder has two parts, the form (or pressure drag) and the skin-friction drag. However, because of the moving boundary, the form drag is no longer arises from pressure effects alone. However we still refer to it here as pressure drag, since the contribution of the moving boundary drops out of the equations. Thus:

$$C_{D_{p}} = \frac{D_{p}}{\rho U_{\infty}^{2} a_{o}}$$

$$= (1+\gamma t) \int_{0}^{2\pi} -\sigma_{rr} \cos(\theta) d\theta ,$$

where σ_{rr} is the normal stress, whereby

$$C_{D_{p}} = (1+\gamma t) \int_{0}^{2\pi} - \left[-p + \frac{2}{R_{e}} \frac{\partial v_{r}}{\partial r} \right] \cos(\theta) d\theta$$
$$= (1+\gamma t) \int_{0}^{2\pi} C_{p} \cos(\theta) d\theta$$

where C_p is the pressure coefficient, given by (3.92). The above definition gives positive C_{D_p} in the flow direction. Integrating, we obtain

$$C_{D_{p}} = -\frac{(1+\gamma T)^{2}}{R_{e}} \int_{0}^{2\pi} \frac{\partial \omega}{\partial r} \Big|_{r=1+\gamma T} \sin(\theta) d\theta . \qquad (3.93a)$$

Substituting for ω and integrating we obtain,

$$C_{D_p} = \pi (1 + \gamma T) \left\{ -2\gamma (1+\gamma T) + \frac{2}{\sqrt{\pi T R}} + \gamma \left[\frac{T}{\pi R_e} \right]^{1/2} - \frac{1}{R_e} \right\}. (3.93b)$$

The frictional contribution to the drag coefficient is definied as

$$C_{D_{f}} = \frac{D_{f}}{\rho U_{\infty}^{2} a_{o}}$$

$$= \frac{(1+\gamma t)}{R_{e}} \int_{0}^{2\pi} \left[\frac{\partial v_{\theta}}{\partial r} - \frac{v_{\theta}}{r} + \frac{\partial v_{r}}{\partial \theta} \right] \sin(\theta) d\theta$$

$$= \frac{(1+\gamma t)}{R_{e}} \int_{0}^{2\pi} \omega \sin(\theta) d\theta , \qquad (3.94a)$$

where we again define $^{\rm C}_{\rm D}$ such that it will be positive in the flow direction. Substituting and integrating, we find

$$C_{D_{f}} = \frac{\pi (1 + \gamma T)}{R_{e}} \left\{ 2 \left[\frac{R_{e}}{\pi T} \right]^{1/2} + 1 + 3 \gamma \left[\frac{T R_{e}}{\pi} \right]^{1/2} \right\}. \quad (3.94b)$$

The total drag coefficient is the sum of (3.94b) and (3.93b), viz., $^{C}_{D} = ^{C}_{D_{D}} + ^{C}_{D_{f}}$

$$= \pi \left(1 + \gamma T \right) \left\{ -2\gamma (1+\gamma T) + \frac{2}{\sqrt{\pi T R_e}} + \gamma \left[\frac{T}{\pi R_e} \right]^{1/2} - \frac{1}{R_e} \right\}$$

$$+ \frac{\pi \left(1 + \gamma T \right)}{R_o} \left\{ 2 \left[\frac{R_e}{\pi T} \right]^{1/2} + 1 + 3 \gamma \left[\frac{T R_e}{\pi} \right]^{1/2} \right\}.$$
 (3.95)

Similarly, the pressure lift is

$$C_{L_p} = (1 + \gamma t) \int_0^{2\pi} C_p \sin(\theta) d\theta$$
, (3.96a)

and the skin-friction lift is

$$C_{L_{f}} = \frac{(1 + \gamma t)}{R_{e}} \int_{0}^{2\pi} \omega \cos(\theta) d\theta.$$

The lift force is positive in the direction normal to flow. By substituting and integrating, we obtain

$$C_{L_{\mathbf{p}}} = -2 \pi \Omega \left(1 + \gamma t\right) \left\{ \frac{1}{2 R_{\mathbf{e}}} + \left[\frac{4}{3 \pi} - \frac{5 \gamma}{2} \right] \left[\frac{T}{\pi R_{\mathbf{e}}} \right]^{1/2} \right\}, \tag{3.96b}$$

$$C_{L_f} = \frac{(1+\gamma t)}{R_o} \int_0^{2\pi} (-\tau_{r\theta}) \cos(\theta) d\theta \qquad (3.97a)$$

$$-\frac{8}{3}\left(1+\gamma T\right)\left[\frac{T}{\pi R_{e}}\right]^{1/2}\Omega , \qquad (3.97b)$$

where, $\mathbf{C}_{\mathbf{L}}$ is defined to be positive downward. The total lift is therefore

$$C_{L} = C_{L_{p}} + C_{L_{f}}$$

$$= -2 \pi \Omega (1 + \gamma t) \left\{ \frac{1}{2 R_{e}} + \left[\frac{4}{3 \pi} - \frac{5 \gamma}{2} \right] \left[\frac{T}{\pi R_{e}} \right]^{1/2} \right\}$$

$$+ \frac{8}{3} (1 + \gamma T) \left[\frac{T}{\pi R_{e}} \right]^{1/2} \Omega . \qquad (3.98)$$

In order to maintain rotation of the cylinder, torque must be applied to overcome the dissipation of energy by viscous effects. This torque is defined through the torque coefficient as

$$C_{T} = \frac{T}{\rho U_{\infty}}^{2} a^{2}$$

$$= \frac{(1+\gamma t)^{2}}{R_{e}} \int_{0}^{2\pi} \left[\frac{\partial v_{\theta}}{\partial r} - \frac{v_{\theta}}{r} \right]_{r=(1+\gamma t)} d\theta$$

$$= \frac{(1+\gamma t)^{2}}{R_{e}} \int_{0}^{2\pi} \left[\omega - 2\Omega \right]_{r=(1+\gamma t)} d\theta \qquad (3.99a)$$

$$= -\frac{2\pi}{R_{e}} \frac{(1+\gamma T)^{2}}{R_{e}} \left\{ \frac{1}{2} + \left[\frac{R_{e}}{\pi} T \right]^{1/2} + \frac{7}{2} \gamma \left[\frac{T R_{e}}{\pi} \right]^{1/2} \right\} \Omega \qquad (3.99b)$$

3-8 Results

The results presented in the following pages are for the following parameter values;

$$R_d = 2 R_e = 100 \text{ and } 500,$$

 $\Omega = 0.0 \text{ and } 1.0 ,$
 $\gamma = 0.05 \text{ and } 0.1$

These parameter values are chosen as representative for the problem under investigation, to explore the various physical effects. Note that although the solution is valid only for small T, the graphs were plotted for values of T up to 1.0, in order to show the behavior for large times.

3-8-1 Stream Lines

The composite solution given by equation (3.84) is used to plot the stream lines, using a specially coded subroutine written by the author for this specific purpose. No smoothing of any kind is carried out; only linear interpolation was used. We plotted equally-incremented instantaneous stream lines (a total 25) in the region enclosed by a circular domain which is triple the cylinder radius. However, since we have a moving boundary (in the radial and tangential direction), the separation region is small in size; the plotting routine could not detect this effects for small times. For this reason we include a detailed sample plot of the stream lines for early times (see figures III-1 and III-18).

3-8-2 Pressure Coefficient

The pressure coefficient, given by equation (3.92) indicate the singular behavior of the flow. We note from the plotted figures that as the Reynolds number increases the pressure coefficient decreases, after the short adjustment period for the impulsive start. This occurs until T=1.0. The effect of increasing γ is to reduce the average pressure coefficient (although it might increase the value of the pressure).

It appears that higher-order solution should be derived, since the present second-order solution does not fully indicate the rotation effect, as expected. The results obtained do not show any reasonable

asymmetry of the pressure coefficient; furthermore equation (3.92) still has some nonperiodic terms (although of smaller order). Those short-comings are expected to be rectified with higher approximations.

3-8-3 Drag

In the first stage of motion, the cylinder displaces the fluid on the surface with infinite acceleration. The cylinder thus experiences infinite resistance of the fluid because of its impulsive motion. There is also a discontinuity in the tangential velocity at the cylinder This discontinuity gives rise to infinite friction drag as indicated by the graphs (figures III-3, 7, 11, 15, 20, 26, 32, 38). Thus, the general features are the singular behavior of the drag coefficients at $t = 0^+$, the sharp drop in the beginning and the gradual drop for larger T. The effect of increasing the Reynolds number is to increase the ratio $\left[\begin{array}{c} \mathbf{C_{D_{p}}} \neq \mathbf{C_{D_{f}}} \end{array}\right]$, which means a greater contribution from the pressure drag. The effect of increasing γ is to increase the drag. This is expected, since high γ will tend to push the fluid away from the surface more rapidly, causing more resistance. Although rotation tends to decrease the drag in most cases, this decrease is more than offset by the effect of the expanding surface, which increases the drag.

3-8-4 Lift

The lift starts from a value of zero, since the pressure and the friction are initially uniform. The main contribution to the lift is initially from the pressure. Then friction lift eventually becomes dominant. Increasing the Reynolds number shows two effects. First, it reduces the total lift, and second, it shortens the period for which the

friction lift is dominant. The lift coefficients are presented in figures III-21, 27, 33 and 39.

3-8-5 **Moment**

The moment coefficient also reflects the initial singularity of impulsive rotation. It rapidly decreases until it become nearly constant. As expected, the moment increases with increasing R_d , γ and Ω . The moment coefficient is presented in figures III-22, 28, 34 and 40.

3-8-6 Surface Vorticity

A vortex sheet, represented by the singular terms in equation (3.88), forms on the cylinder surface at $t=0^+$. The vorticity subsequently diffuses out into the fluid. The non-linearity of the solution is indicated in the surface vorticity plots (figures III-4, 8, 12, 16, 23, 29, 35 and 41). The larger the Reynolds number, the larger the initial surface vorticity, which produces a larger diffusion rate. As time advances the maximum surface vorticity decreases. The effect of γ (with the values used here) on the surface vorticity is not clear in the figures. However from equation (3.88) we can see that it increases the surface vorticity. The value of the surface vorticity is affected by rotation in a different way; it appears that the surface vorticity is decreased early by the (dominant) singular Ω term, which leads to the very early separation.

3-8-7 Separation Progression

As described before, we predict separation by identifying the points on the cylinder surface at which the shear stress vanish. The vorticity graphs are helpful in following the progression of the separation points, keeping in mind the difference in magnitude (-2 Ω) between the two values, vorticity and shear stress.

In general two recirculating zones appear at $T \simeq 0.4$ for the non-rotating cases. These zones gradually become larger. With rotation, the situation is different; one recirculating region starts at once, and another region appears later. The first region shrinks gradually, while the second enlarges.

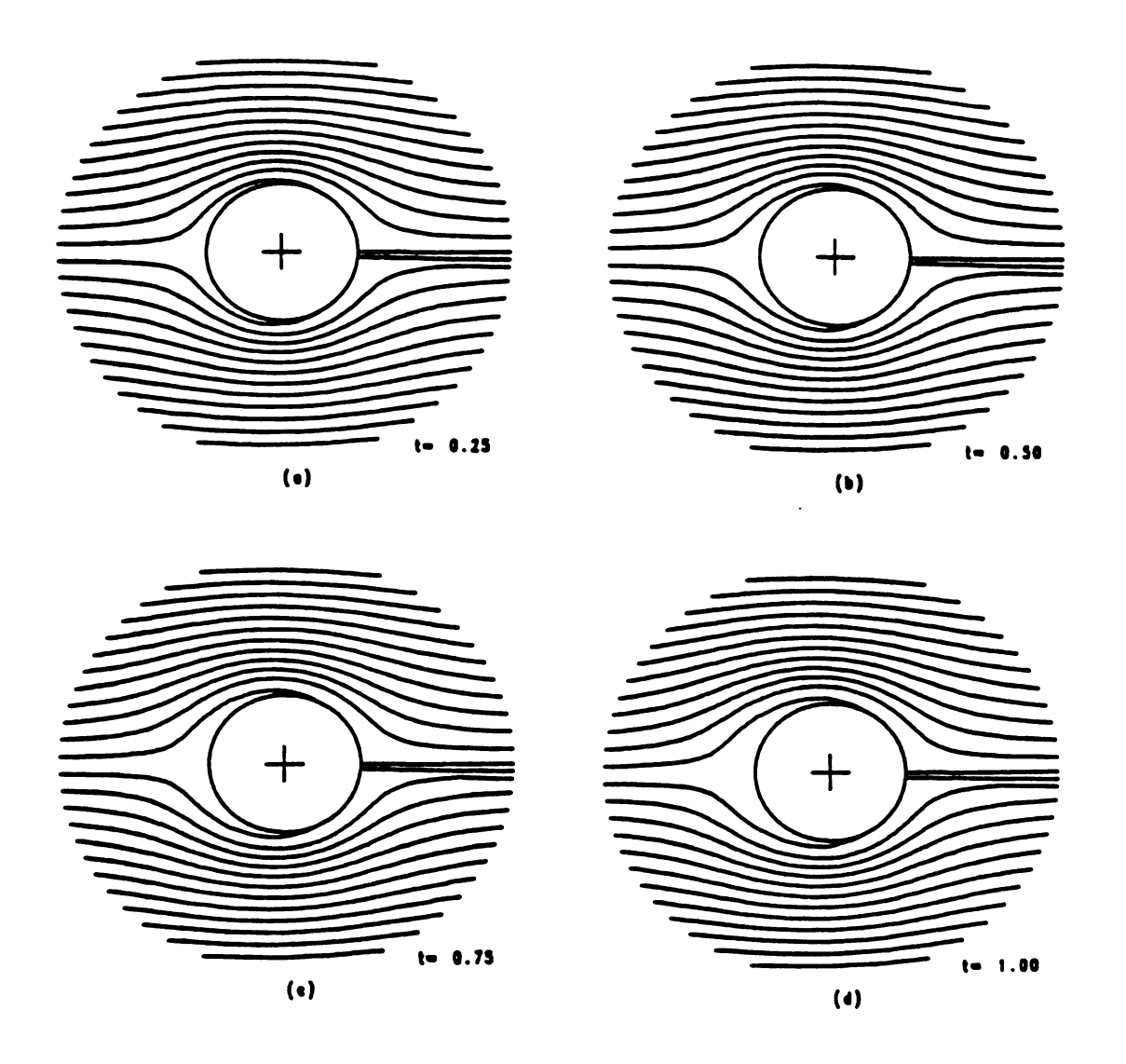


Figure III-1 Typical flow Development with γ = 0.05 , Ω = 0.0 and R_d = 100 ,at T equal (a) 0.25 ,(b) 0.50 ,(c) 0.75 and (d) 1.0.

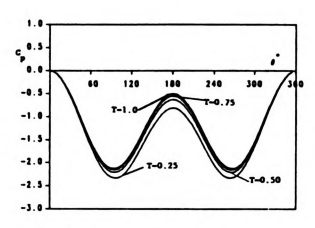


Figure III-2 Development of Pressure Coefficient C_p , for Flow With $\gamma = 0.05$, $\Omega = 0.0$ and $R_d = 100$.

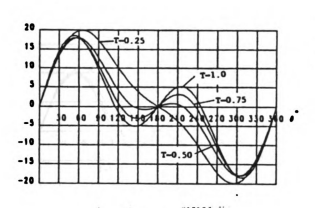


Figure III-4 Development of Surface Vorticity ω for Flow With γ = 0.05 , Ω = 0.0 and R_d = 100.

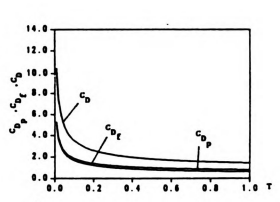


Figure III-3 Development of the Drag Coefficients C_{D_p} , C_{D_f} , C_{D} for Flow With $\gamma=0.05$, $\Omega=0.0$ and $R_d=100$.

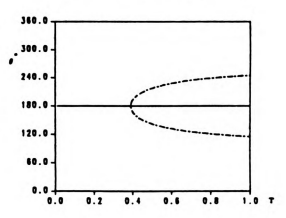


Figure III-5 Separation Points History For Flow With $\gamma = 0.05 \ , \ \Omega = 0.0 \ \text{and} \ R_d = 100.$

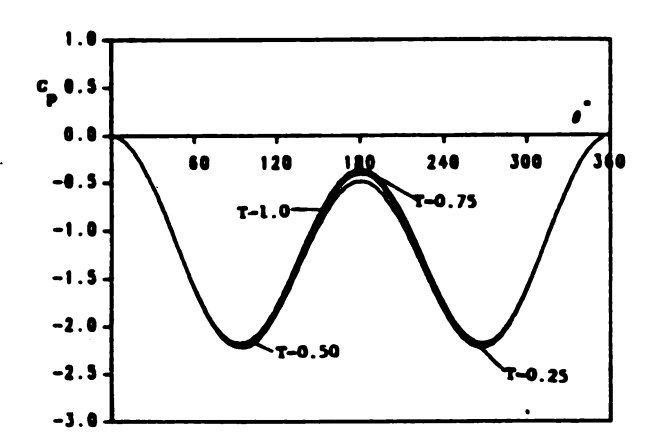


Figure III-6 Development of Pressure Coefficient C_p , for Flow With $\gamma=0.05$, $\Omega=0.0$ and $R_d=500$.

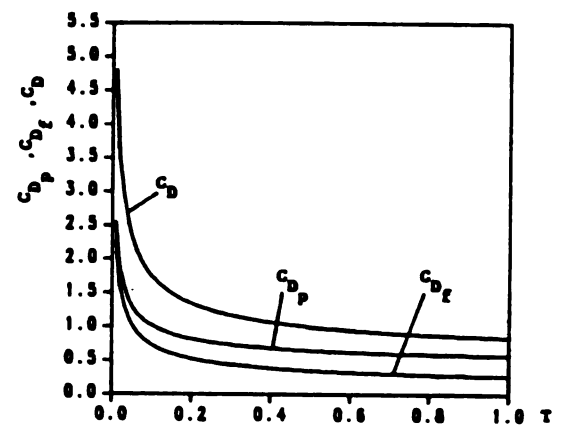


Figure III-7 Development of the Drag Coefficients C_{D_p} , C_{D_g} , C_{D} for Flow With $\gamma=0.05$, $\Omega=0.0$ and $R_d=500$.

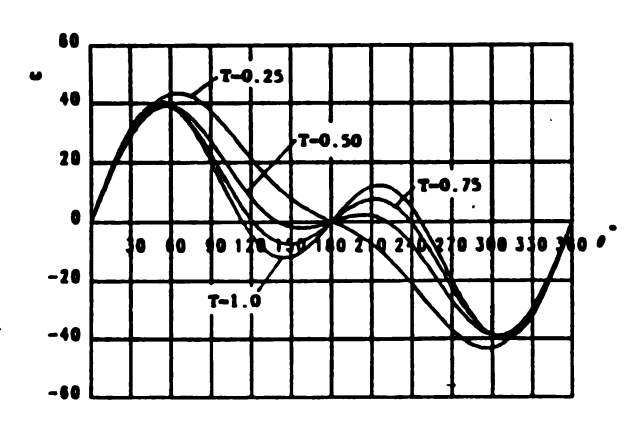


Figure III-8 Development of Surface Vorticity ω for Flow With $\gamma=0.05$, $\Omega=0.0$ and $R_{\rm d}=500$.

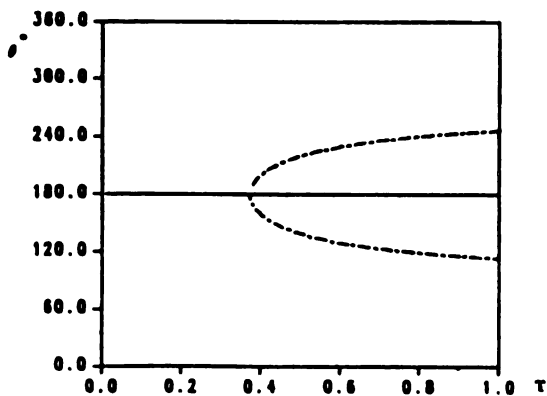


Figure III-9 Separation Points History For Flow With $\gamma = 0.05$, $\Omega = 0.0$ and $R_{d} = 500$.

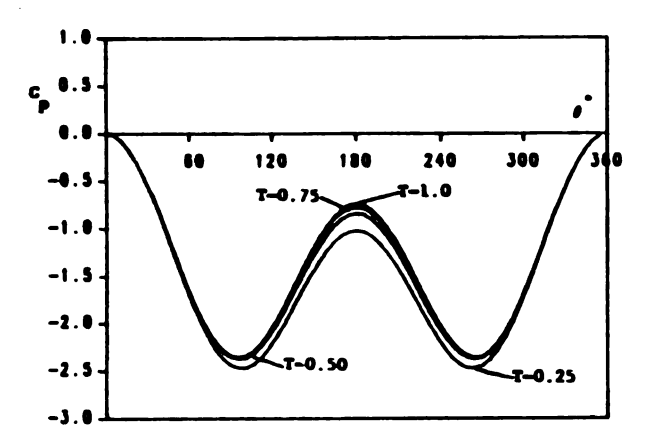


Figure III-10 Development of Pressure Coefficient C_p , for Flow With $\gamma = 0.10$, $\Omega = 0.0$ and $R_d = 100$.

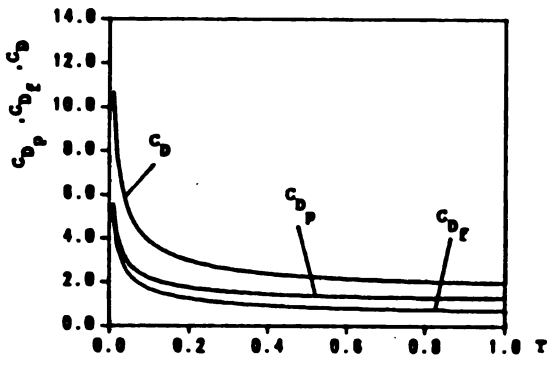


Figure III-11 Development of the Drag Coefficients C_{D_p} , C_{D_f} , C_{D} for Flow With $\gamma = 0.10$, $\Omega = 0.0$ and $R_d = 100$.

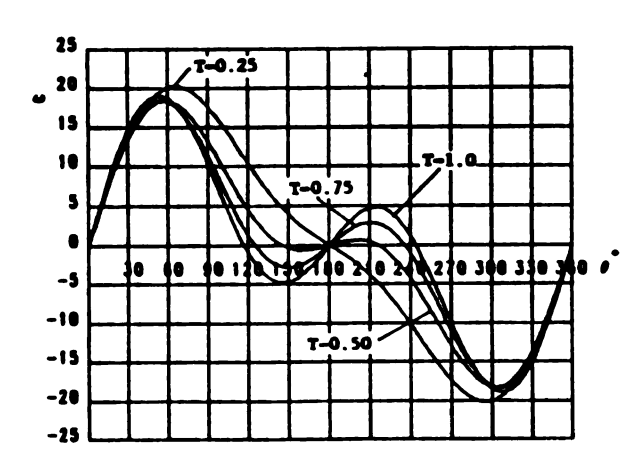


Figure III-12 Development of Surface Vorticity ω for Flow With $\gamma=0.10$, $\Omega=0.0$ and $R_{\rm d}=100$.

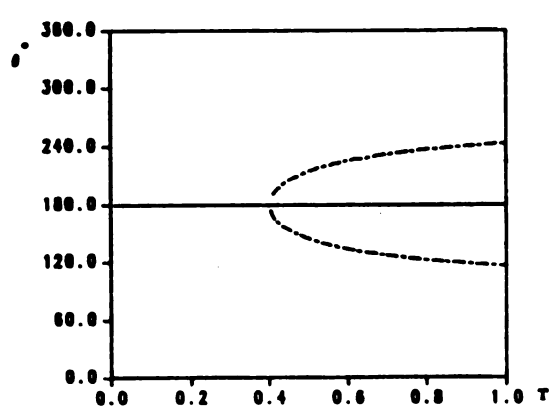


Figure III-13 Separation Points History For Flow With γ = 0.10 , Ω = 0.0 and R_d = 100.

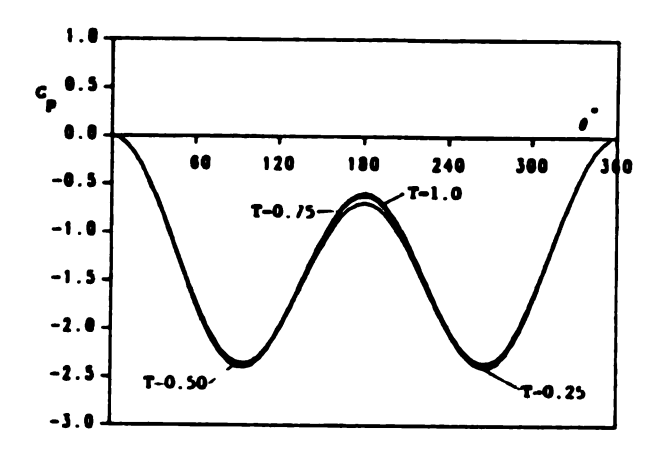


Figure III-14 Development of Pressure Coefficient C_p , for Flow With $\gamma=0.10$, $\Omega=0.0$ and $R_d=500$.

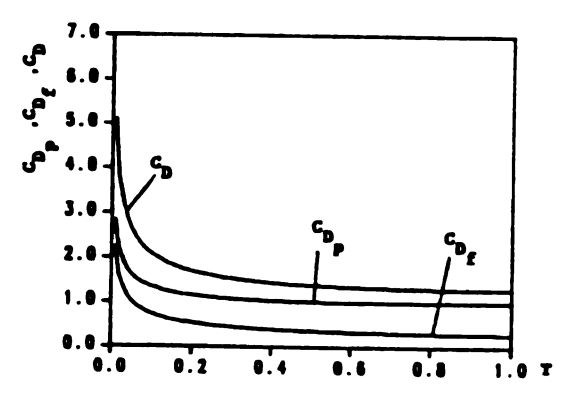


Figure III-15 Development of the Drag Coefficients C_{D_p} , C_{D_g} , C_D for Flow With $\gamma = 0.10$, $\Omega = 0.0$ and $R_d = 500$.

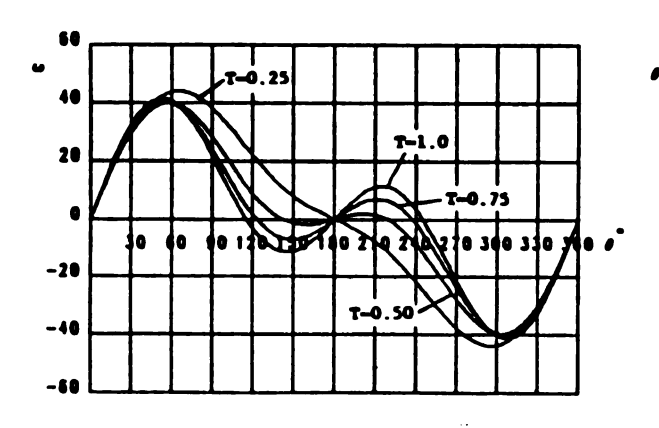


Figure III-16 Development of Surface Vorticity ω for Flow With $\gamma = 0.10$, $\Omega = 0.0$ and $R_{\rm d} = 500$.

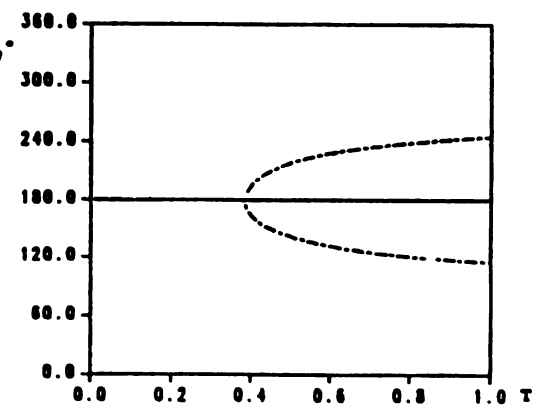


Figure III-17 Separation Points History For Flow With γ = 0.10 , Ω = 0.0 and R_d = 500.

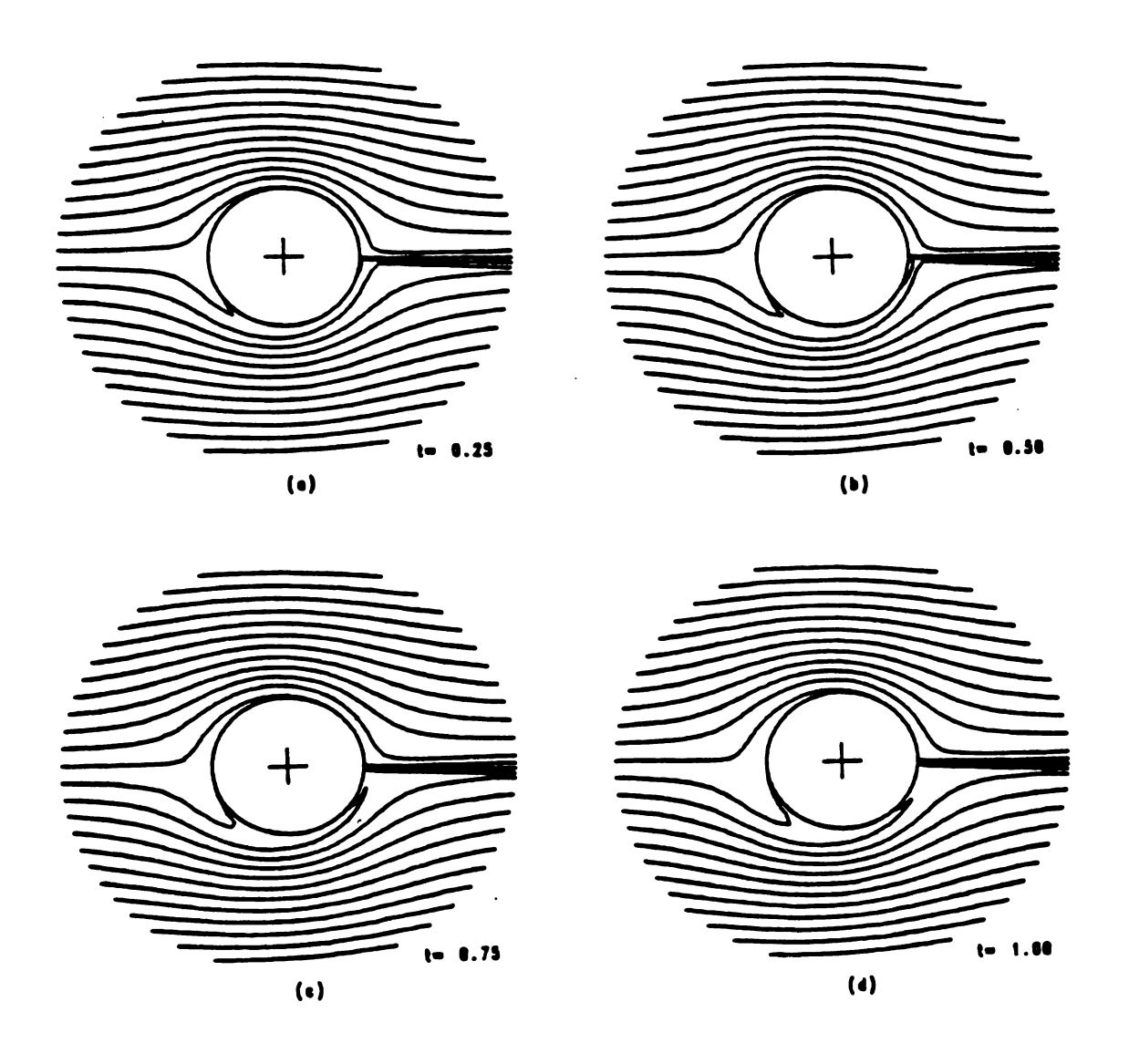


Figure III-18 Typical flow Development with γ = 0.05 , Ω = 1.0 and R_d = 100 ,at T equal (a) 0.25 ,(b) 0.50 ,(c) 0.75 and (d) 1.0.

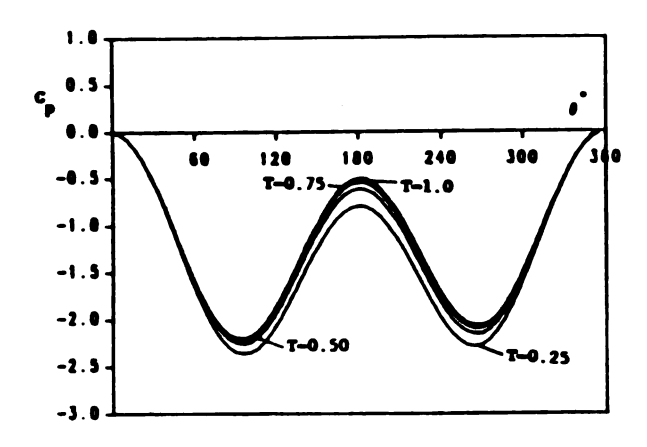


Figure III-19 Development of Pressure Coefficient C_p , for Flow With $\gamma=0.05$, $\Omega=1.0$ and $R_d=100$.

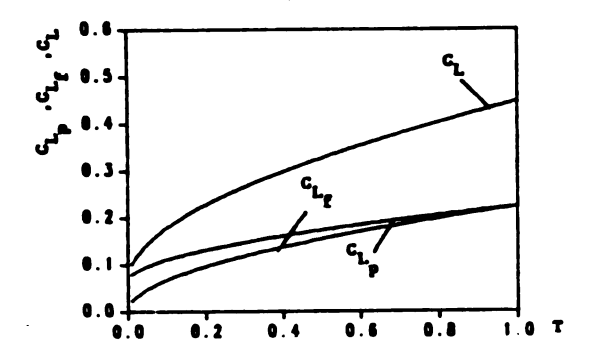


Figure III-21 Development of the lift Coefficients C_{L_p} , C_{L_f} , C_{L} for Flow With $\gamma = 0.05$, $\Omega = 1.0$ and $R_d = 100$.

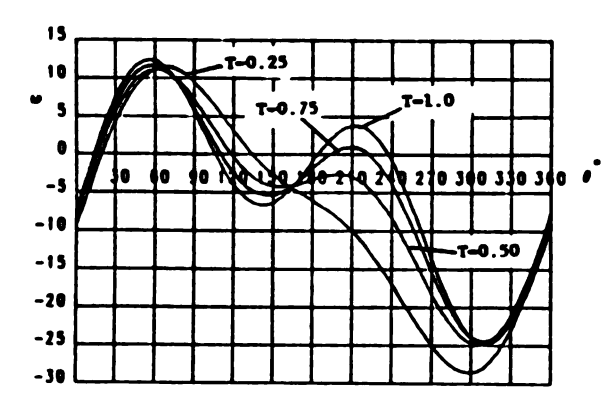


Figure III-23 Development of Surface Vorticity ω for Flow With $\gamma=0.05$, $\Omega=1.0$ and $R_{\rm d}=100$.

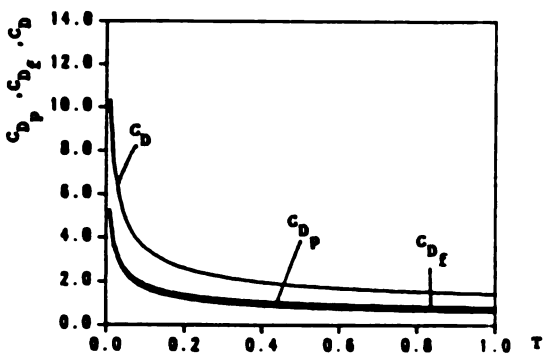


Figure III-20 Development of the Drag Coefficients C_{D_p} , C_{D_f} , C_{D} for Flow With $\gamma = 0.05$, $\Omega = 1.0$ and $R_d = 100$.

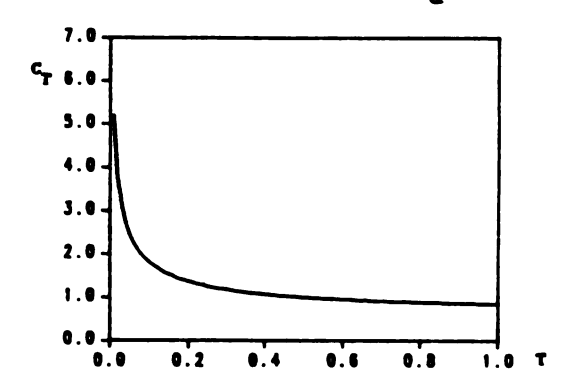


Figure III-22 Development of the Moment Goefficient C_T for Flow With $\gamma=0.05$, $\Omega=1.0$ and $R_A=100$.

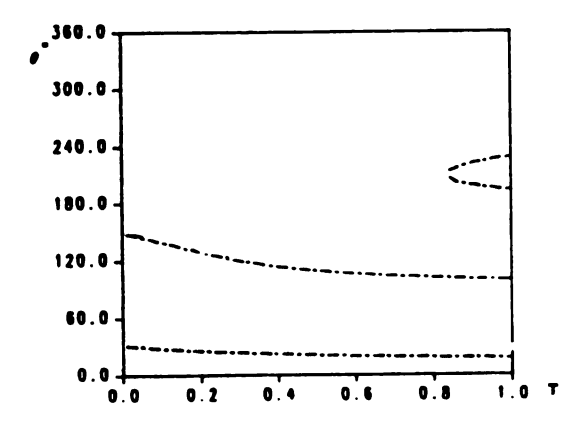


Figure III-24 Separation Points History For Flow With $\gamma=0.05$, $\Omega=1.0$ and $R_{\rm d}=100$.

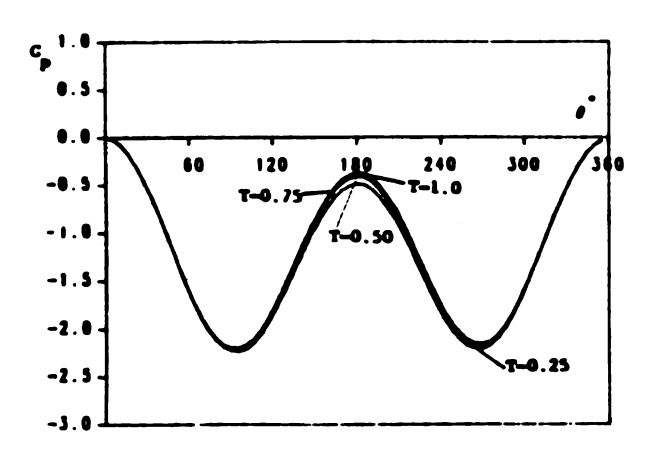


Figure III-25 Development of Pressure Goefficient C_p , for Flow With $\gamma=0.05$, $\Omega=1.0$ and $R_d=500$.

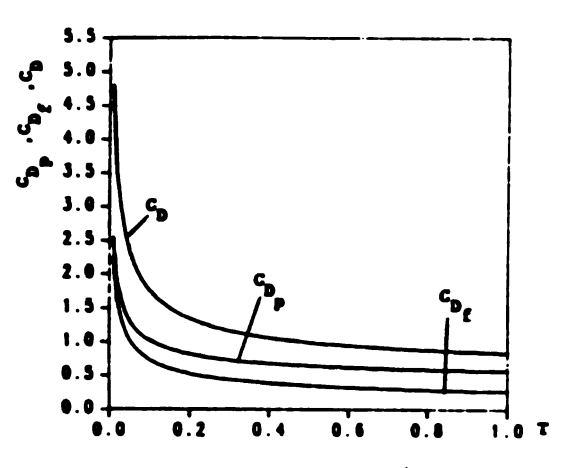


Figure III-26 Development of the Drag Coefficients C_{D_p} , C_{D_f} , C_D for Flow With $\gamma=0.05$, $\Omega=1.0$ and $R_d=500$.

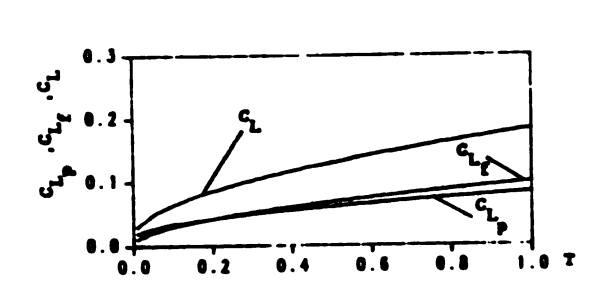


Figure III-27 Development of the lift Coefficients C_{L_p} , C_{L_f} , C_L for Flow With $\gamma = 0.05$, $\Omega = 1.0$ and $R_d = 500$.

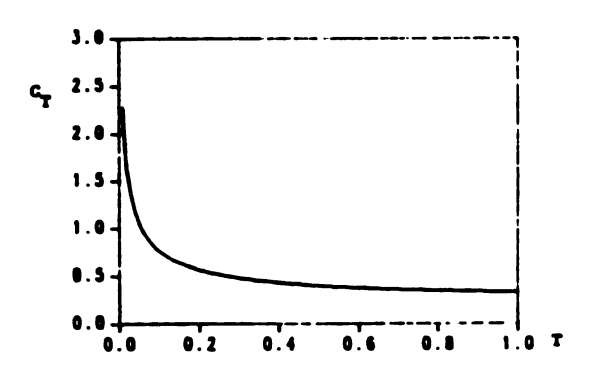


Figure III-28 Development of the Homent Coefficient C_T for Flow With $\gamma=0.05$, $\Omega=1.0$ and $R_d=500$.

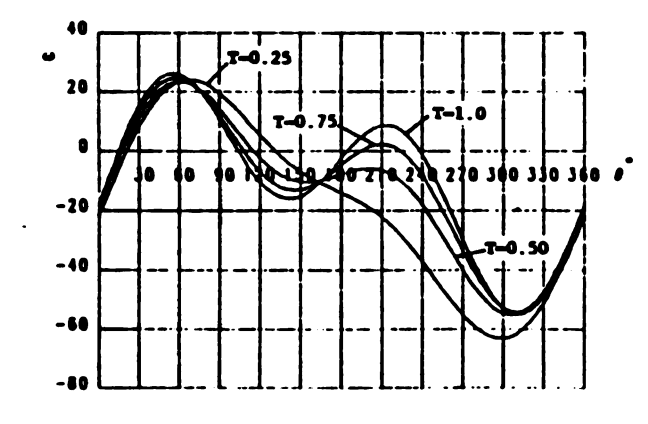


Figure III-29 Development of Surface Vorticity ω for Flow With $\gamma=0.05$, $\Omega=1.0$ and $R_{\rm d}=500$.

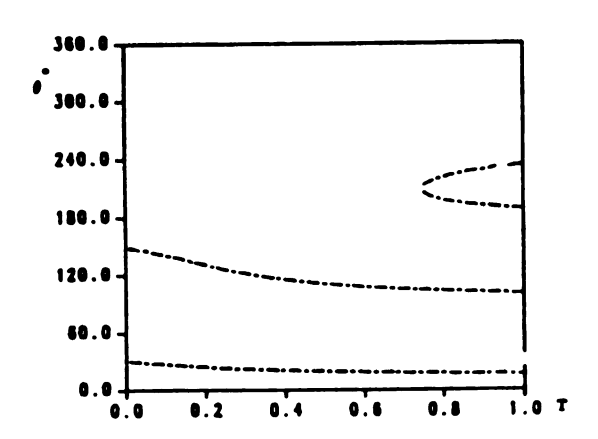


Figure III-30 Separation Points
History For Flow With $\gamma = 0.05$, $\Omega = 1.0$ and $R_d = 500$.

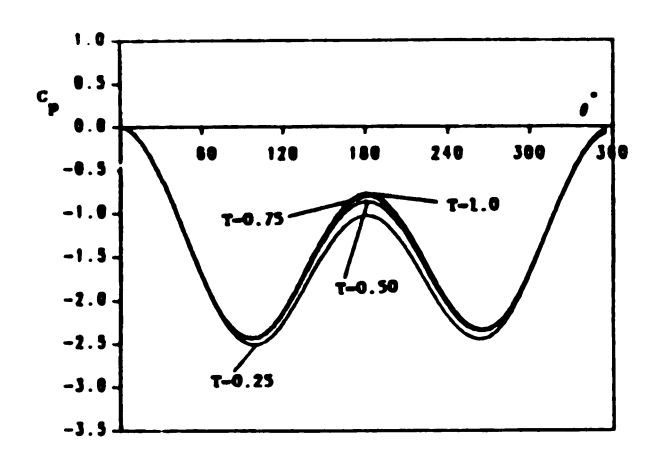


Figure III-31 Development of Pressure Coefficient C_p , for Flow With $\gamma = 0.10$, $\Omega = 1.0$ and $R_d = 100$.

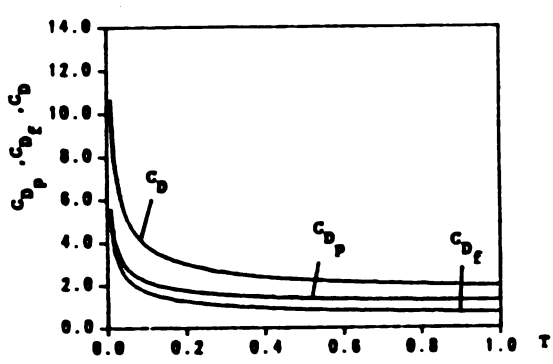


Figure III-32 Development of the Drag Coefficients $C_{\mathrm{D}_{\mathrm{p}}}$, $C_{\mathrm{D}_{\mathrm{f}}}$, C_{D} for Flow With $\gamma = 0.10$, $\Omega = 1.0$ and $R_{\mathrm{d}} = 100$.

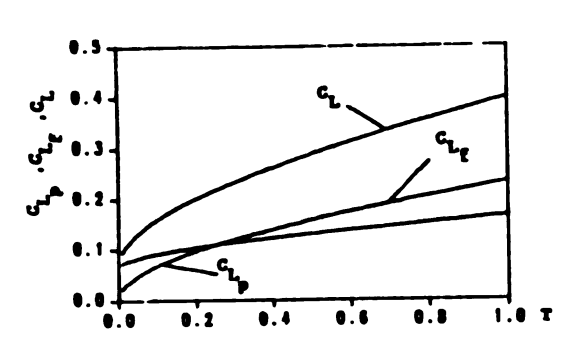


Figure III-33 Development of the lift Coefficients C_{L_p} , C_{L_f} , C_{L} for Flow With $\gamma=0.10$, $\Omega=1.0$ and $R_{d}=100$.

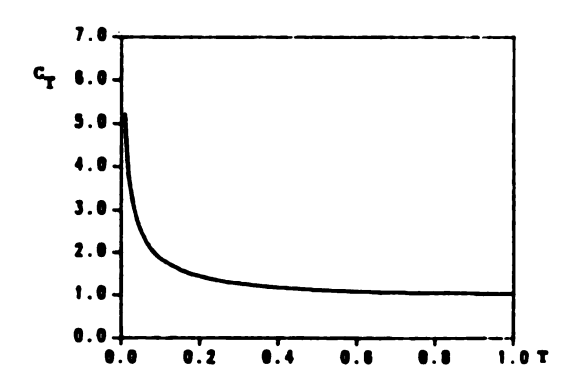


Figure III-34 Development of the Moment Coefficient C_T for Flow With $\gamma = 0.10 \ , \ \Omega = 1.0 \ \text{and} \ R_d = 100 \, .$

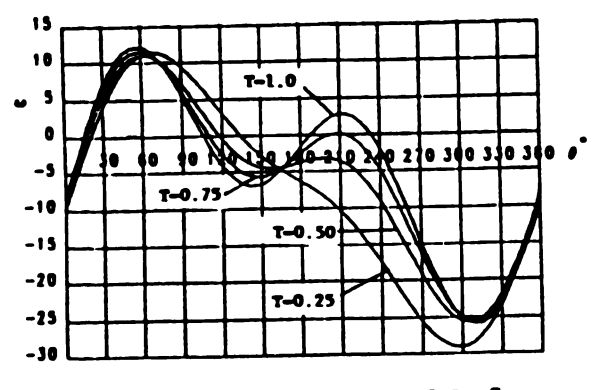


Figure III-35 Development of Surface Vorticity ω for Flow With $\gamma=0.10$, $\Omega=1.0$ and $R_{\rm d}=100$.

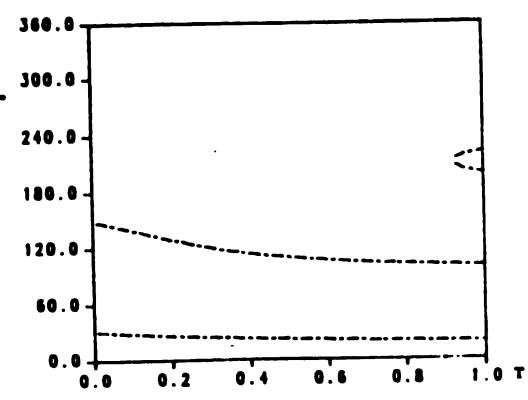
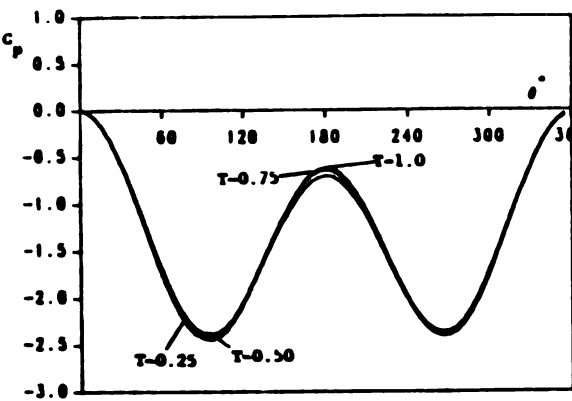
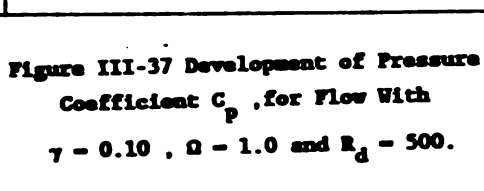


Figure III-36 Separation Points
History For Flow With $\gamma = 0.10$, $\Omega = 1.0$ and $R_d = 100$.



Coefficient C_p , for Flow With



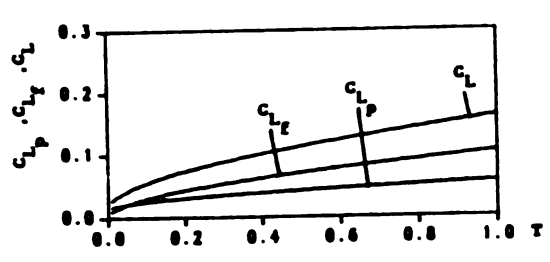


Figure III-39 Development of the lift Coefficients C_{L_p} , C_{L_f} , C_L for Flow With $\gamma = 0.10$, $\Omega = 1.0$ and $R_d = 500$.

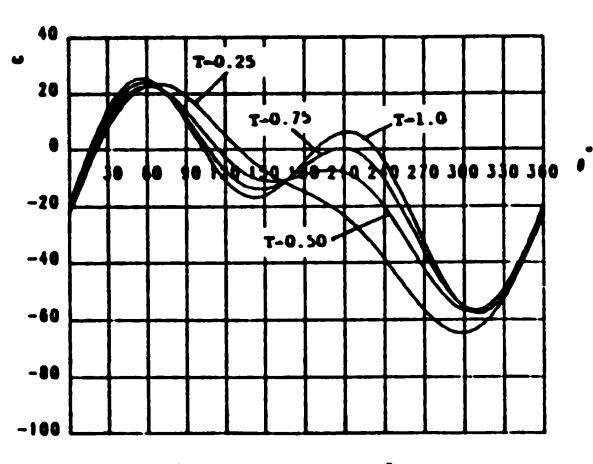


Figure III-41 Development of Surface Vorticity w for Flow With γ = 0.10 , Ω = 1.0 and $R_{\rm d}$ = 500.

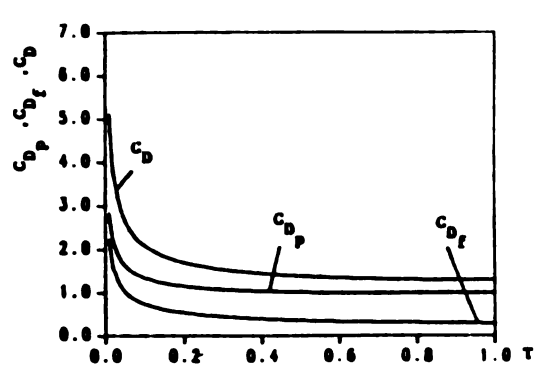
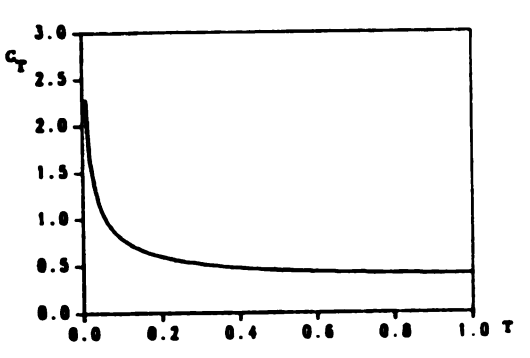


Figure III-38 Development of the Drag Coefficients C_{D_p} , C_{D_f} , C_D for Flow With γ = 0.10 , Ω = 1.0 and R_d = 500.



w Figure III-40 Development of the Homent Coefficient C_T for Flow With $\gamma = 0.10$, $\Omega = 1.0$ and $R_d = 500$.

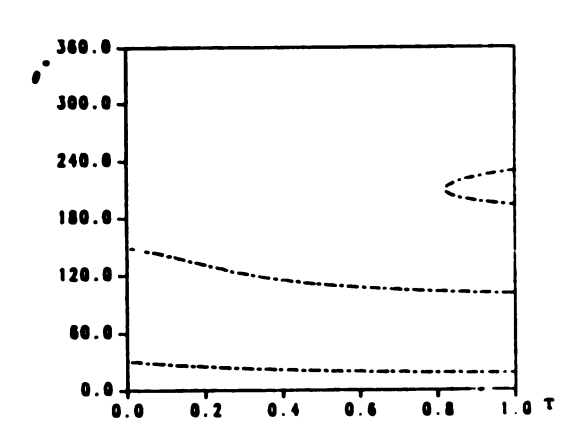


Figure III-42 Separation Points History For Flow With γ = 0.10 , Ω = 1.0 and R_d = 500.

CHAPTER IV

NUMERICAL SOLUTION

The analytical solution obtained in chapter III by the method of matched asympototic expansions to the second order is valid only for small t. For large t we integrate the Navier-Stokes equations numerically.

The choice of a suitable numerical scheme is dependent on the nature of the problem to be solved, together with the required accuracy, the time available on the computer, and the type of computer available. It seems that most frequently-used schemes are first-order accurate in time and second-order accurate in space. This is mainly because of the complexity of higher-order schemes, and the extra time and memory required in most cases. In fluid mechanics, there are two basic methods, namely, the method of primitive variables, and the vorticity-stream function method.

We preferred to use the latter method because there are fewer dependent variables, requiring less memory; also, the speed of computation is faster than for the first method. Although there are many algorithms for the second method, we select the explicit forward-in-time, centered-space for the vorticity equation and the Fast Fourier Transform (FFT) for the Poisson equation. Although it has previously been reported that [42] this scheme often fails, even with a factor of safety, it did worked very well for the present problem, because we took advantage of the expanding boundary to obtain a much less restrictive stability criteria.

4-1 Grid Structure

Due to the curved boundary on the surface of the cylinder, rectangular grids are unsuitable for computation. The most common coordinate system used in the study of flow over a circular cylinder is the modified polar coordinate system. It transform the circular arc into a flat boundary by

$$\xi = \frac{1}{\pi} \ln(r/r_{\circ}(t)) \qquad \text{or} \qquad r = r_{\circ}(t) \exp(\pi \xi) ,$$

$$\theta = \pi \zeta . \qquad (4.1)$$

Here we have generalized r_0 (the cylinder radius) to be a function of t. Thus, for constant $\Delta \xi$, meshes are finer near the surface of the cylinder and coarser far from the cylinder.

As usual, the infinite outer boundary is simulated by a circle of large diameter. This circle is chosen to be 30 to 50 times (depending on the mesh size) the instantaneous diameter. Tests on numerical accuracy show that this ratio is adequate. For the numerical computations the mesh size most often used is $\Delta \zeta = \frac{1}{32} = 0.03125$; for reasons to be shown later, the denominator is chosen to be multiple powers of 2, with $\Delta \xi = 0.025$. This gives us a total number of meshes (memory storage) per variable of 41x64. Tests have been carried out to determine the effect of changing these numbers; the results will be presented later.

4-2 Formulation

The equations to be solved are

$$\frac{\partial \omega}{\partial t} - \frac{1}{r} \left\{ \frac{\partial}{\partial r} \left[\omega \frac{\partial \psi}{\partial \theta} \right] - \frac{\partial}{\partial \theta} \left[\omega \frac{\partial \psi}{\partial r} \right] \right\} - \frac{1}{R_e} \nabla^2 \omega \qquad (2.23)$$

and

$$\nabla^2 \psi = \omega \tag{2.24}$$

where

$$\nabla^2 = \frac{\partial}{\partial r} + \frac{1}{r} \frac{\partial}{\partial r} + \frac{1}{r} \frac{\partial^2}{\partial \theta^2} ,$$

subjected to the initial conditions

$$\psi(r,\theta,0^+) = r \sin(\theta) - \gamma\theta , \qquad r \neq r_0 , \qquad (2.25)$$

$$\psi(\mathbf{r},\theta,0^{-}) = \mathbf{r} \sin(\theta), \qquad (2.25b)$$

$$\omega(r,\theta,0^+) = 0$$
, $r \neq r_0$, (2.26)

where from (2.29), for a truncated right cone,

$$r_0$$
 (t) = 1 + γ t. (2.29)

the boundary conditions are

$$\psi(\mathbf{r}_0, \theta, \mathbf{t}) = -\gamma \theta (1 + \gamma \mathbf{t}), \qquad (2.27)$$

$$\psi_r(r_0,\theta,t) = \Omega(1+\gamma t), \qquad (2.28)$$

and

$$\psi = r \sin(\theta) - \gamma \theta (1+\gamma t)$$
, as $r \to \infty$, (2.30)

$$\omega = 0$$
, as $r \to \infty$. (2.31)

As in chapter III we subtract the non-periodicity in θ a priori by using the following transformation

$$\psi = -\gamma \theta \ (1 + \gamma t) + \hat{\psi} \tag{4.2}$$

Thus, dropping the superscript and making use of (4.1) yields

$$\frac{\partial \omega}{\partial t} - \frac{\gamma}{\pi (1 + \gamma t)} \frac{\partial \omega}{\partial \xi} + \frac{1}{g(\xi, t)} \left\{ \frac{\partial}{\partial \xi} \left[\omega u \right] + \frac{\partial}{\partial \zeta} \left[\omega v \right] \right\} - \frac{1}{R_{\alpha} g(\xi, t)} \nabla^{2} \omega , \qquad (4.3)$$

and

$$\nabla^2 \psi = g(\xi, t) \ \omega(\xi, \zeta, t), \tag{4.4}$$

where

$$\nabla^2 = \frac{\partial^2}{\partial \xi^2} + \frac{\partial^2}{\partial \zeta^2} ,$$

with

$$u = \pi \gamma (1 + \gamma t) - \frac{\partial \psi}{\partial \zeta},$$
 (4.5)

$$v = \frac{\partial \psi}{\partial \dot{\varepsilon}}$$
 , (4.6)

and the Jacobian

$$g(\xi,t) = \pi^2 (1 + \gamma t)^2 e^{2\pi \xi}$$
 (4.7)

The boundary and initial conditions are now

$$\psi(\xi,\zeta,0^{+}) = e^{\pi\xi} \sin(\pi\zeta), \qquad (4.8)$$

$$\omega(\xi,\zeta,0^{+})=0, \qquad \qquad \xi\neq 0 , \quad (4.9)$$

$$\psi(0,\zeta,t)=0, \qquad (4.10)$$

$$\psi_{\xi}(0,\zeta,t) = \pi (1 + \gamma t)^{2} \Omega,$$
 (4.11)

$$\psi = (1 + \gamma t) e^{\pi \xi} \sin(\pi \zeta), \quad \text{as } r \to \infty, \quad (4.12)$$

$$\omega = 0 , \qquad \text{as } r \to \infty . \tag{4.13}$$

4-2-1 Finite Difference Scheme for The Vorticity Equation

As mentioned earlier, the algorithm used for the vorticity equation is the explicit forward-in-time, centered-space finite difference scheme, i.e.,

$$\omega_{\mathbf{i},\mathbf{j}}^{\mathbf{n+1}} = \omega_{\mathbf{i},\mathbf{j}}^{\mathbf{n}} + \frac{\Delta \mathbf{t} \gamma}{\pi (1 + \gamma \mathbf{t}^{\mathbf{n}}) \Delta \mathcal{E}} \left[\omega_{\mathbf{i} + \frac{1}{2},\mathbf{j}}^{\mathbf{n}} - \omega_{\mathbf{i} - \frac{1}{2},\mathbf{j}}^{\mathbf{n}} \right]$$

$$-\frac{\Delta t}{\Delta \xi g_{i}^{n}} \left[(\omega u)_{i+\frac{1}{2},j}^{n} - (\omega u)_{i-\frac{1}{2},j}^{n} \right]$$

$$-\frac{\Delta t}{\Delta \zeta g_{\mathbf{i}}^{n}} \left[(\omega v)^{n}_{\mathbf{i},\mathbf{j}+\frac{1}{2}} - (\omega v)^{n}_{\mathbf{i},\mathbf{j}-\frac{1}{2}} \right]$$

$$+ \frac{\Delta t}{\Delta \xi^2 g_i^n R_a} \left[\omega_{i+1,j}^n - 2\omega_{i,j}^n - \omega_{i-1,j}^n \right]$$

+
$$\frac{\Delta t}{\Delta \zeta^{2}} g_{i}^{n} R_{e} \left[\omega_{i,j+1}^{n} - 2\omega_{i,j}^{n} + \omega_{i,j-1}^{n} \right]. \quad (4.14)$$

This scheme is of order (Δt , $\Delta \xi^2$, $\Delta \zeta^2$) and is consistent with equation (4.3).

The governing equations are quasi-linear with variable coefficients, for which the stability criterion is difficult to apply. Practical experience shows [44] that instability usually begins as a local phenomenon. We are thus considering stability as related to small perturbations, such that second-order effects become negligibly small. The assumption is that perturbations to the true solution will normally be sufficiently small in magnitude that damping will result with use of the proper stability criterion. While the Kreiss matrix theorem $^{\left[43\right]}$ forms the basis for treatment of variable-coefficient problems, in practice the Von Neumann condition is found to be a useful tool in judging a difference scheme. Reference [43] stated that when a difference scheme is found to be conditionally stable, the Von Neumann condition nearly always gives the correct stability range, and that it is only at the limits of the range that the analysis may need to be supplemented. Thus we assume that the given problem is properly posed and we make use of Von Neumann's analysis of stability theory on the

basis of Fourier analysis. We therefore assume a typical Fourier component solution to equation (4.14) in the form

$$\omega_{i,j}^{n} = \omega_{o} w^{n} e^{(i\kappa_{1}+j\kappa_{2})\hat{j}}$$
 (4.15)

Here the wave number κ_1 refers to the ξ -component variation, κ_2 refers to the wave number for the ζ -component, and \hat{j} is the complex number $\sqrt{-1}$. The reference amplitude is modified by w^n where w is the growth rate factor and n is the index of time advancement.

$$|w| \leq 1$$

if the component solution is to remain bounded as n becomes large.

We assume a first order velocity variation of the form

$$u_{i,j}^{n} = u_{\circ} (1 + \delta_{i,j}^{n}), \qquad \delta_{i,j}^{n} \ll 1,$$
 $v_{i,j}^{n} = v_{\circ} (1 + \Delta_{i,j}^{n}), \qquad \Delta_{i,j}^{n} \ll 1,$

and we further simplify by assuming

$$\kappa_1 - \kappa_2 - \kappa$$

substituting equation (4.15) into equation (4.14) we obtain

$$\begin{aligned} \mathbf{w} &= 1 + \frac{2\Delta t}{g_{1}^{n} R_{e}} \left(\frac{1}{\Delta \xi^{2}} + \frac{1}{\Delta \zeta^{2}} \right) \left(\cos(\kappa) - 1 \right) \\ &- \hat{\mathbf{j}} \left(\frac{\Delta t}{g_{1}^{n}} \left[\frac{\mathbf{u}_{o}}{\Delta \xi} + \frac{\mathbf{v}_{o}}{\Delta \zeta} \right] - \frac{\Delta t \gamma}{\pi (1 + \gamma t^{n}) \Delta \xi} \right) \sin(\frac{1}{2} \kappa) , \end{aligned}$$

or,

$$w = 1 + 2 \alpha \left(\cos(\kappa) - 1 \right) - \hat{j} \sqrt{2} \beta \sin(\frac{1}{2} \kappa) ,$$

where

$$\alpha = \frac{\Delta t}{g_{i}^{n} R_{e}} \left(\frac{1}{\Delta \xi^{2}} + \frac{1}{\Delta \zeta^{2}} \right) ,$$

and

$$\beta = \frac{1}{\sqrt{2}} \left[\frac{\Delta t}{g_{i}^{n} R_{e}} \left[\frac{u_{o}}{\Delta \xi} + \frac{v_{o}}{\Delta \zeta} \right] - \frac{\Delta t \gamma}{\pi (1 + \gamma t^{n}) \Delta \xi} \right].$$

Thus,

$$|w|^2 = \left[1 + 2 \alpha \left(\cos(\kappa) - 1\right)\right]^2 + \beta^2 \left[1 - \cos(\kappa)\right], \quad (4.16)$$

and,

$$\frac{d \left| w \right|^2}{d(\cos(\kappa))} = 4 \alpha \left[1 + 2 \alpha (\cos(\kappa) - 1) \right] - \beta^2$$
 (4.17)

$$\frac{d^2 \left| w \right|^2}{d(\cos(\kappa))} = 8 \alpha^2. \tag{4.18}$$

Since α is always positive, $\left|\mathbf{w}\right|^2$ has no maximum in (-1,1). After some manipulation on (4.17), we also find that $\left|\mathbf{w}\right|^2$ has no minimum in (-1,1). The only possibilities for an extremum is therefore at the end points.

For $\cos(\kappa) = 1$, |w| = 1 and the stability condition is identically satisfied. When $\cos(\kappa) = -1$ we obtain

$$|w|^2 = (1 - 4\alpha)^2 + 2\beta^2$$
,

which implies that

$$1 \geq 2\alpha + \frac{\beta^2}{4 \alpha} \quad ,$$

$$\Delta t \leq \frac{\pi^{2} \left(1 + \gamma t^{n}\right)^{2} R_{e}}{2\left[\frac{1}{\Delta \xi^{2}} + \frac{1}{\Delta \zeta^{2}}\right] + \frac{1}{8}\left[\frac{1}{\Delta \xi^{2}} + \frac{1}{\Delta \zeta^{2}}\right] \left(\frac{u_{o}}{\Delta \xi} + \frac{v_{o}}{\Delta \zeta} - \frac{\pi(1 + \gamma t^{n})R_{e}}{\Delta \xi}\right)^{2}}\right]}.$$

$$(4.19)$$

At each time step we evaluate Δt from (4.19), allowing for Δt to be within a certain percentage (90%) of the calculated value. Because the allowable Δt always increases as we advance in time, Δt was limited here to a maximum value (usually Δt =0.01), in order to attain the desired level of accuracy. In the above formula we use the value of g_1^n which gives the minimum Δt . This is the value at the surface or $g_1^n = \pi^2 \left(1 + \gamma t\right)^2$.

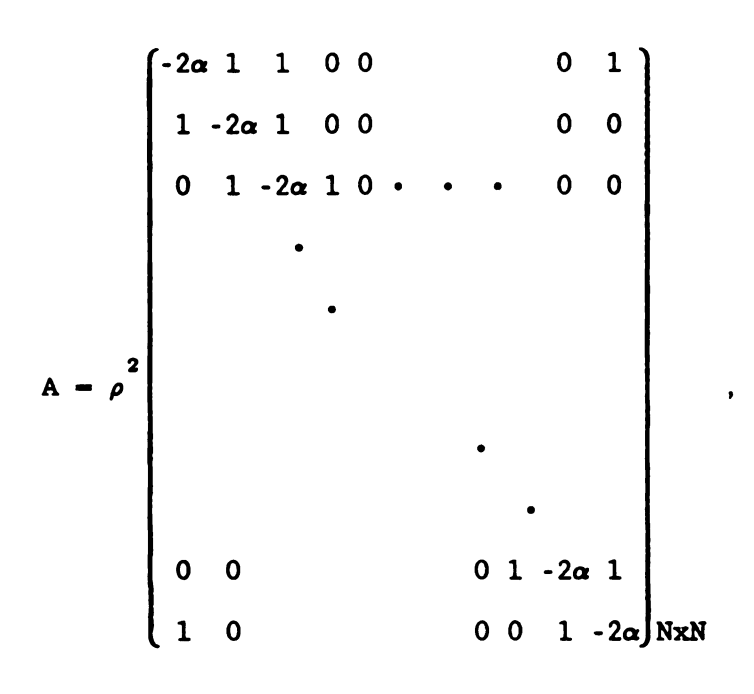
4-2-2 Finite Difference Scheme for Poisson Equation

For Poisson equation, we used the standard second-order discretization, which gives, for equation (4.4),

$$\vec{A} = \vec{B} , \qquad (4.20)$$

where

and



where,

$$\alpha = (\rho^2 + 1)/\rho^2$$

$$\rho^2 - \Delta \xi^2 / \Delta \zeta^2$$

and

$$\vec{\Psi} = (\hat{\Psi}_2, \hat{\Psi}_3, \hat{\Psi}_3, \dots, \hat{\Psi}_{M-1})^T$$

where

$$\hat{\Psi}_{i} - (\psi_{i,1}, \psi_{i,2}, \dots, \psi_{i,N})$$
, $i = 2,3,\dots,M-1$.

Also,

$$\vec{B} = (B_2, B_3, \dots, B_{M-1})$$
,

with

$$B_{i} = (B_{i,1}, B_{i,2}, \dots, B_{i,N})$$
, $i = 2,3,\dots,M-1$

and

$$B_{2,j} = -\psi_{1,j} + g_2^n \omega_{2,j}^n$$
,

$$B_{M-1,j} = -\psi_{M,j} + g_{M-1}^n \omega_{M-1,j}^n$$
,

and

$$B_{i,j} - g_{i,j}^n \omega_{i,j}^n$$
, i-3,4,...,M-2.

In all cases,

$$j = 1, 2, 3, \dots, N$$

It is easy to see that we have M-2xN unknowns in M-2xN coupled equations. A large class of modern methods for obtaining fast solutions for elliptic equations are available. Because those methods require complex coding, we decided to use the simplest and most common method in use today, known as the Fast Fourier Transform (FFT). Although there are many articles dealing with this important topic, we feel that they overemphasize the final step, which is the economical evaluation of the transform itself. We present here the necessary steps before using the FFT.

Let us redefine the matrix A as

$$\mathbf{A} = \rho^2 \left[\mathbf{P} - 2\alpha \mathbf{I} \right]_{\mathbf{N} \times \mathbf{N}} ,$$

where

It is known [45] that any matrix of the form

$$\mathbf{C} = \begin{bmatrix} \mathbf{a_1} & \mathbf{a_2} & \mathbf{a_3} & & & & & & \mathbf{a_N} \\ \mathbf{a_N} & \mathbf{a_1} & \mathbf{a_2} & \mathbf{a_3} & & & & \mathbf{a_{N-1}} \\ \mathbf{a_{N-1}} & \mathbf{a_N} & \mathbf{a_1} & \mathbf{a_2} & & & & \mathbf{a_{N-2}} \\ & & & & & & & \\ & & & & & \\ & & & & & \\ & & & & & \\ & & & & & \\ & & & & & \\ & & & & & \\ & & & & & \\ & & & & & \\ & & & & & \\ & & & & & \\ & & & & & \\ & & & & & \\ & & & & \\ & & & & \\ & & & & \\ & & & & \\ & & & & \\ & & & & \\ & & & & \\ & & & & \\ & & & & \\ & & & & \\ & & & & \\ & & \\ & & & \\ & & & \\ & & & \\ & & & \\ & & & \\ & & & \\ & & \\$$

is called a circulant matrix. The matrix P is therefore a circulant matrix. The eigenvalues for a general circulant C are

$$v_k - \sum_{j=1}^{N} a_j r_k^{j-1}$$

where

$$r_k = \cos(\frac{2\pi k}{N}) + \hat{j} \sin(\frac{2\pi k}{N})$$
, $k = 1, 2, 3, ..., N$

The corresponding eigenvectors are

$$Q_k = N^{-1/2}$$
 (1, r_k , r_k^2 , ..., r_k^{N-2} , r_k^{N-1}),

We thus conclude that the matrix A has eigenvalues equal to

$$\lambda_{k} = 2 \rho^{2} \left[\cos(\frac{2\pi k}{N}) - 1 \right],$$
 (4.21)

and the resulting matrix of eigenvectors is

where

$$\mathbf{w} = \mathbf{e}^{\mathbf{\frac{2\pi a}{N}} \hat{\mathbf{j}}} \qquad \qquad \hat{\mathbf{j}} = \sqrt{-1}$$

with

$$a = -1$$

Now we define

$$\hat{\psi}_{i} = Q \hat{\psi}_{i} . \tag{4.23}$$

For each i we have now

$$Q \dot{\psi}_{i-1} + A Q \dot{\psi}_{i} + Q \dot{\psi}_{i+1} - B_{i}$$

To diagonalize A we multiply by Q^{-1} , which has the same structure as Q, but with

$$a = + 1$$
.

The process of evaluating Q^{-1} B_i is widely known as the FFT. Here we used the original version of the scheme as proposed by Cooly and Tukey^[46], known as Radix-2(which utilize having $N=2^n$, where n is an integer). After solving the resulting tri-diagonal systems the same algorithm is applied to evaluate the inverse transform(here $\hat{\psi}_i$ is evaluated from definition(4.21)).

4-2-3 Numerical Boundary and Initial Conditions

4-2-3a Boundary conditions

From (4.10) to (4.13) we have

$$\psi(0,\zeta,t)=0, \qquad (4.10)$$

$$\psi_{\xi}(0,\zeta,t) = \pi(1+\gamma t)^{2} \Omega$$
, (4.11)

$$\psi = (1 + \gamma t) e^{\pi \xi} \sin(\pi \zeta)$$
, as $r \to \infty$, (4.12)

$$\omega = 0$$
, as $r \to \infty$. (4.13)

It should be clear that we can not make explicit use of all of these boundary conditions. We can only make use of them by relating them implicitly. The boundary conditions (4.10), (4.12) and (4.13) do not need differencing, so we use them as they are. Differentiating (4.10) with respect to ζ and substituting in (4.4), we obtain

$$\frac{\partial^3 \psi}{\partial \xi} = \frac{\partial (g\omega)}{\partial \xi} , \quad \text{at } \xi = 0 , \quad (4.24)$$

and we have, by a Taylor series expansion about $\xi = 0$,

$$\psi_{i+1} - \psi_i + \Delta \xi \frac{\partial \psi}{\partial \xi} \Big|_{\xi=0} + \frac{\Delta \xi^2}{2!} \frac{\partial^2 \psi}{\partial \xi^2} \Big|_{\xi=0} + \frac{\Delta \xi^3}{3!} \frac{\partial^3 \psi}{\partial \xi^3} \Big|_{\xi=0} + O(\Delta \xi^4) . \quad (4.25)$$

By substituting the Taylor expansion for the right hand side of (4.24) in (4.25) we obtain

$$\psi_{w+1} = \psi_{w} + \Delta \xi \pi (1 + \gamma t^{n})^{2} \Omega + \frac{\Delta \xi^{2}}{2!} g_{w}^{n} \omega_{w}^{n} + \frac{\Delta \xi^{3}}{3!} \left[\frac{(g\omega)_{w+1}^{n} - (g\omega)_{w}^{n}}{\Delta \xi} \right] + 0(\Delta \xi^{4}).$$

In the above formula, subscript w indicates the surface of the cylinder, or ξ =0; we also made use of (4.10). Thus, we arrive at the boundary condition for the surface vorticity:

$$\omega_{w}^{n} = \frac{3(\psi_{w+1} - \psi_{w})}{\Delta \xi^{2} g_{w}^{n}} - \frac{3 \pi (1 + \gamma t^{n})^{2} \Omega}{\Delta \xi g_{w}^{n}} - \frac{g_{w+1}^{n} \omega_{w+1}^{n}}{2 g_{w}^{n}}. \quad (4.26)$$

4-2-3b Initial conditions and flow initialization

The initial conditions as given by (4.8) and (4.9) are unsuitable for initializing the flow field. Since we are dealing with an impulsively-started circular cylinder, the flow will initially be potential [2]. The potential flow is just the first-order outer solution obtained in the previous chapter analytically (see Eq.(4.27)).

By making the necessary modifications due to different coordinates used here, we have

$$\psi(\xi,\zeta,t) = \left((1+\gamma t)e^{\pi\xi} - \frac{1}{(1+\gamma t)e^{\pi\xi}} \right) \sin(\pi\zeta) . \quad (4.27)$$

When t = 0 the above formula yields the initial flow field. However this same formula is used to determine the flow far away from the surface of the cylinder at any time (for i = M, or $\xi = \Delta \xi (M-1)$). Use of the initial condition (4.9) will not initialize the computation process. To initialize the computation we use (4.27) in (4.26) with $\omega_{w+1}^1 = 0$. Although the results are initially in error,

experiements [47,48] have shown that slightly later the scheme (any numerical scheme) will correct itself. That means that the very early

numerical results are unreliable. This is still an unsolved problem which require further research.

4-2-4 Scheme implementation

When using a finite difference method, the objective is to calculate the values of ψ and ω at the intersections of the mesh lines shown in Figure 4.1, for each discrete time step. We use (4.14) to compute $\omega_{1,j}^{n+1}$ from known values of $\psi_{1,j}^n$, $u_{1\pm\frac{1}{2},j}^n$, $v_{1,j\pm\frac{1}{2}}^n$, g_1^n and $\omega_{1,j}^n$ or $\omega_{1\pm\frac{1}{2},j}$ for all (i,j), in turn. Values for $\psi_{1,j}^{n+1}$ are obtained by using the advanced time value of $\omega_{1,j}^{n+1}$ in the poisson equation(4.20). We use

$$u_{i,j+\frac{1}{2}}^{n} = \pi \gamma (1 + \gamma t^{n}) - \left[\frac{\psi_{i,j+1}^{n} - \psi_{i,j}^{n}}{\Delta \zeta} \right].$$
 (4.28)

Then, by using suitable permutation we obtain

$$u_{i+\frac{1}{2},j}^{n} = \frac{1}{4} \left[u_{i+1,j+\frac{1}{2}}^{n} + u_{i+1,j-\frac{1}{2}}^{n} + u_{i-1,j+\frac{1}{2}}^{n} + u_{i-1,j-\frac{1}{2}}^{n} \right]$$

Similar relationships can easily be obtained for other values.

66

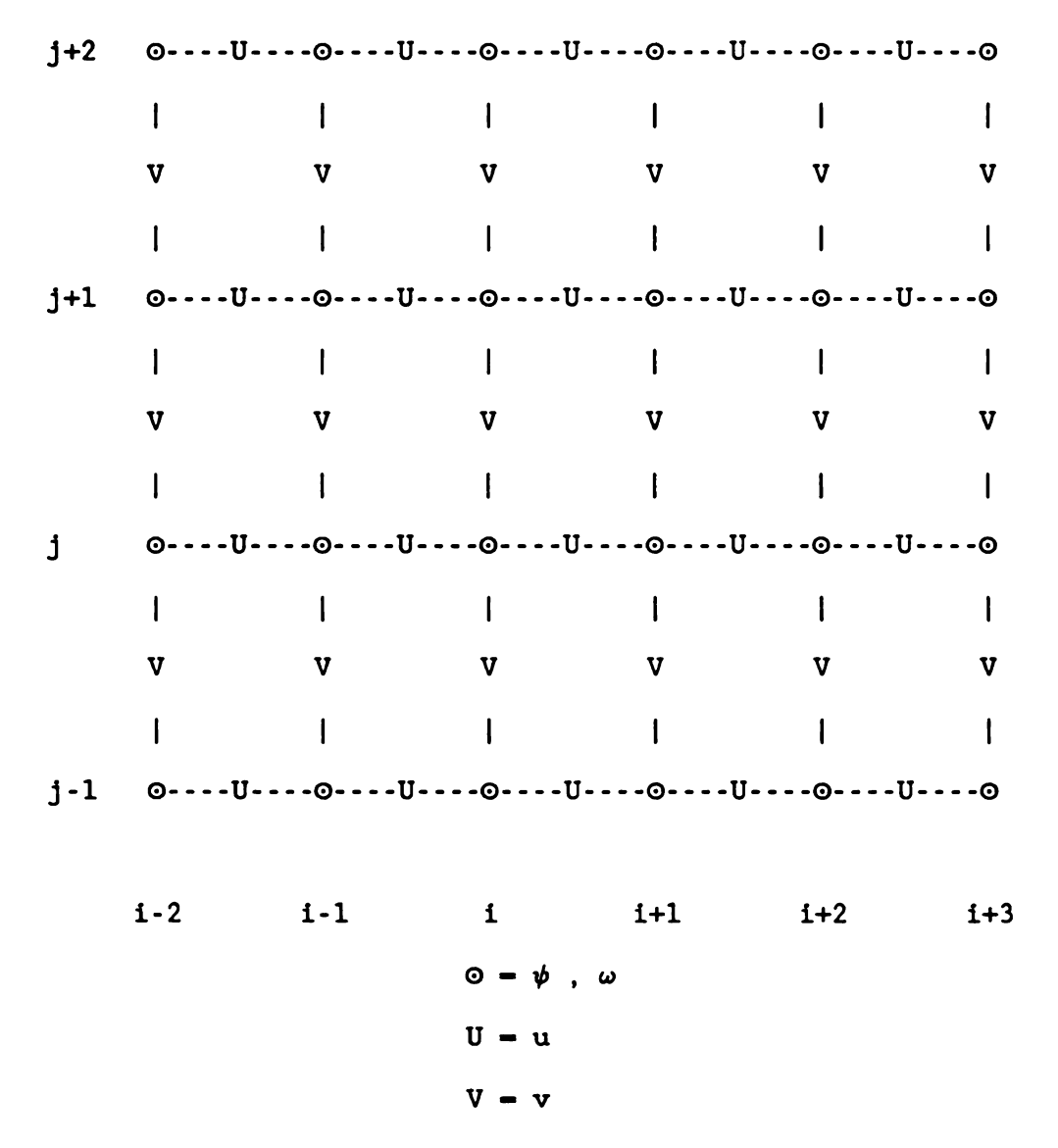


Figure IV-1 Location of the Points of Definition of the Variables Relative to the Mesh

4-3 Pressure Distribution and Pressure Coefficient

As in chapter III, upon integrating Navier-Stokes equation in the $\boldsymbol{\theta}$ direction, we obtain

$$c_{p} = \frac{p - p_{o}}{U_{\infty}^{2} \rho}$$

$$- (1 + \gamma t) \int_0^{\theta} \left[-2\gamma \Omega + \frac{1}{R_e} \frac{\partial \omega}{\partial r} \right]_{r=r_e}^{d\theta}$$

changing to the ξ -and ζ system of coordinats, this becomes

$$C_{p} = \pi(1 + \gamma t) \int_{0}^{\zeta} \left[\frac{1}{\pi(1 + \gamma t) R_{e}} \frac{\partial \omega}{\partial \xi} - 2\gamma \Omega \right]_{\xi=0} d\zeta . \qquad (4.29)$$

Because "the trapizoidal rule for integrating periodic functions is remarkably accurat" [49], we use it to integrate the above equation, and for all other numerical integration in this study. Special care is required for the integration of equation (4.29); and this will be discussed later.

4-4 Drag, Lift and Moment

Following the same steps as in chapter III we obtain

$$C_{D_p} = -(1+\gamma t)^2 \int_0^{2\pi} \left[\frac{1}{R_e} \frac{\partial \omega}{\partial r} \right]_{r=r_0} \sin(\theta) d\theta$$
.

When using ξ - ζ system of coordinates, this becomes

$$C_{D_{p}} = -(1+\gamma t) \int_{0}^{2} \left[\frac{\partial \omega}{\partial \xi} \right]_{\xi=0} \sin(\pi \zeta) d\zeta . \qquad (4.30)$$

For the skin-friction drag we obtain

$$C_{D_f} = \frac{\pi(1+\gamma t)}{R_o} \int_0^2 \omega \sin(\pi \zeta) d\zeta . \qquad (4.30b)$$

The above definitions give positive drag in the flow direction. The total drag coefficient is thus

$$C_D - C_{D_p} + C_{D_f}$$

$$-\pi \left(1+\gamma t\right) \int_{0}^{2} \left\{ \left[\frac{1}{R_{e}} + \gamma(1+\gamma t) \right] \omega - \frac{1}{\pi R_{e}} \frac{\partial \omega}{\partial \xi} \right\}_{\xi=0} \sin(\pi \zeta) d\zeta . \tag{4.31}$$

The pressure lift is

$$C_{L_{p}} = (1 + \gamma t)^{2} \int_{0}^{2\pi} \left[\frac{1}{R_{e}} \frac{\partial \omega}{\partial r} \right]_{r=r_{0}} \cos(\theta) d\theta .$$

The lift is positive downward. Adjusting to the ξ - ζ system of coordinates, C_{L_n} becomes

$$C_{L_{p}} = \frac{(1+\gamma t)}{R_{e}} \int_{0}^{2} \left[\frac{\partial \omega}{\partial \xi} \right]_{\xi=0} \cos(\pi \zeta) d\zeta . \qquad (4.32)$$

The skin-friction lift is given by

$$C_{L_f} = \frac{\pi(1+\gamma t)}{R_e} \int_0^2 -\omega \cos(\pi \zeta) d\zeta , \qquad (4.33)$$

and the total lift is thus

$$C_{L} = C_{L_{p}} + C_{L_{f}}$$
 (4.34)

Finally, the moment coefficient is given by

$$C_{T} = \frac{\pi (1+\gamma t)^{2}}{R_{e}} \int_{0}^{2} \omega \bigg|_{\xi=0} d\zeta \qquad (4.35)$$

4-5 RESULTS

The numerical calculations were computed on the Albert Case Center for Computer-Aided Design Prime Computer, at Michigan State University.

The calculations were carried out using a mesh system of M = 41 nodes in

the ξ (radial) direction, and N=64 nodes in the ζ (meridian) direction, with $\Delta \xi$ =0.025 and $\Delta \zeta$ = $\frac{1}{32}$ = 0.03125 . In all of the figures T=t U_{∞}/a_0 is defined as the nondimensional time, for consistency with the previous chapters.

Although Ece and Walker [31] found it impossible to advance in time beyond certain value (typically T = 1.125 for Ω = 0.6), we had no difficulty in pushing the calculation to larger T. The computation was terminated at a value of T deemed sufficient for understanding the phenomena.

4-5-1 Stream Lines

For the non-rotating case all of the computed results show the formation of two primary bubbles. Although we could not predict the exact time of their appearance from the graphs of the stream lines, the separation-point plots (figures IV-6, 11, 16 and 21) indicate very clearly the appearance of bubbles between T=0.4 and T = 0.5, for all the Reynolds numbers studied. Secondary bubbles did not appear at R_d = 100, but at higher Reynolds number their existence is certain. The higher the Reynolds number, the earlier their appearance. The size of the primary bubbles increases with R_d . However the increase of γ not only delays separation but also decreases the bubble size.

With rotation (Ω = 1.0), primary separation takes place in the upper portion of the cylinder, somewhere between θ = 30 and 120. A secondary separation bubble appears with increasing R_d , but it disappears at some later time. With rotation, separation begins right

away after the motion has stared. Both primary and secondary bubbles decay with time. A solid rotation of the fluid with the cylinder will eventually be.

4-5-2 Pressure Coefficient

In order to integrate equation (4.29), which gives the pressure coefficient as a function of both θ and T, the trapezoidal rule [48] is used, since it is integrate periodic function with sufficient accuracy. Accumulation of round-off error, in addition to numerical error, makes it difficult to achieve perfect periodicity when we evaluating the integral at different point on the circle. To overcome this difficulty, we subtract the value of the error for a full period, divided into equal factors for each integration step. We believe that the above non periodicity due to integration is one of the main reasons that the pressure coefficient is seldom presented in published (numerical) work.

The acceleration for impulsive starting makes the pressure extremely high in the beginning of motion, however, the pressure rapidly decreases as time increases. Without rotation, the pressure has nearly attained a steady state value at T = 10 (when the integration is terminated). However, with rotation the pressure is unable to reach a steady state at T = 10.

The effect of the separated flow region is reflected in the pressure distribution, since in this region the pressure tends to be constant. Increasing the Reynolds number decreases the average pressure coefficient. Increasing γ has the same effect as that of increasing R_d since the fluid is pushed by the moving boundary at a higher rate. The well known effect of shifting the stagnation point due to rotation is clear in the pressure-coefficient figures.

4-5-3 Drag

After the singular behavior at $T=0^+$, arising from the impulsive start, the drag coefficient decreases dramatically to a reasonable value. It then increases continuously with time, but the rate of increase is very slow. The latter increase in drag seems to be mainly the consequence of the increase in size of the recirculating zone. For the same reason, increasing R_d has exactly the same effect on the drag, since it increases the separation-zone size.

4-5-4 Lift

The fact that the lift coefficient starts from zero and increases almost suddenly to a large value, may be caused by the rapid diffusion of the vorticity into the fluid. The subsequent sharp drop in the lift coefficient may be due to the interaction with the newly established-flow condition, such as the appearance of the secondary bubble.

4-5-5 Moment

The singular behavior arising from the sudden rotation is clearly indicated in the moment-coefficient figures. It increases with Reynolds number, or γ , as expected. However, increasing γ sharply increases C $_{\rm T}$ after the initial adjustment period. Looking at both the moment-coefficient and the separation figures, it seems that the change in the separation region has an effect on the pressure coefficient as related to the fluid pressure.

4-5-6 Surface Vorticity

The vorticity at the surface increases with the Reynolds number, although it is singular at $T = 0^+$. This quantity might help understand

some complex events, such as separation in the case of the non-rotating cylinder. The diagrams (figures IV-5, 10, 15, 20, 27, 34, 41, 48, 53, 58, 65 and 72) explain the appearance of the secondary bubbles, in both rotating and non-rotating cases.

In the rotating cases the vorticity on the rearward side of the cylinder (150° to 240°) tends to be constant as we advance in time. By comparing the rotating cases with the non-rotating cases, it seems that the value of the vorticity is lowered by a constant in the former cases. The maximum value of the vorticity increases with increasing Reynolds number and γ .

4-5-7 Effect of Outer Numerical Boundary

For external flow the boundary condition at infinitely is placed at a reasonably far distance from the body. It is clear that we must check whether any appreciable error is incurred by the finiteness of the domain.

Before introducing the results of such a test, it is appropriate to note that two coordinate system are used in this work. The first is the system that has the moving boundary, which is difficult to use for numerical computation. Instead, we use the system defined by (4.1) which allows us to move in physical space a distance $\left((1+\gamma(t+\Delta t)) - (1+\gamma(t+\Delta t))\right)$

 $(1+\gamma t)$ $\Big]$ $e^{-\pi \xi}$ away (in the radial direction) from the previous timespace node. Since we are using an explicit scheme which transfers signals to the next node at next time step, the signals will not be restricted to a fixed computational domain.

Figures IV-74 to IV-83 indicate that the outer boundary may has no effect on the computations. Comparing figures IV-74 to IV-77 with

figures IV-3 to IV-6 and figures IV-78 to IV-83 with IV-23 to IV-28 it shows that our choice of the outer limit is satisfactory.

4-6 Transforming to the Steady-State Three-Dimensional Case

In order to recover the original problem of three-dimensional steady flow over a projectile at an angle of attack, we use the definition of the forces and moment, and relation (2.7), thereby

$$C_{D_{total}}^{} - \rho U_{\infty}^{^{2}} a_{0} \int_{0}^{z} C_{D}^{} dz$$

$$- \rho U_{\infty}^{^{2}} a_{0} \int_{0}^{z} C_{D}^{}(t(z)) dz .$$

similar expression may be obtained for the lift and moment coefficients ,i.e.,

$$C_{L_{total}} - \rho U_{\infty}^{2} a_{0} \int_{0}^{z} C_{L}(t(z)) dz$$
,

and

$$C_{T_{total}} - \rho U_{\infty}^{2} a_{0}^{2} \int_{0}^{z} C_{T}(t(z)) dz .$$

for a truncated right cone, however different projectile shapes may be substituted into this formula to obtain corresponding force and moment coefficient.

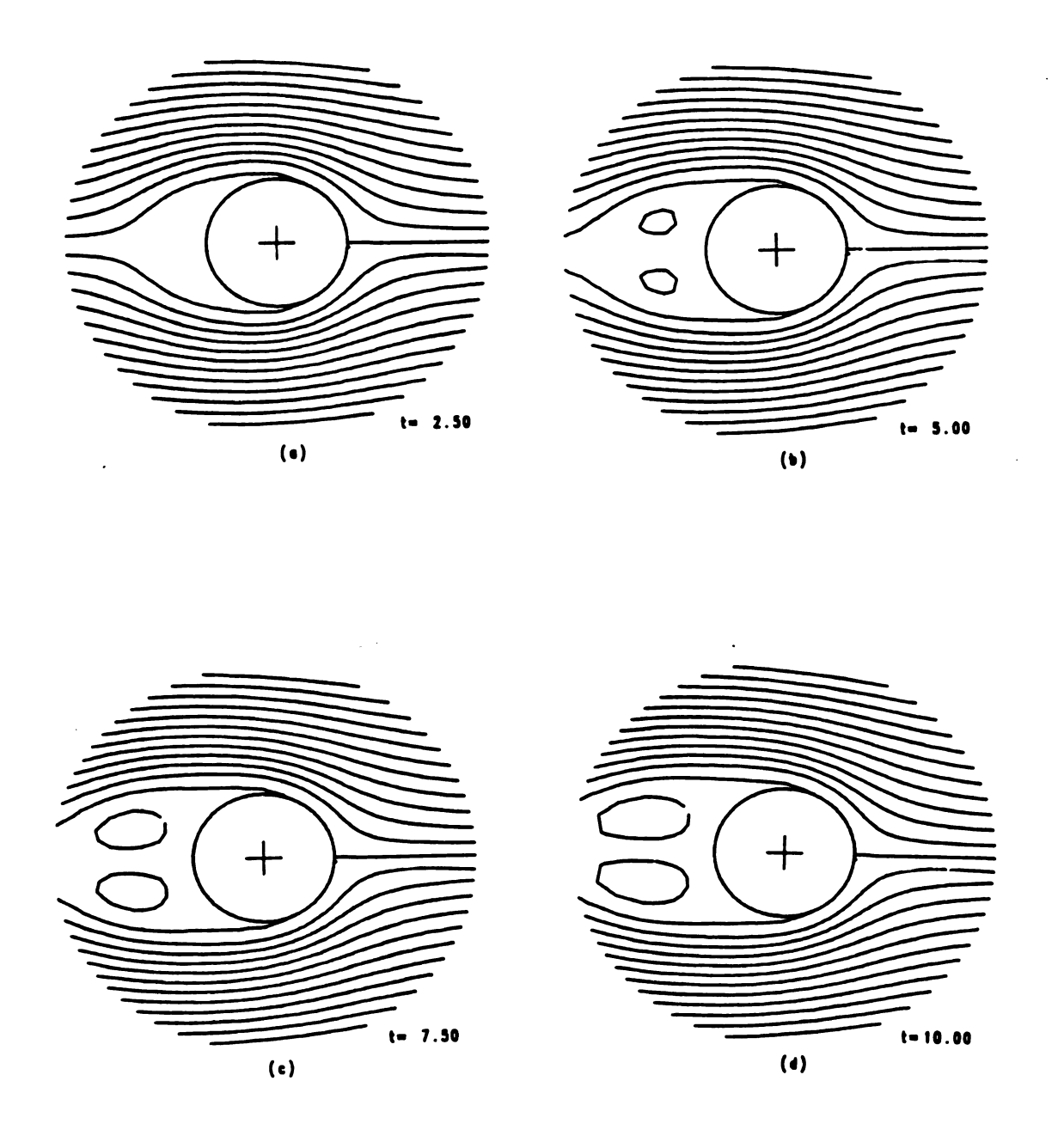


Figure IV-2 Streamlines Development with γ = 0.05 , Ω = 0.0 and R_d = 100 ,at T equal (a) 2.50 ,(b) 5.0 ,(c) 7.50 and (d) 10.0.

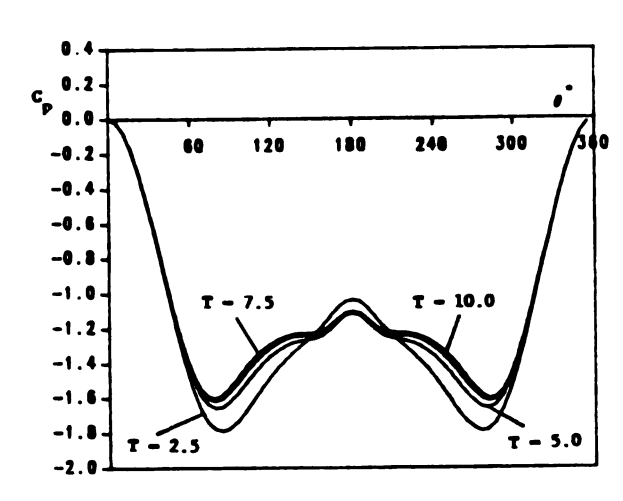


Figure IV-3 Development of Pressure Coefficient G_p , for Flow With $\gamma=0.05$, $\Omega=0.0$ and $R_d=100$.

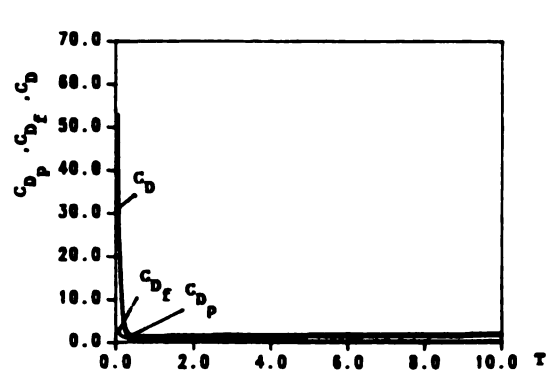


Figure IV-4 Development of the Drag Coefficients C_{D_p} , C_{D_f} , C_{D} for Flow With $\gamma = 0.05$, $\Omega = 0.0$ and $R_d = 100$.

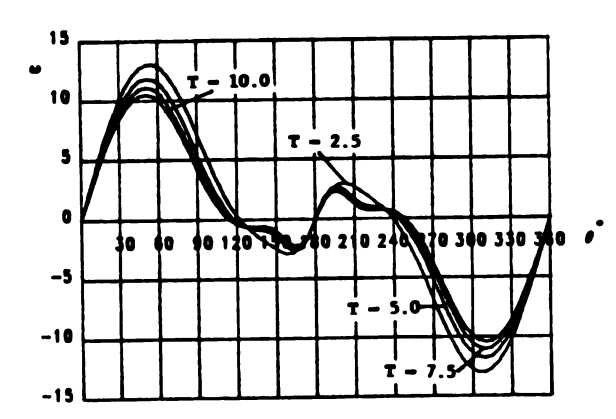


Figure IV-5 Development of Surface Vorticity ω for Flow With $\gamma=0.05$, $\Omega=0.0$ and $R_{\rm d}=100$.

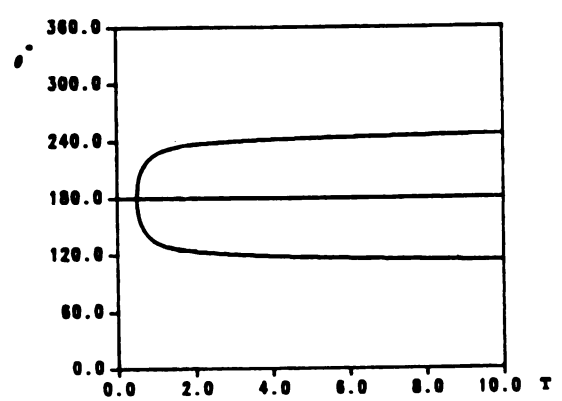


Figure IV-6 Separation Points History For Flow With $\gamma=0.05$, $\Omega=0.0$ and $R_{\rm d}=100$.

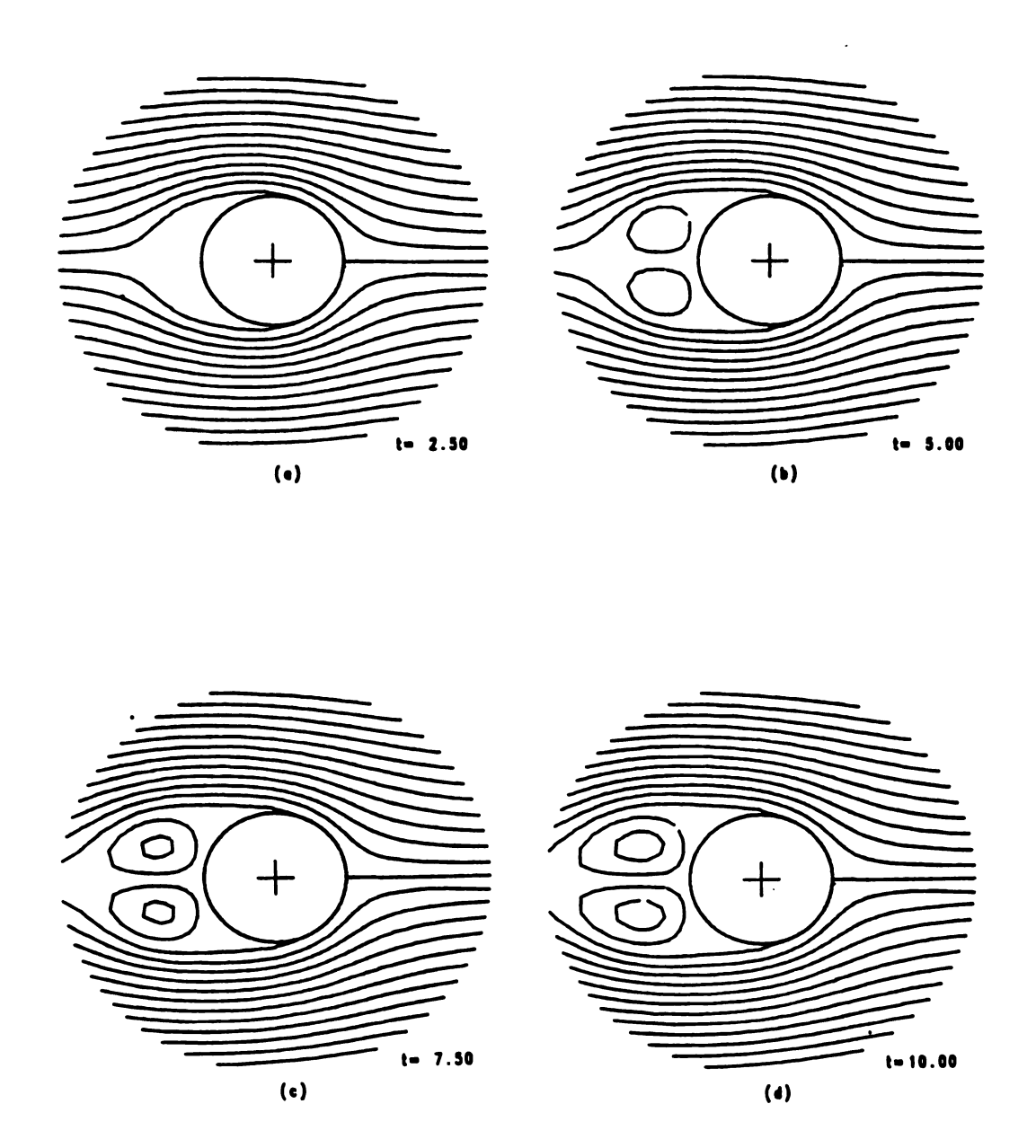


Figure IV-7 Streamlines Development with γ = 0.05 , Ω = 0.0 and R_d = 500 ,at T equal (a) 2.50 ,(b) 5.0 ,(c) 7.50 and (d) 10.0.

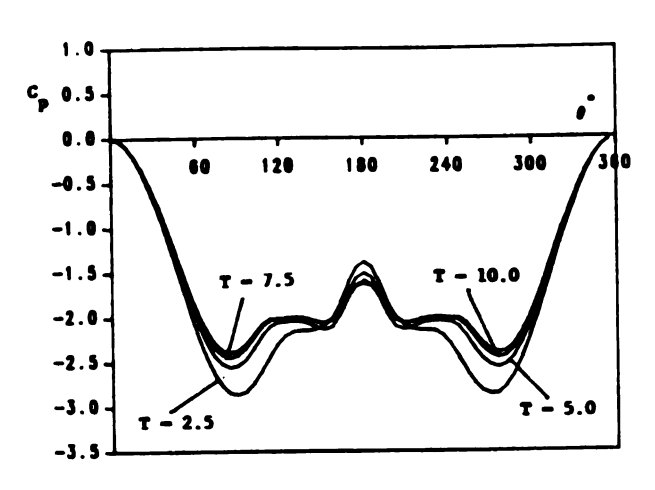


Figure IV-8 Development of Pressure Coefficient C , for Flow With $\gamma=0.05$, $\Omega=0.0$ and $R_{\rm d}=500$.

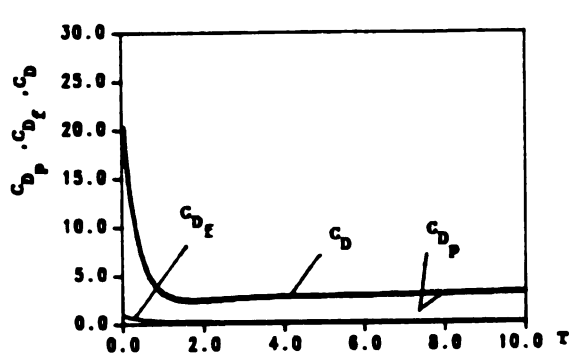


Figure IV-9 Development of the Drag Coefficients C_{D_p} , C_{D_f} , C_{D} for Flow With γ = 0.05 , Ω = 0.0 and R_d = 500.

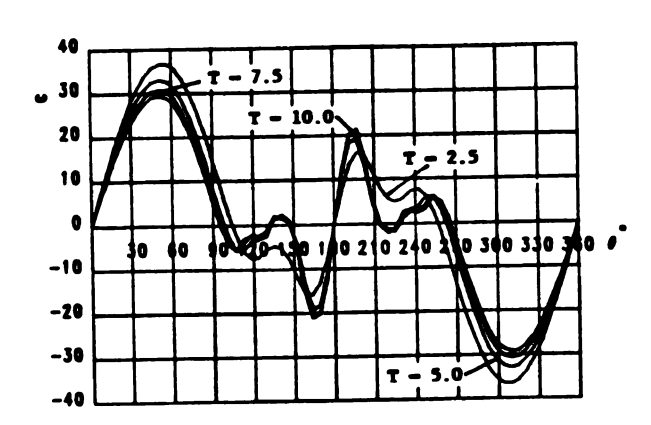


Figure IV-10 Development of Surface Vorticity ω for Flow With $\gamma=0.05$, $\Omega=0.0$ and $R_{\rm d}=500$.

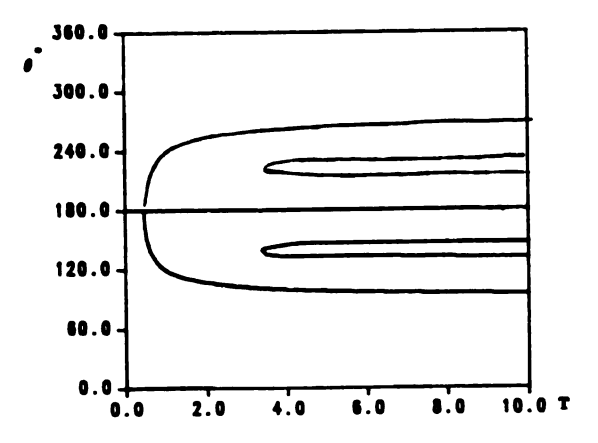


Figure IV-11 Separation Points History For Flow With $\gamma = 0.05$, $\Omega = 0.0$ and $R_d = 500$.

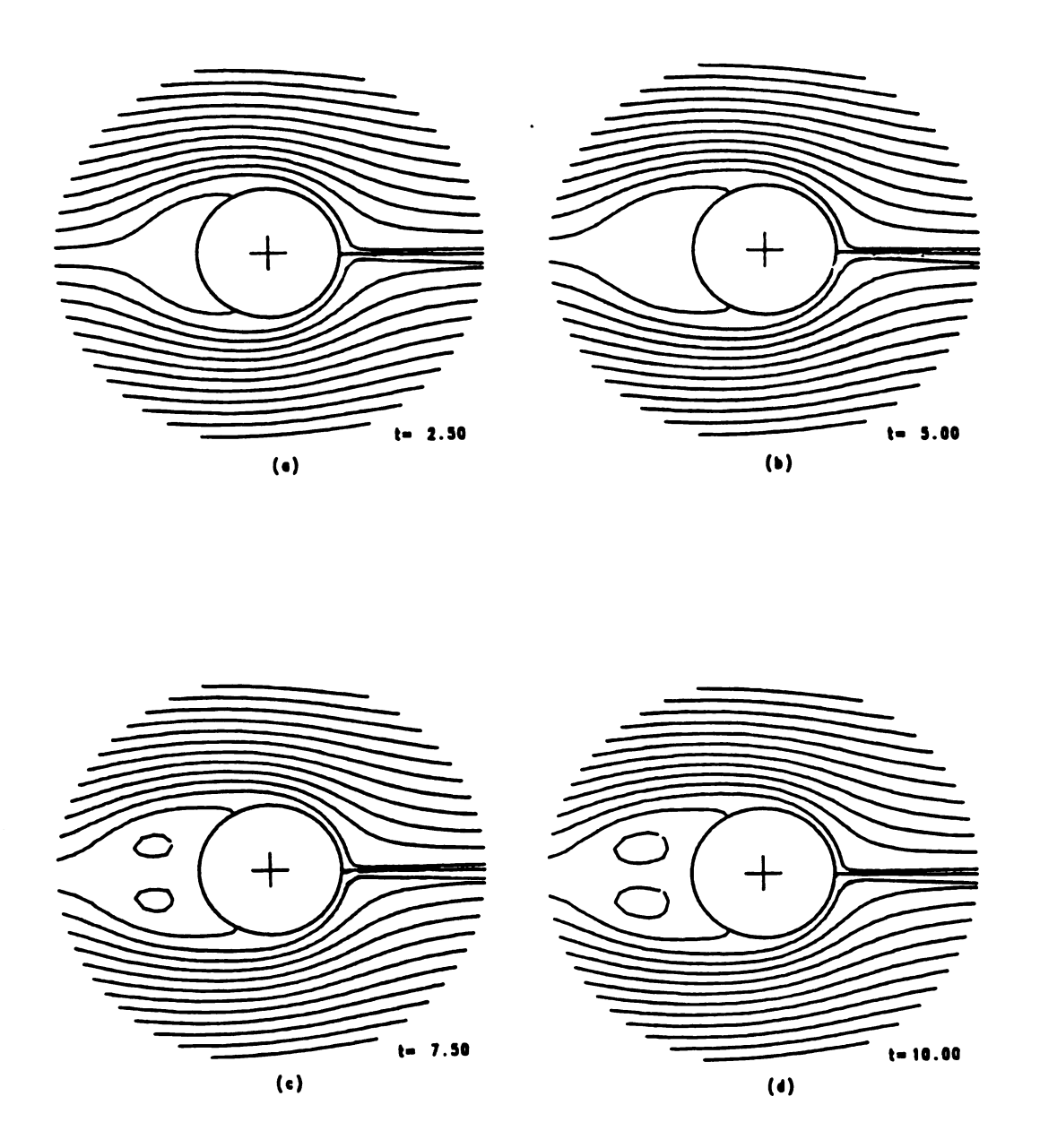


Figure IV-12 Streamlines Development with γ = 0.10 , Ω = 0.0 and R_d = 100 ,at T equal (a) 2.50 ,(b) 5.0 ,(c) 7.50 and (d) 10.0.

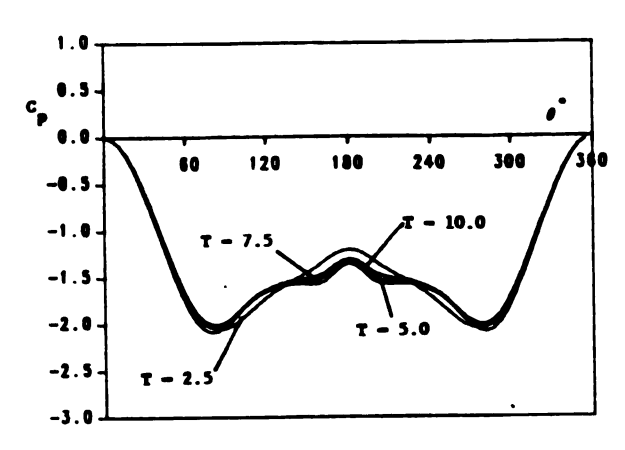


Figure IV-13 Development of Pressure Coefficient C_p , for Flow With $\gamma=0.10$, $\Omega=0.0$ and $R_d=100$.

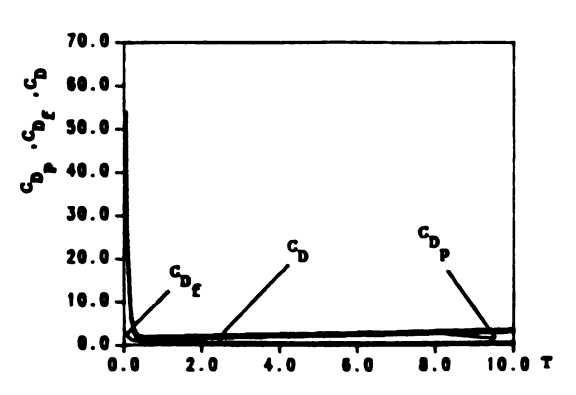


Figure IV-14 Development of the Drag Coefficients C_{D_p} , C_{D_f} , C_{D} for Flow With γ = 0.10 , Ω = 0.0 and R_d = 100.

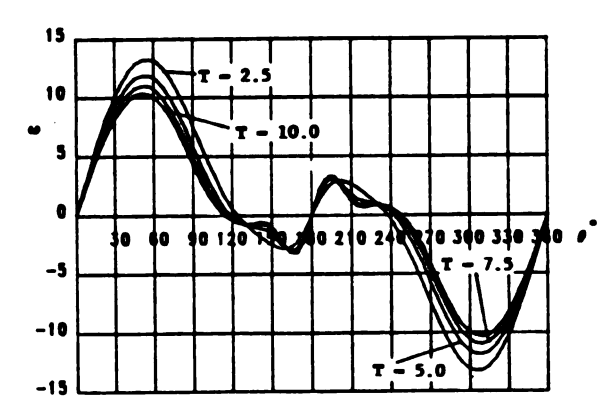


Figure IV-15 Development of Surface Vorticity ω for Flow With $\gamma=0.10$, $\Omega=0.0$ and $R_{\rm d}=100$.

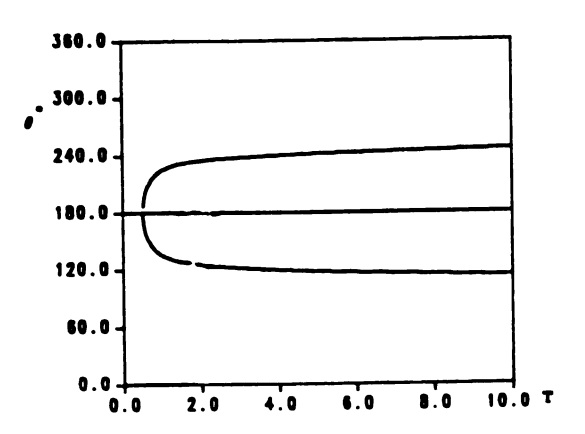


Figure IV-16 Separation Points History For Flow With $\gamma=0.10$, $\Omega=0.0$ and $R_{\rm d}=100$.

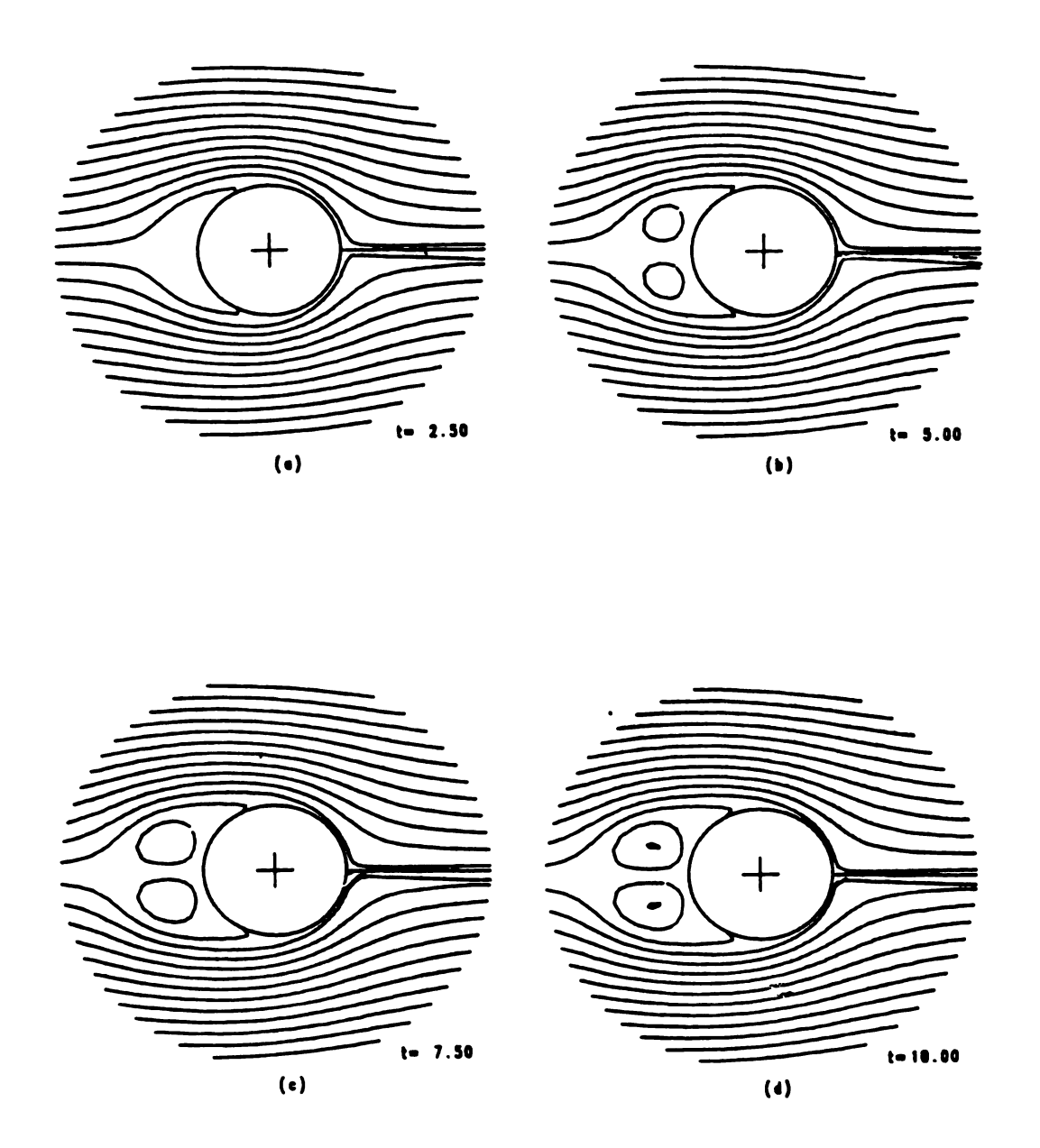


Figure IV-17 Streamlines Development with γ = 0.10 , Ω = 0.0 and R_d = 500 ,at T equal (a) 2.50 ,(b) 5.0 ,(c) 7.50 and (d) 10.0.

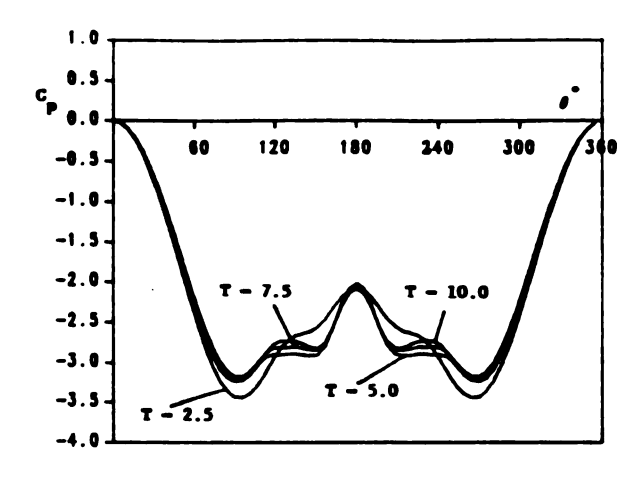


Figure IV-18 Development of Pressure Coefficient C_p , for Flow With $\gamma = 0.10$, $\Omega = 0.0$ and $R_d = 500$.

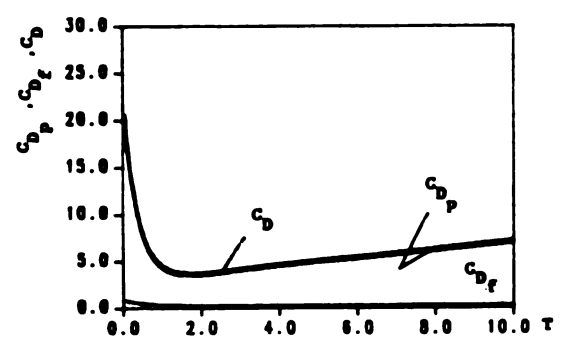


Figure IV-19 Development of the Drag Coefficients G_{D_p} , G_{D_g} , G_{D} for Flow With $\gamma=0.10$, $\Omega=0.0$ and $R_{d}=500$.

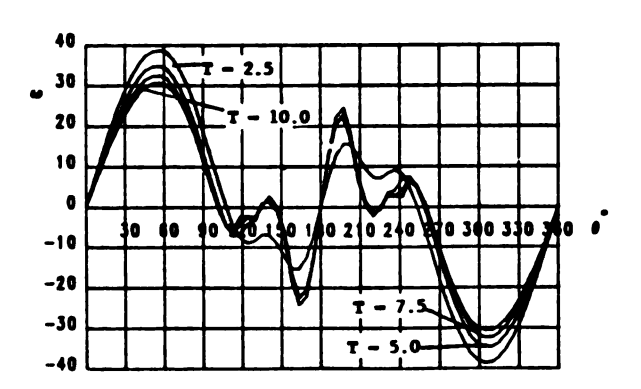


Figure IV-20 Development of Surface Vorticity ω for Flow With γ = 0.10 , Ω = 0.0 and R_d = 500.

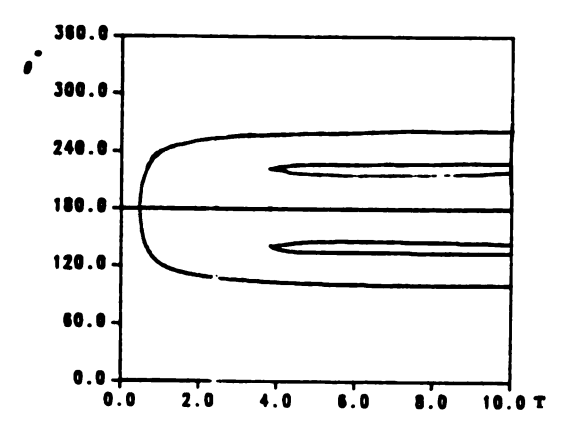


Figure IV-21 Separation Points History For Flow With γ = 0.10 , Ω = 0.0 and R_d = 500.

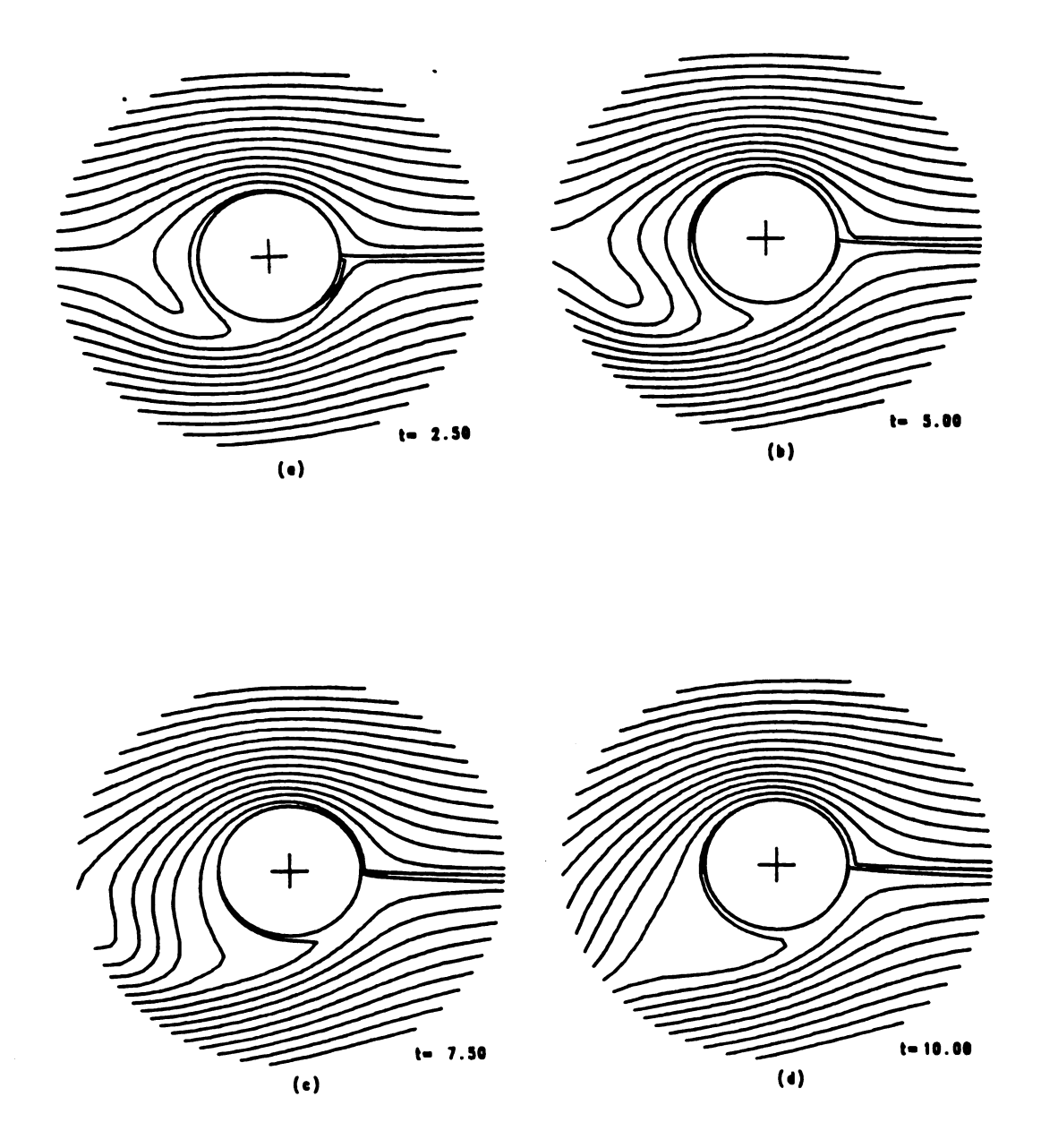


Figure IV-22 Streamlines Development with γ = 0.05 , Ω = 1.0 and R_d = 100 ,at T equal (a) 2.50 ,(b) 5.0 ,(c) 7.50 and (d) 10.0.

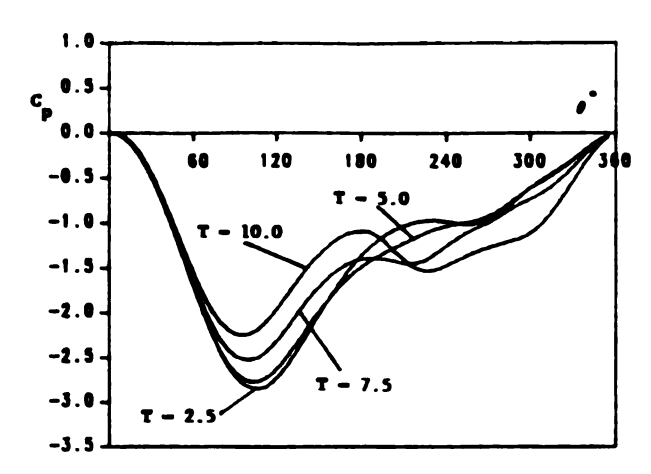


Figure IV-23 Development of Pressure Coefficient C_p , for Flow With $\gamma = 0.05$, $\Omega = 1.0$ and $R_d = 100$.

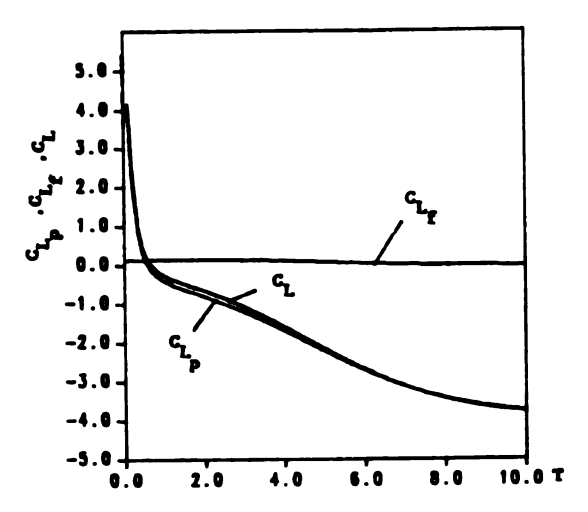


Figure IV-25 Development of the lift Coefficients G_{L_p} , G_{L_f} , G_{L} for Flow With $\gamma=0.05$, $\Omega=1.0$ and $R_d=100$.

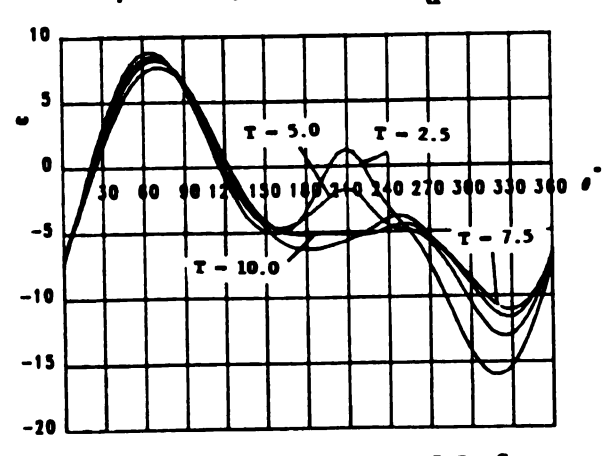


Figure IV-27 Development of Surface Vorticity ω for Flow With $\gamma=0.05$, $\Omega=1.0$ and $R_{\rm d}=100$.

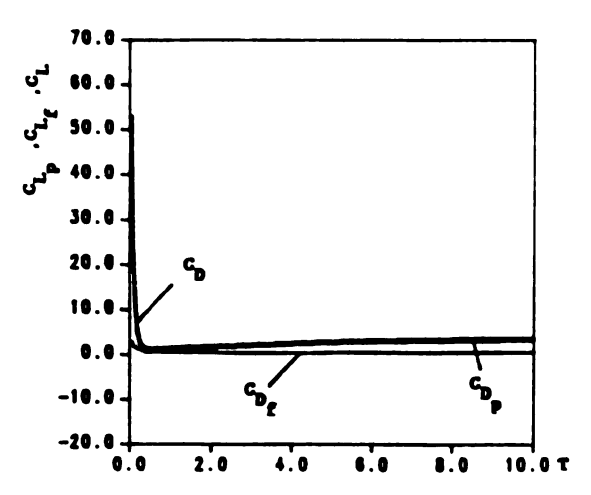


Figure IV-24 Development of the Drag Coefficients C_{D_p} , C_{D_f} , C_D for Flow With γ = 0.05 , Ω = 1.0 and R_d = 100.

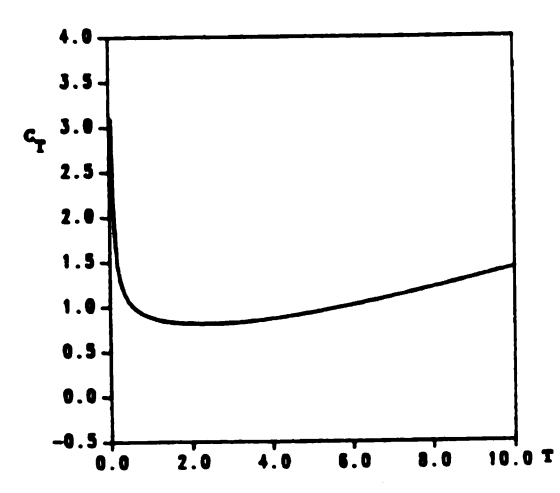


Figure IV-26 Development of the Moment Coefficient C_T for Flow With $\gamma=0.05$, $\Omega=1.0$ and $R_d=100$.

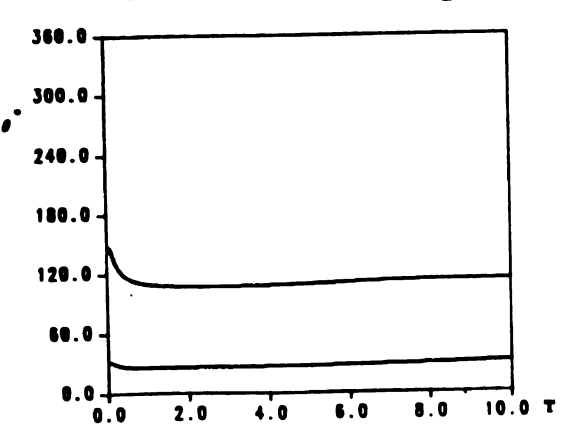


Figure IV-28 Separation Points History For Flow With γ = 0.05 , Ω = 1.0 and R_d = 100.

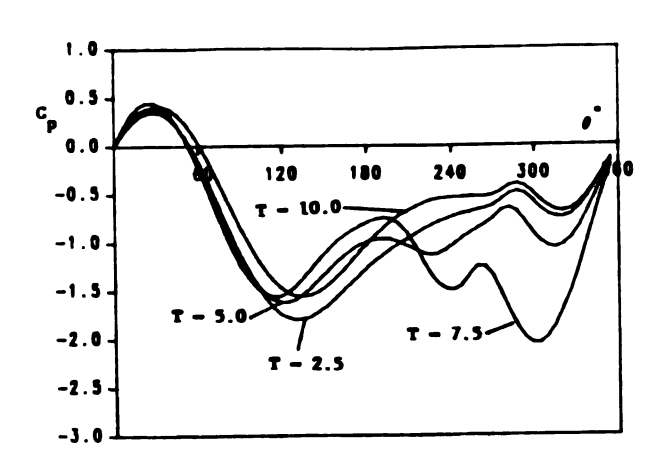


Figure IV-30 Development of Pressure Coefficient C_p , for Flow With $\gamma = 0.05$, $\Omega = 1.0$ and $R_d = 500$.

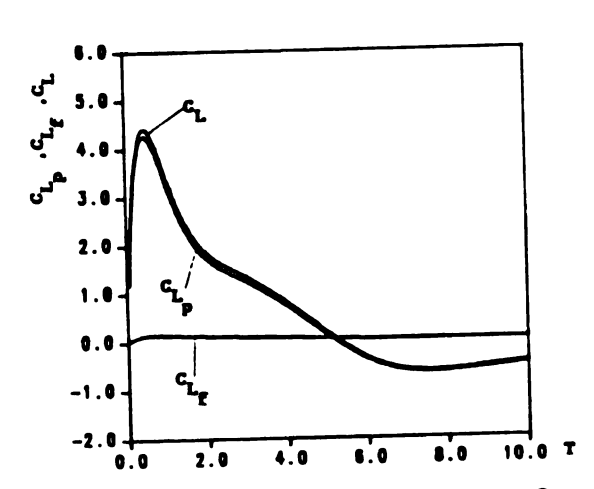


Figure IV-32 Development of the lift Coefficients C_L, C_L for Flow With

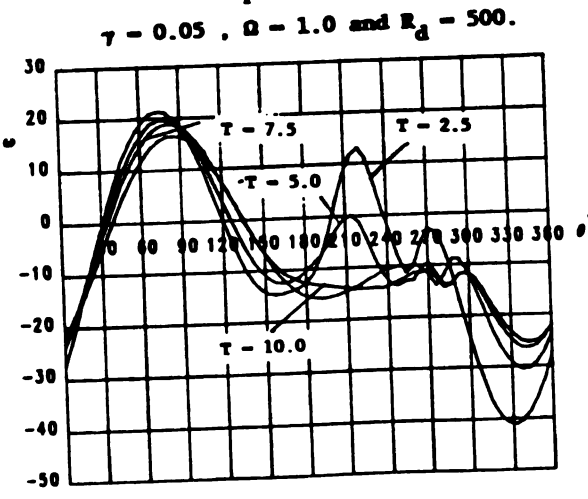


Figure IV-34 Development of Surface Verticity ω for Flow With γ = 0.05 , Ω = 1.0 and $R_{\rm d}$ = 500.

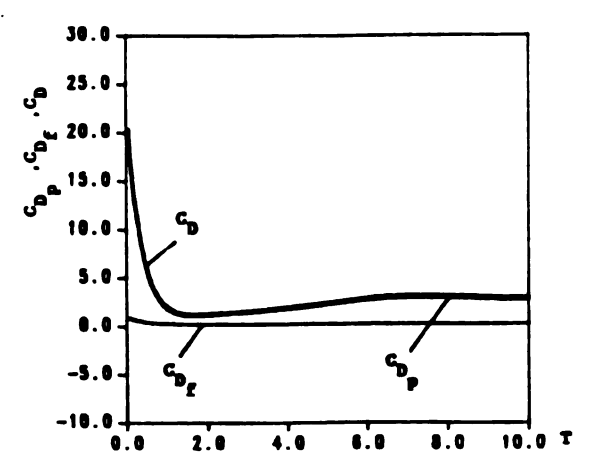


Figure IV-31 Development of the Drag Coefficients C_{D_p} , C_{D_f} , C_D for Flow With γ = 0.05 , Ω = 1.0 and R_d = 500.

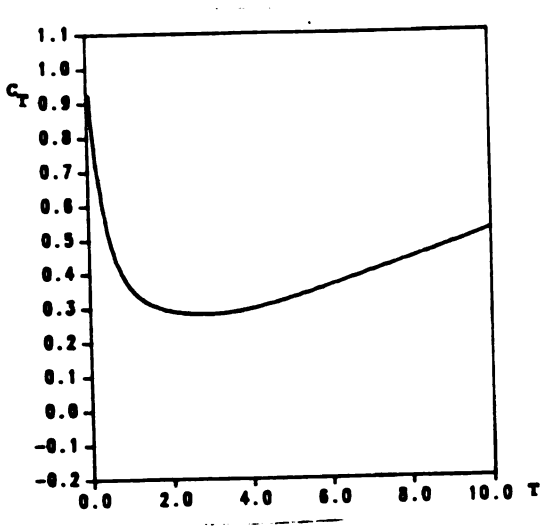


Figure IV-33 Development of the Homent Coefficient G_T for Flow With $\gamma=0.05$, $\Omega=1.0$ and $R_d=500$.

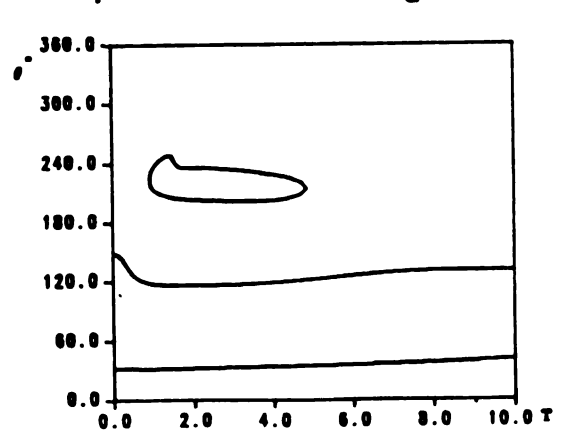


Figure IV-35 Separation Points History For Flow With $\gamma=0.05$, $\Omega=1.0$ and $R_{\rm d}=500$.

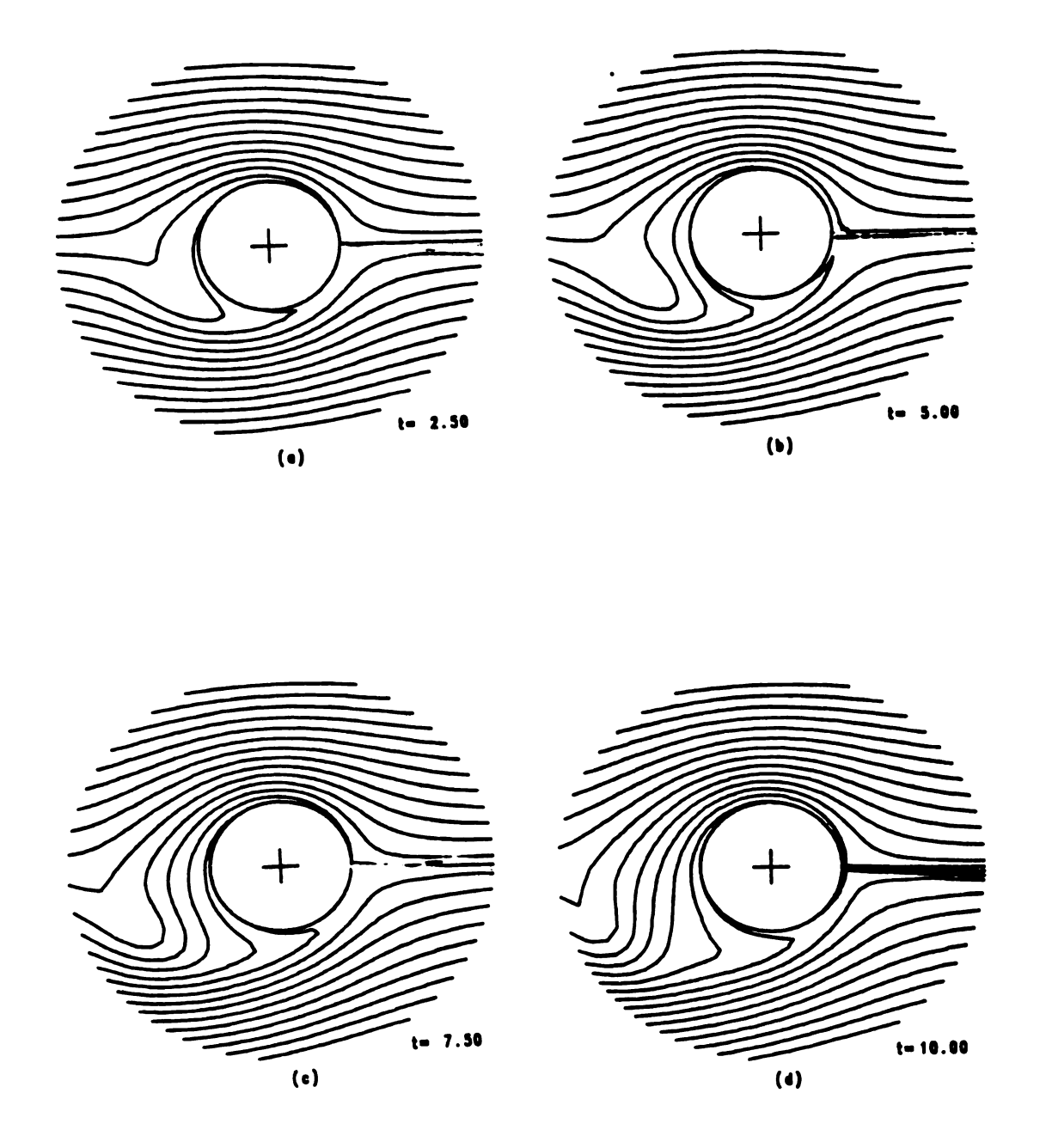


Figure IV-36 Streamlines Development with γ = 0.10 , Ω = 1.0 and R_d = 100 ,at T equal (a) 2.50 ,(b) 5.0 ,(c) 7.50 and (d) 10.0.

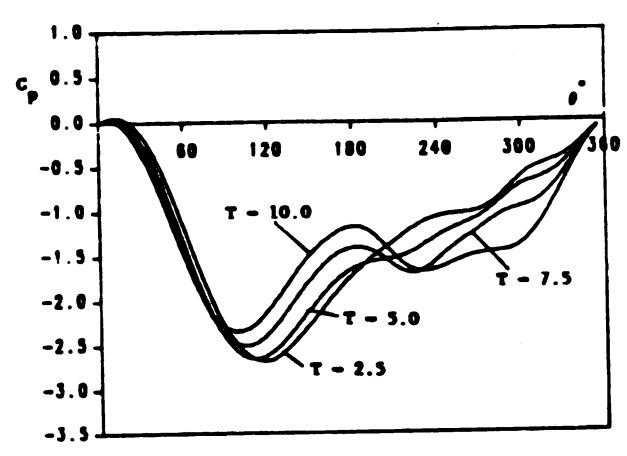


Figure IV-37 Development of Pressure Coefficient C_p, for Flow With $\gamma = 0.10$, $\Omega = 1.0$ and $R_d = 100$.

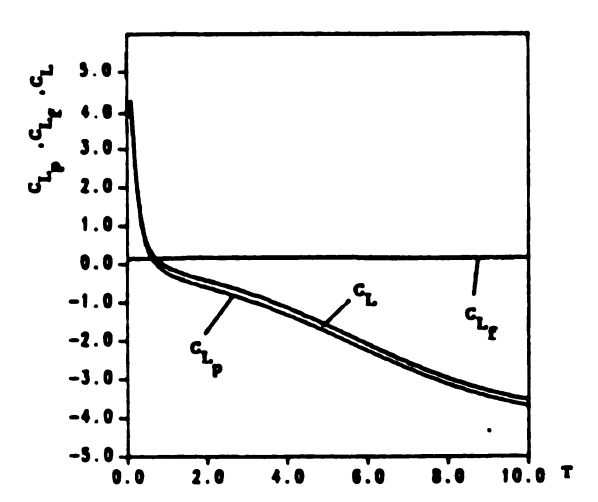


Figure IV-39 Development of the lift Coefficients C_{L_p} , C_{L_f} , C_L for Flow With $\gamma = 0.10$, $\Omega = 1.0$ and $R_d = 100$.

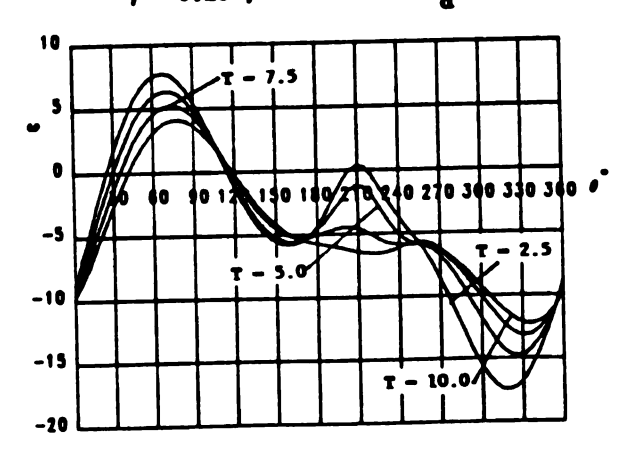


Figure IV-41 Development of Surface Vorticity ω for Flow With $\gamma=0,10$, $\Omega=1.0$ and $R_{\rm d}=100$.

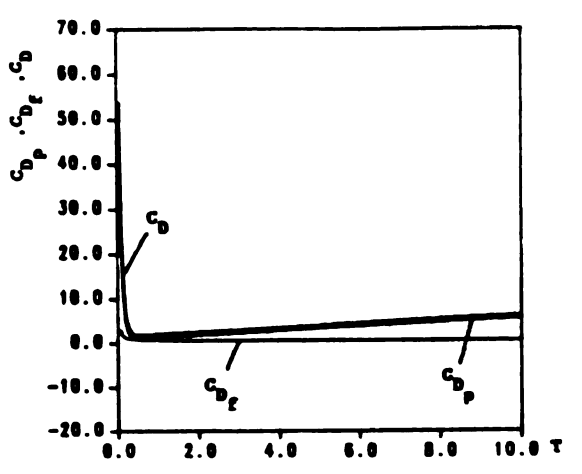


Figure IV-38 Development of the Drag Coefficients G_{D_p} , G_{D_g} , G_D for Flow With

 γ = 0.10 , Ω = 1.0 and R_d = 100.

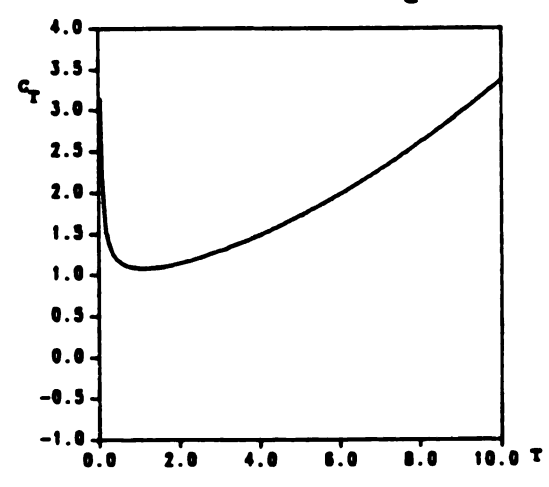


Figure IV-40 Development of the Moment Goefficient C_T for Flow With $\gamma = 0.10$, $\Omega = 1.0$ and $R_d = 100$.

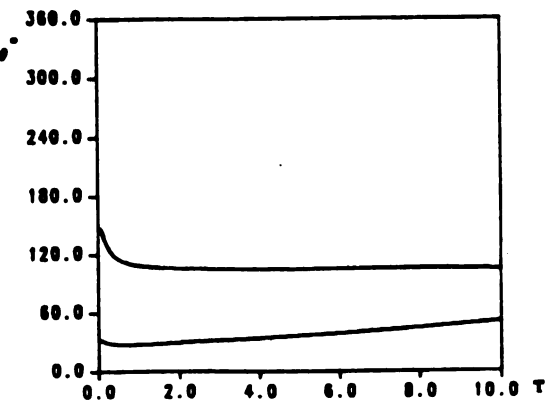


Figure IV-42 Separation Points
History For Flow With $\gamma = 0.10$, $\Omega = 1.0$ and $R_d = 100$.

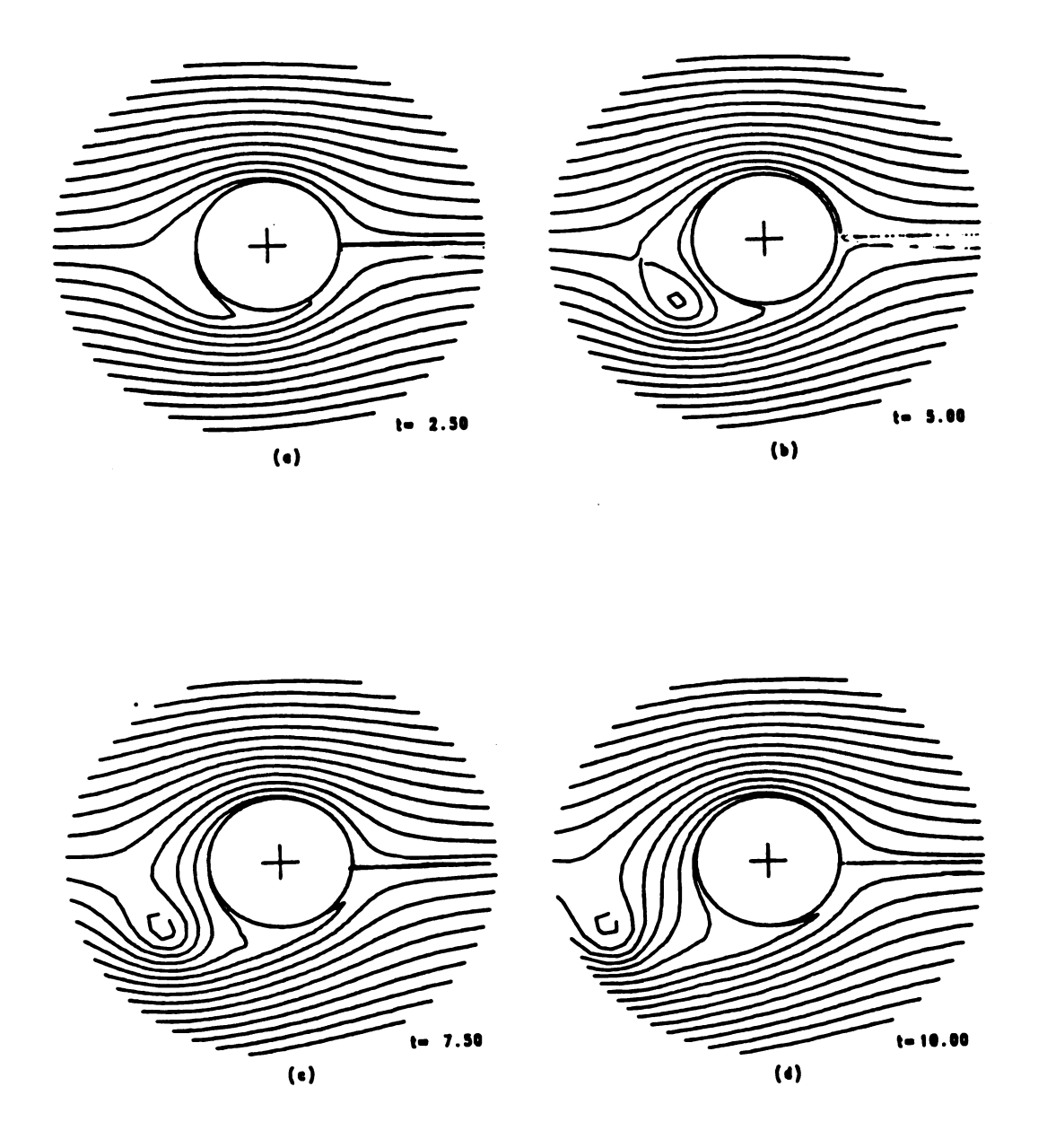


Figure IV-43 Streamlines Development with γ = 0.10 , Ω = 1.0 and R_d = 500 ,at T equal (a) 2.50 ,(b) 5.0 ,(c) 7.50 and (d) 10.0.

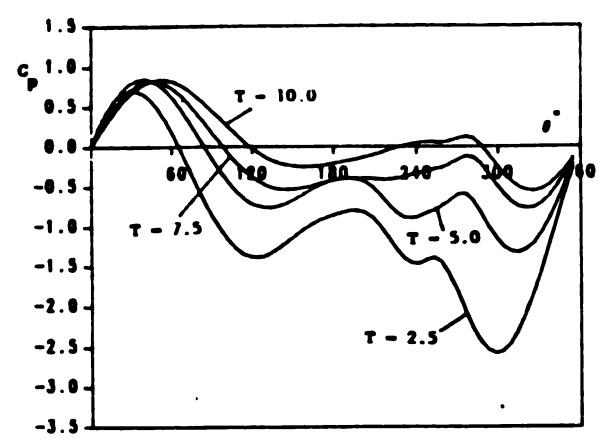


Figure IV-44 Development of Pressure Coefficient C_p , for Flow With $\gamma=0.10$, $\Omega=1.0$ and $R_d=500$.

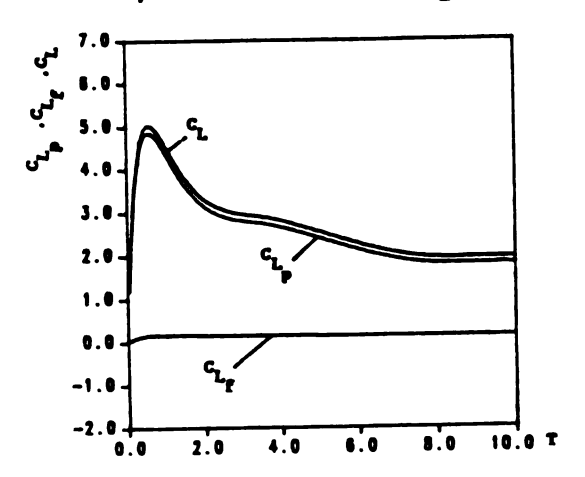


Figure IV-46 Development of the lift Coefficients C_{L_p} , C_{L_f} , C_L for Flow With $\gamma=0.10$, $\Omega=1.0$ and $R_d=500$.

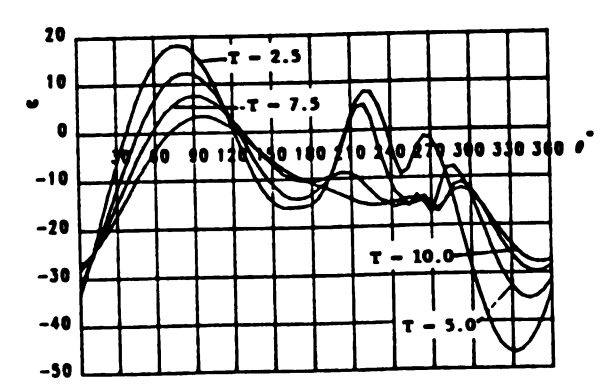


Figure IV-48 Development of Surface Vorticity ω for Flow With $\gamma=0.10$, $\Omega=1.0$ and $R_{\rm d}=500$.

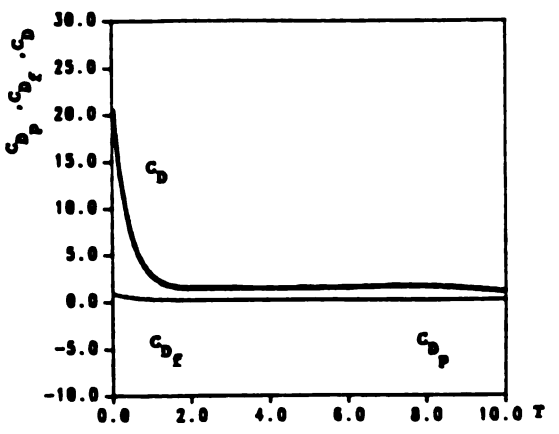


Figure IV-45 Development of the Drag Coefficients C_{D_p} , C_{D_f} , C_D for Flow With $\gamma = 0.10$, $\Omega = 1.0$ and $R_d = 500$.

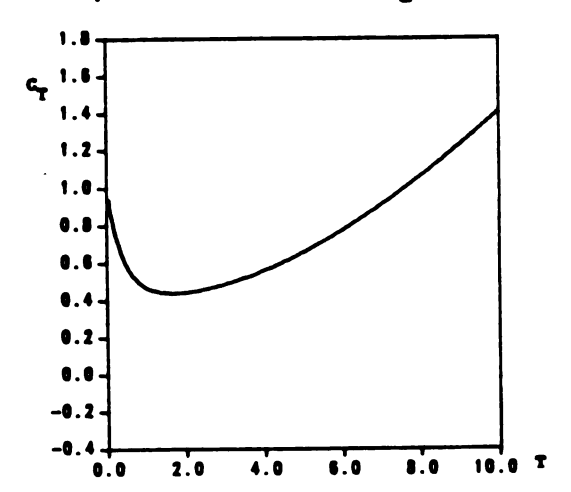


Figure IV-47 Development of the Homent Coefficient C_T for Flow With $\gamma=0.10$, $\Omega=1.0$ and $R_d=500$.

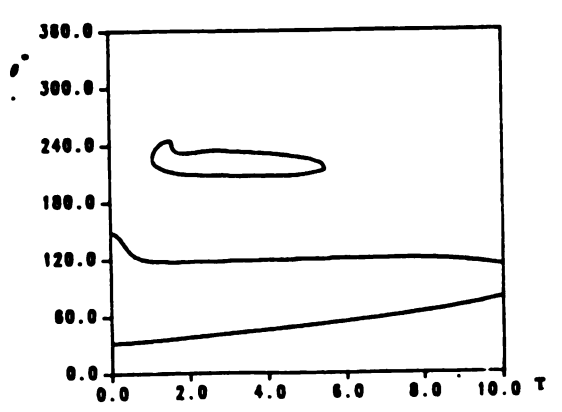


Figure IV-49 Separation Points History For Flow With $\gamma = 0.10$, $\Omega = 1.0$ and $R_{\rm d} = 500$.

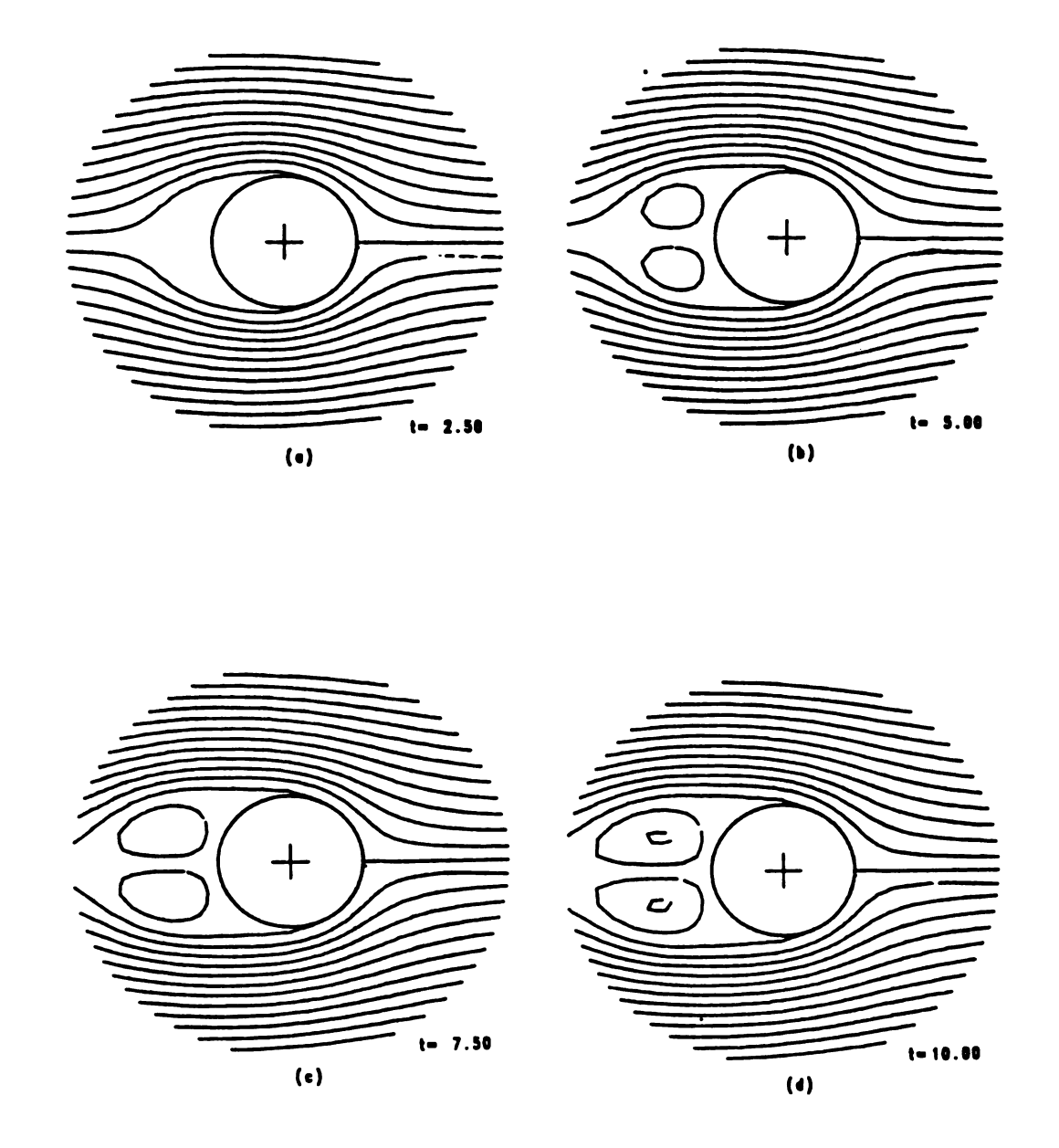


Figure IV-50 Streamlines Development with γ = 0.05 , Ω = 0.0 and R_d = 300 ,at T equal (a) 2.50 ,(b) 5.0 ,(c) 7.50 and (d) 10.0.

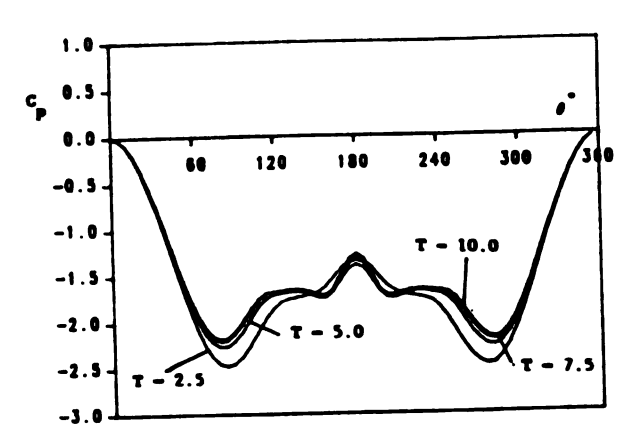


Figure IV-51 Development of Pressure Coefficient C_p , for Flow With $\gamma = 0.05$, $\Omega = 0.0$ and $R_d = 300$.

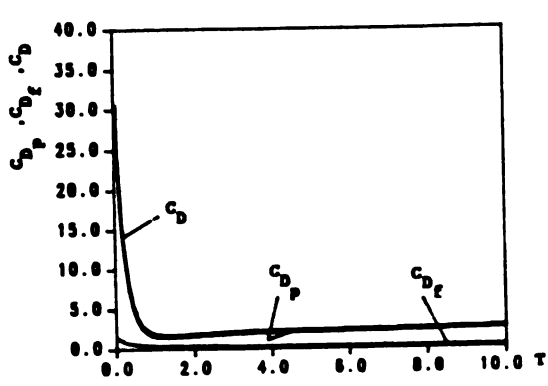


Figure IV-52 Development of the Drag Coefficients C_{D_p} , C_{D_g} , C_{D} for Flow With $\gamma = 0.05$, $\Omega = 0.0$ and $R_d = 300$.

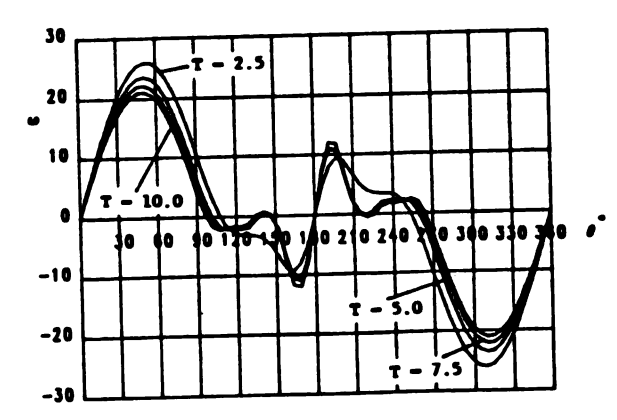


Figure IV-53 Development of Surface Verticity ω for Flow With $\gamma=0.05$, $\Omega=0.0$ and $R_{\rm d}=300$.

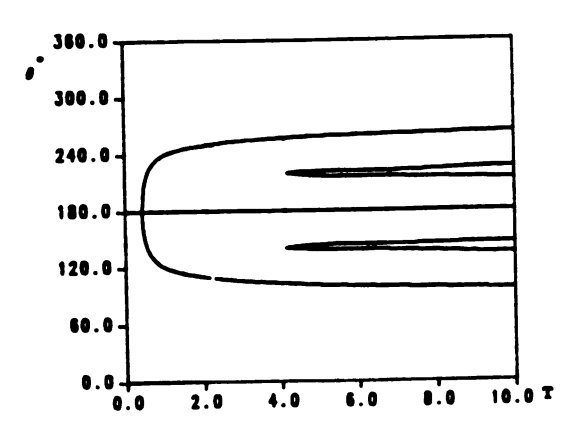


Figure IV-54 Separation Points History For Flow With $\gamma = 0.05$, $\Omega = 0.0$ and $R_d = 300$.

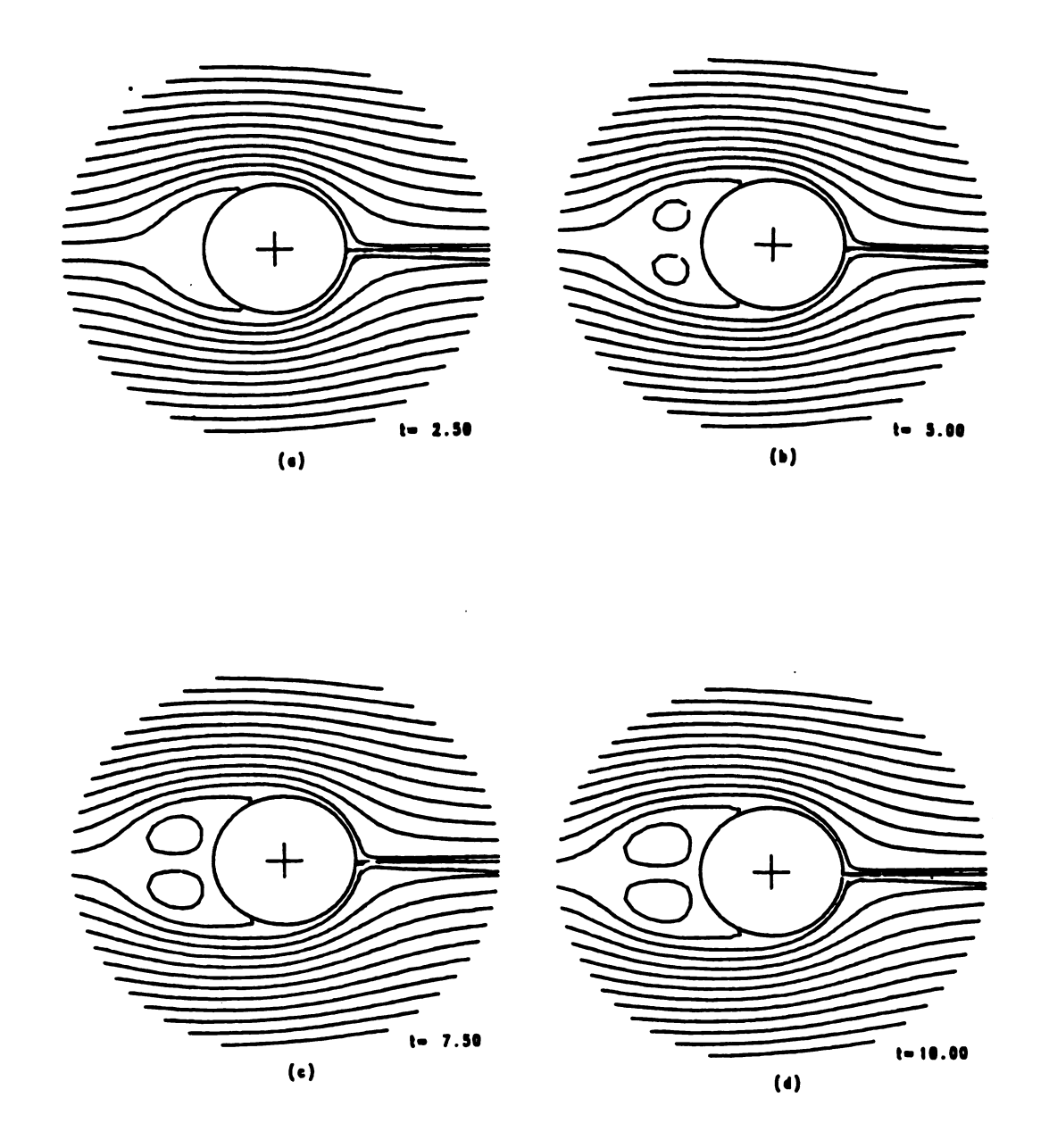


Figure IV-55 Streamlines Development with γ = 0.10 , Ω = 0.0 and R_d = 300 ,at T equal (a) 2.50 ,(b) 5.0 ,(c) 7.50 and (d) 10.0.

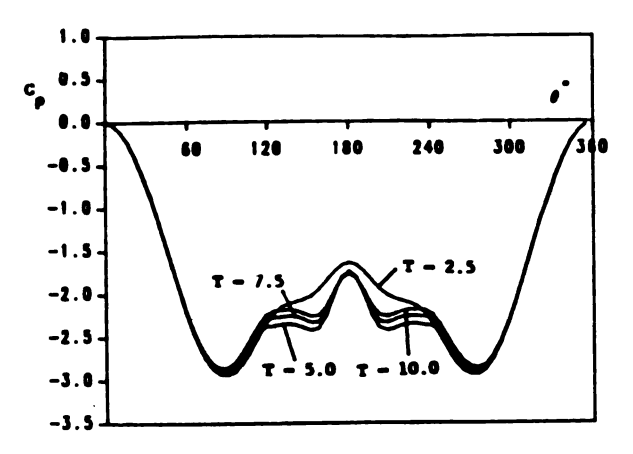


Figure IV-56 Development of Pressure Coefficient C_p, for Flow With $\gamma = 0.10$, $\Omega = 0.0$ and $R_{\rm d} = 300$.

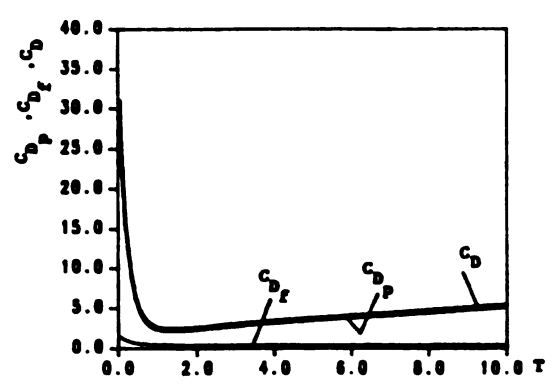


Figure IV-57 Development of the Drag Coefficients C_{D_p} , C_{D_f} , C_{D} for Flow With $\gamma = 0.10$, $\Omega = 0.0$ and $R_d = 300$.

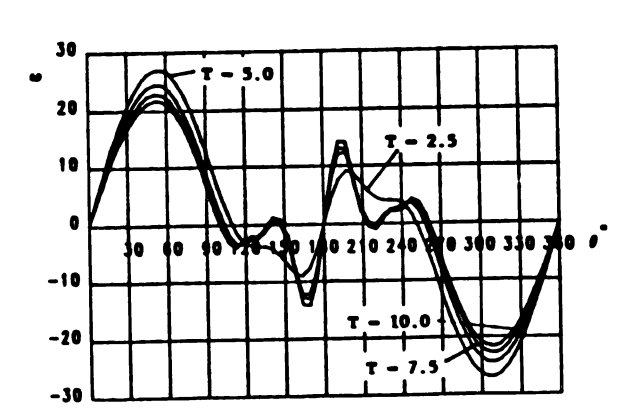


Figure IV-58 Development of Surface Vorticity ω for Flow With γ = 0.10 , Ω = 0.0 and R_d = 300.

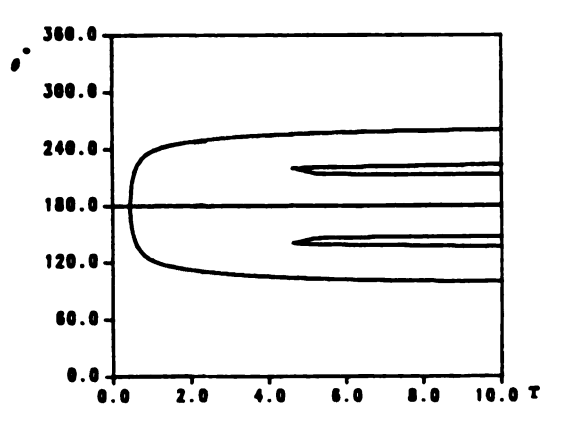


Figure IV-59 Separation Points History For Flow With γ = 0.10 , Ω = 0.0 and R_d = 300.

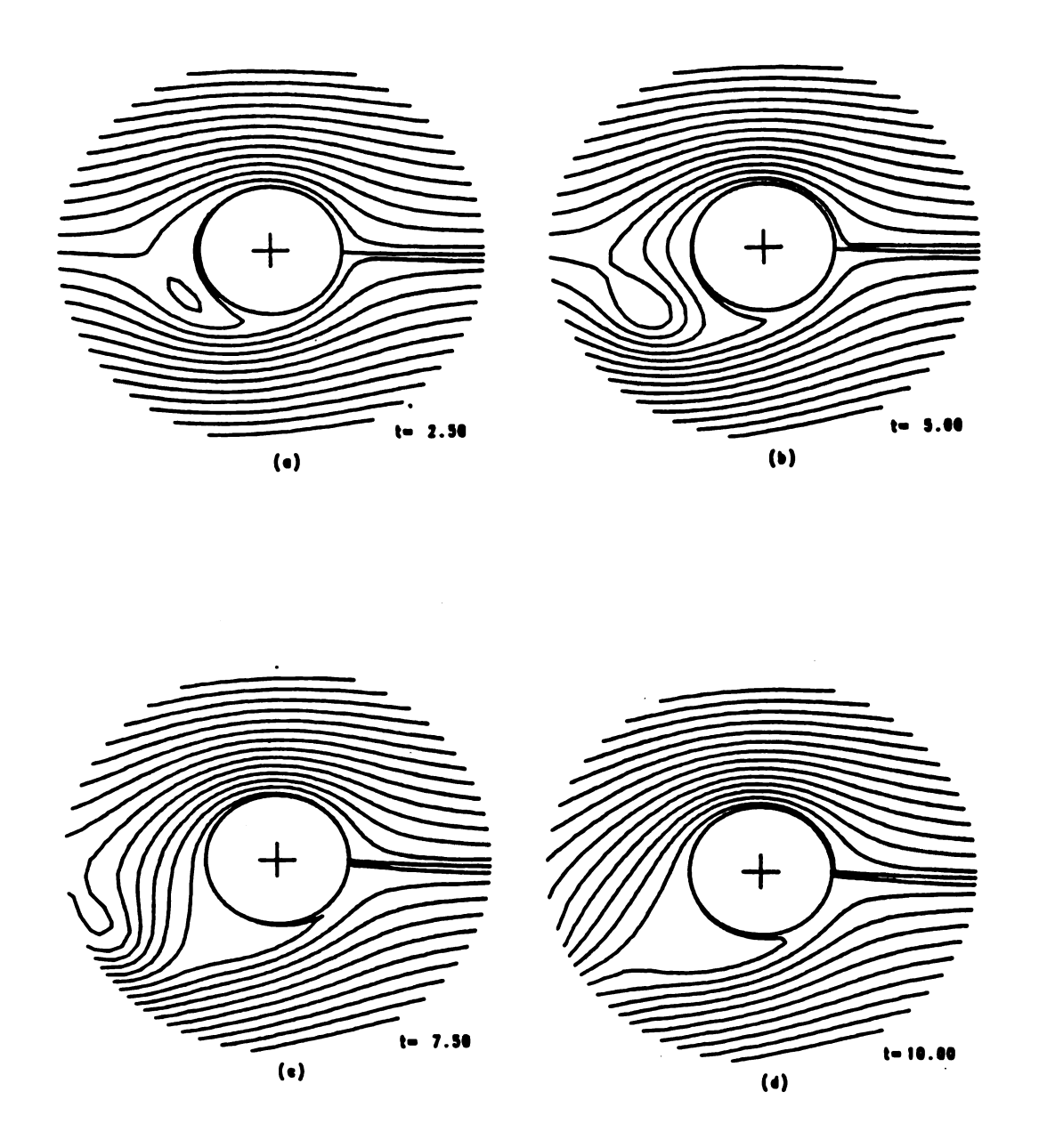


Figure IV-60 Streamlines Development with γ = 0.05 , Ω = 1.0 and R_d = 300 ,at T equal (a) 2.50 ,(b) 5.0 ,(c) 7.50 and (d) 10.0.

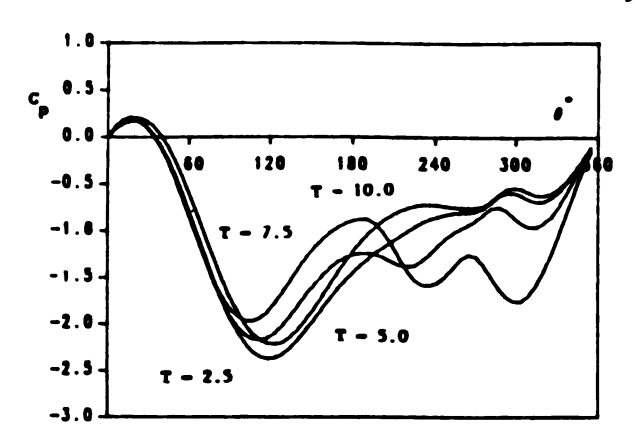


Figure IV-61 Development of Pressure Coefficient C_p , for Flow With $\gamma = 0.05$, $\Omega = 1.0$ and $R_d = 300$.

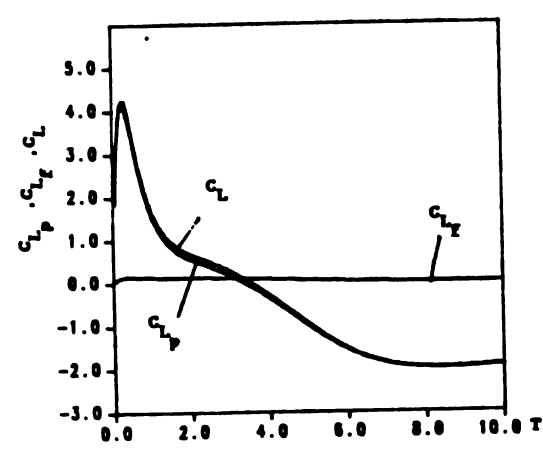


Figure IV-63 Development of the lift Coefficients G_{L_p} , G_{L_f} , G_{L} for Flow With $\gamma=0.05$, $\Omega=1.0$ and $R_d=300$.

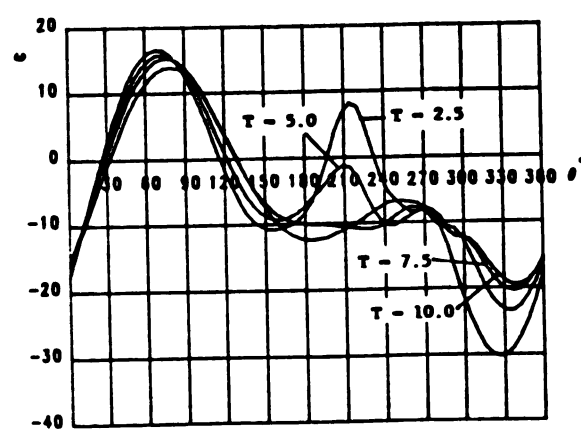


Figure IV-65 Development of Surface Vorticity ω for Flow With $\gamma=0.05$, $\Omega=1.0$ and $R_{\rm d}=300$.

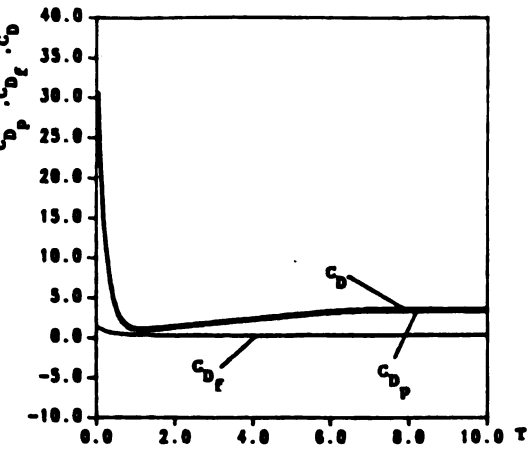
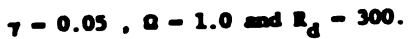


Figure IV-62 Development of the Drag Coefficients C_{Dp}, C_{Df}, C_D for Flow With



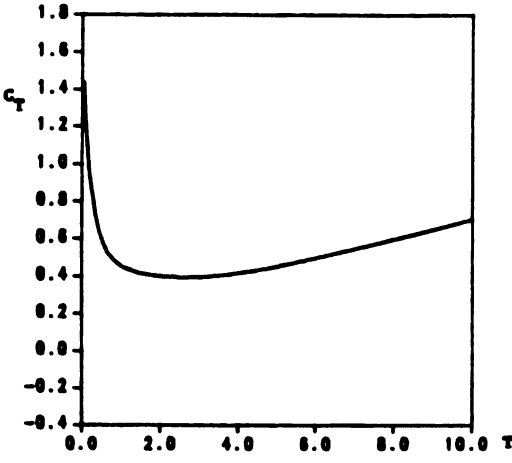


Figure IV-64 Development of the Homent Coefficient $C_{\underline{\underline{T}}}$ for Flow With

$$\gamma = 0.05$$
 , $\Omega = 1.0$ and $R_d = 300$.

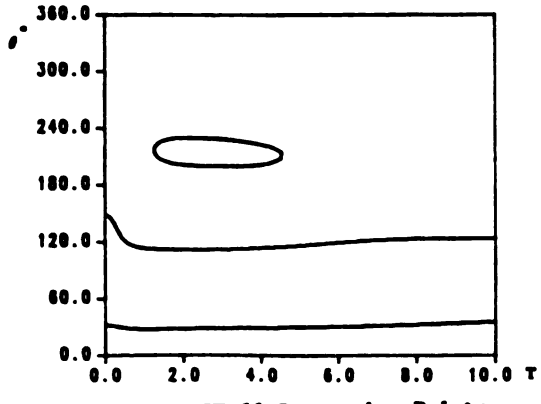


Figure IV-66 Separation Points

History For Flow With

7 = 0.05 , \Omega = 1.0 and R_d = 300.

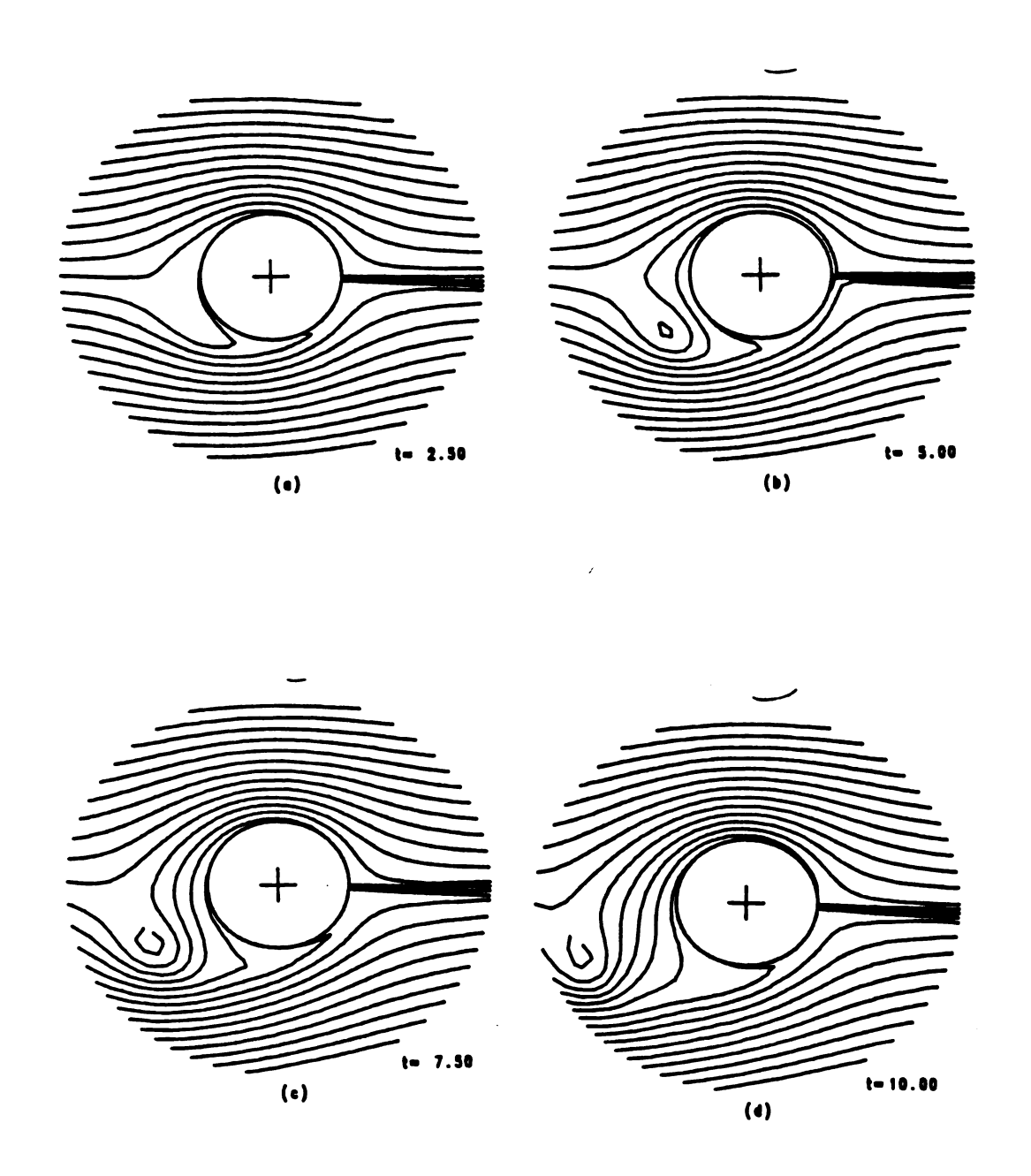


Figure IV-67 Streamlines Development with γ = 0.10 , Ω = 1.0 and R_d = 300 ,at T equal (a) 2.50 ,(b) 5.0 ,(c) 7.50 and (d) 10.0.

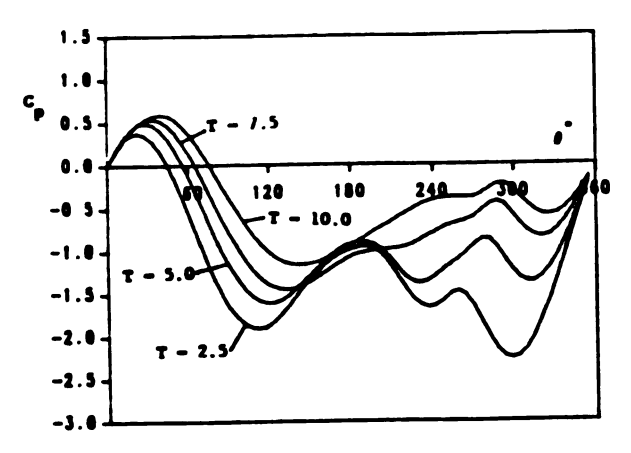


Figure IV-68 Development of Pressure Coefficient C_p , for Flow With $\gamma = 0.10$, $\Omega = 1.0$ and $R_d = 300$.

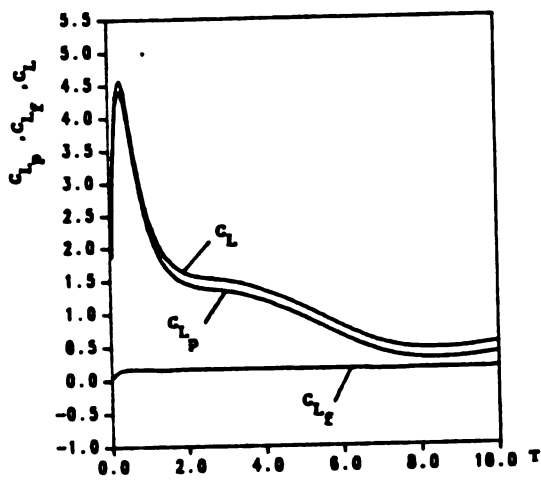


Figure IV-70 Development of the lift Coefficients C_{L_p} , C_{L_f} , C_L for Flow With $\gamma=0.10$, $\Omega=1.0$ and $R_d=300$.

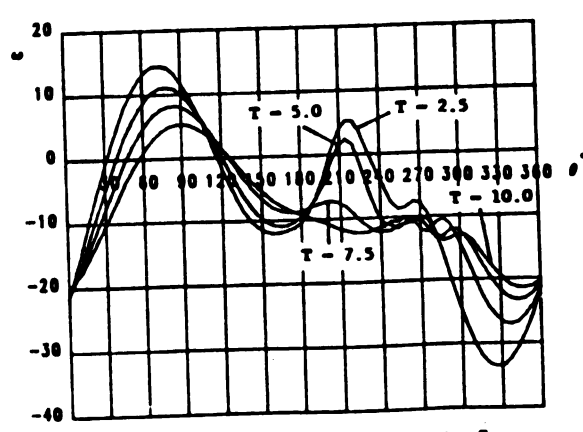


Figure IV-72 Development of Surface Vorticity ω for Flow With γ = 0,10 , Ω = 1.0 and R_d = 300.

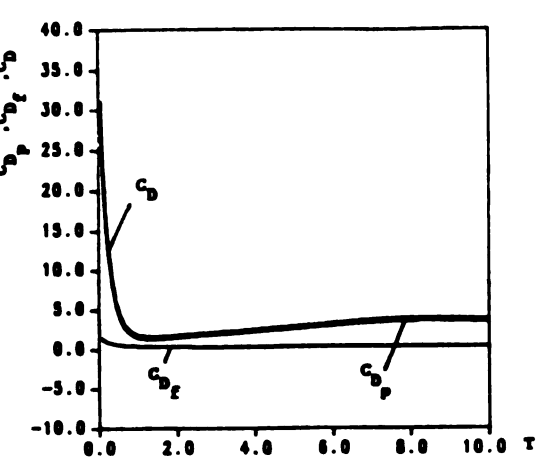


Figure IV-69 Development of the Drag Coefficients $C_{\mathrm{D}_{\mathrm{p}}}$, $C_{\mathrm{D}_{\mathrm{f}}}$, C_{D} for Flow With γ = 0.10 , Ω = 1.0 and R_{d} = 300.

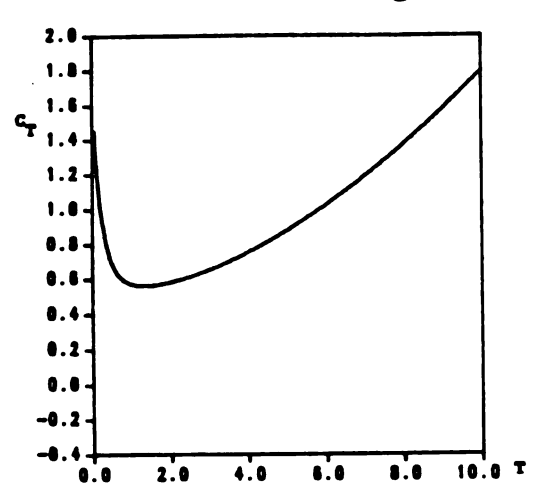


Figure IV-71 Development of the Homent Coefficient C_T for Flow With

 $\gamma = 0.10$, $\Omega = 1.0$ and $R_d = 300$.

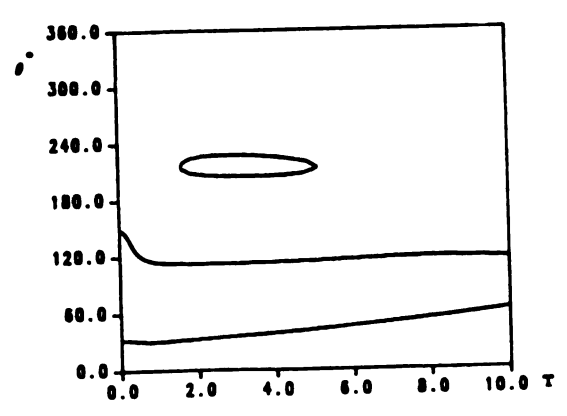


Figure IV-73 Separation Points History For Flow With $\gamma = 0.10$, $\Omega = 1.0$ and $R_{\rm d} = 300$.

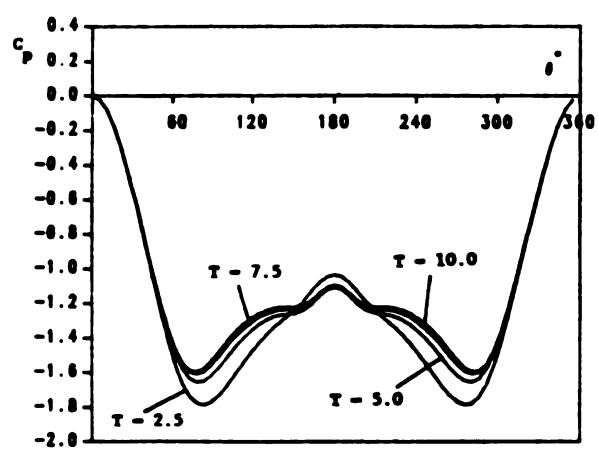


Figure IV-74 Development of Pressure Coefficient C_p , for Flow With $\gamma=0.05$, $\Omega=0.0$, $R_d=100$ and H=61.

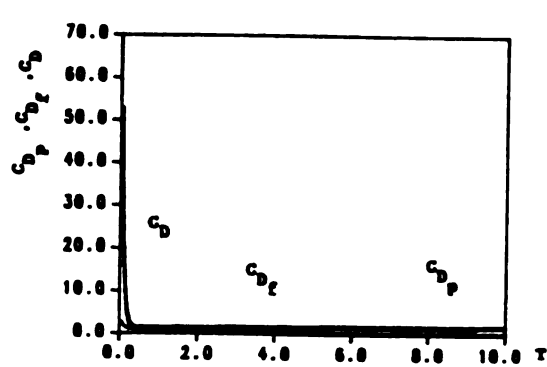


Figure IV-75 Development of the Drag Coefficients C_{D_p} , C_{D_g} , C_{D} for Flow With γ = 0.05 , Ω = 0.0 ,R_d = 100,and H=60.

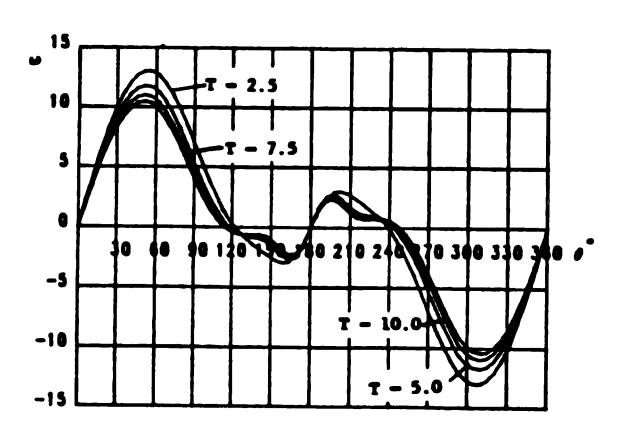


Figure IV-76 Development of Surface Vorticity ω for Flow With $\gamma=0.05$, $\Omega=0.0$, $R_{\rm d}=100$ and H=60.

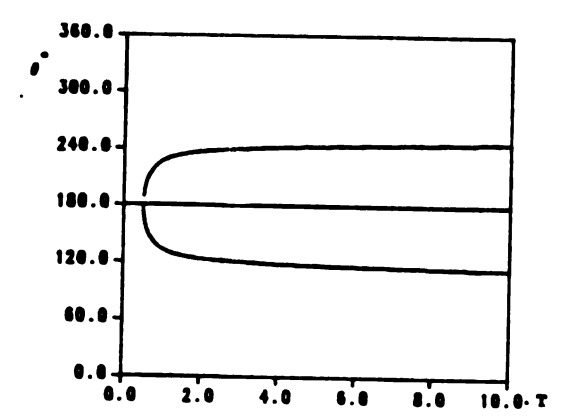


Figure IV-77 Separation Points History For Flow With $\gamma=0.05$, $\Omega=0.0,R_{\rm d}=100$ and H=61.

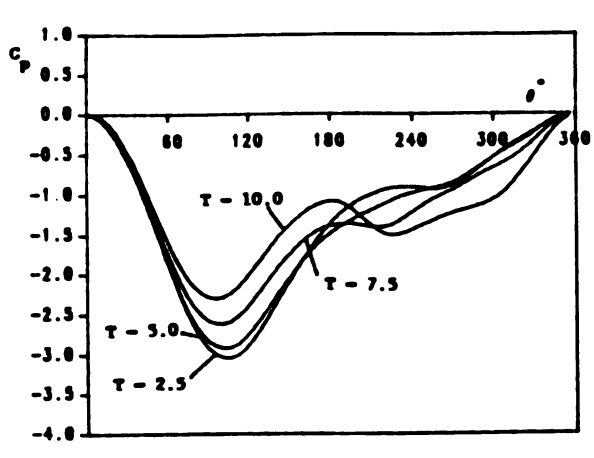
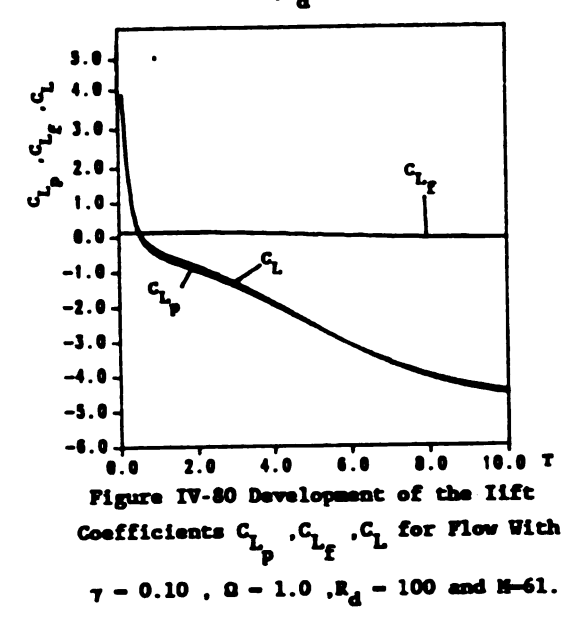


Figure IV-78 Development of Pressure Coefficient C_p , for Flow With $\gamma=0.10$, $\Omega=1.0$, $R_d=100$ and M-61.



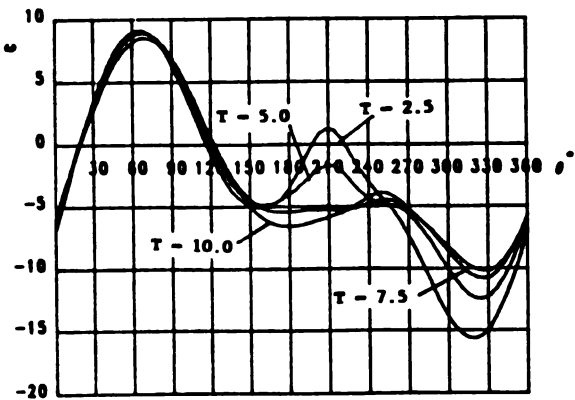


Figure IV-82 Development of Surface Vorticity ω for Flow With $\gamma=0.10$, $\Omega=1.0$, $R_{\rm d}=100$ and H=61.

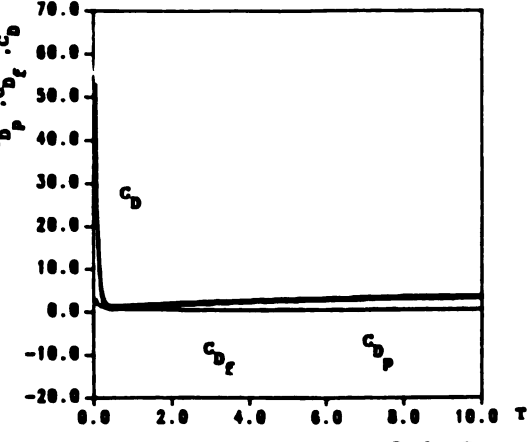
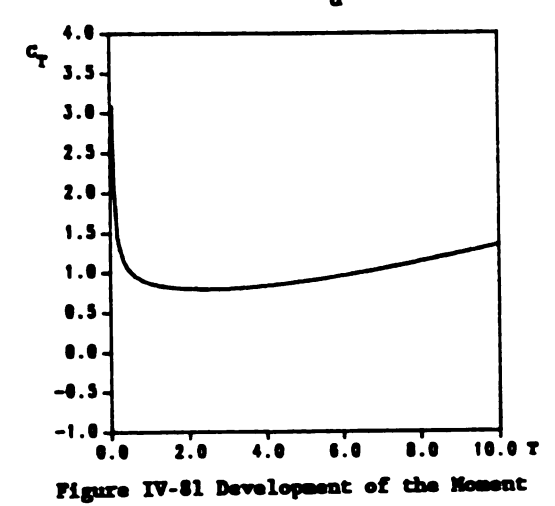


Figure IV-79 Development of the Drag Coefficients C_{D_p} , C_{D_f} , C_{D_f} for Flow With $\gamma = 0.10$, $\Omega = 1.0$, $R_d = 100$ and M-61.



Coefficient C_T for Flow With $\gamma = 0.10$, $\Omega = 1.0$, $R_d = 100$ and H=61.

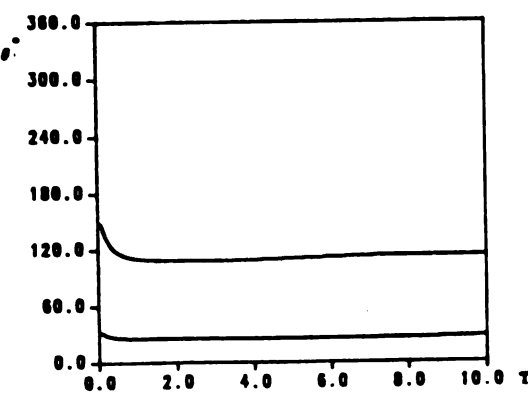


Figure IV-83 Separation Points Bistory For Flow With $\gamma = 0.10$, $\Omega = 1.0$, $R_d = 100$ and M=61.

CHAPTER V

CONCLUSION AND DISCUSSION

We shall compare the numerical and the analytical solution, and then make some general conclusions. Because of the initialization error, the numerical solution for the small time after the start of motion is not valid. Hence, good agreement is not expected in this time interval. There is subsequently a time interval of overlap during which both the analytical and numerical solutions are valid. Figures V-1 to V-14 are shown for this purpose. The lack of agreement is obvious in the early stage of motion. The numerical results subsequently becomes independent of the initial effects, and agreement is excellent, especially for the cases without rotation. The surface vorticity, which is the major variable used in the computations, shows excellent agreement of analytically and numerically calculated values. The numerical values for the pressure distribution show the expected shift of the stagnation point, while the analytical solution did not. This discrepancy may be reduced and perhaps

eliminated, by including the necessary higher-order terms in the analytical solution.

The process of using quantities obtained from the numerical solution as input to compute derivatives or integrals adds additional error. This arises when we integrate the vorticity at the mesh points in order to obtain the drag and the lift. This error can be recognized by comparing the drag (lift) figures for the analytical and numerical solutions and the moment coefficient $C_{\rm T}$ for the above solutions.

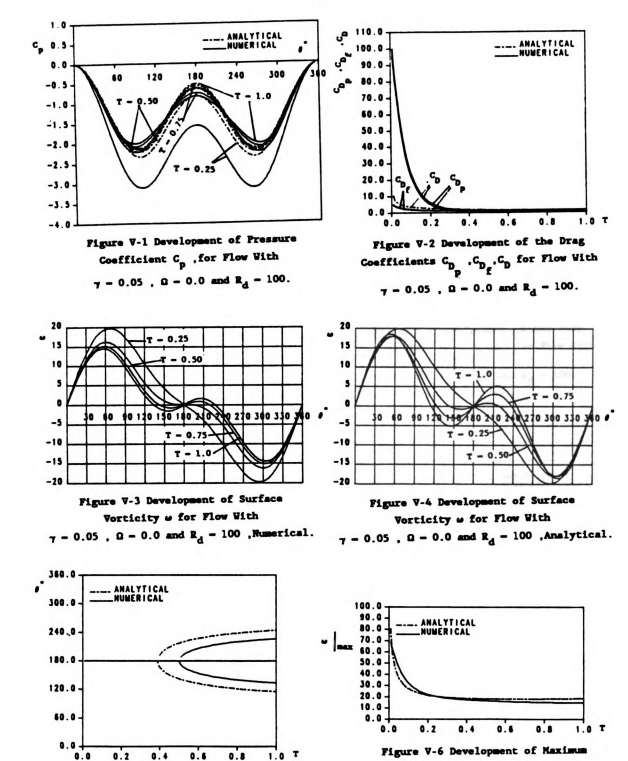
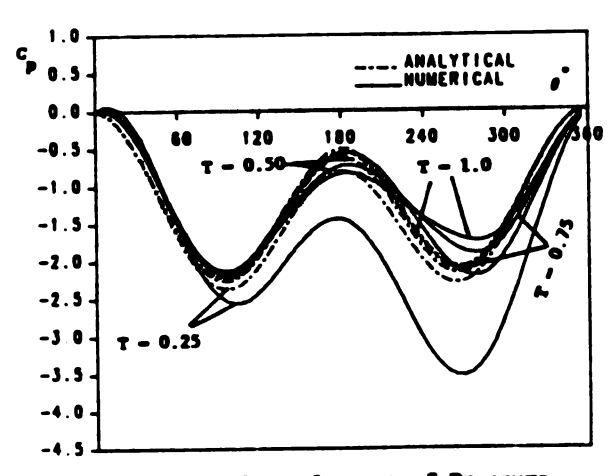


Figure V-5 Separation Points

History For Flow With $\gamma = 0.05$, $\Omega = 0.0$ and $R_A = 100$.

Surface Vorticity for Flow With $\gamma = 0.05$, $\Omega = 0.0$ and $R_d = 100$.



Pigure V-7 Development of Pressure Coefficient C_p , for Flow With $\gamma = 0.05$, $\Omega = 1.0$ and $R_d = 100$.

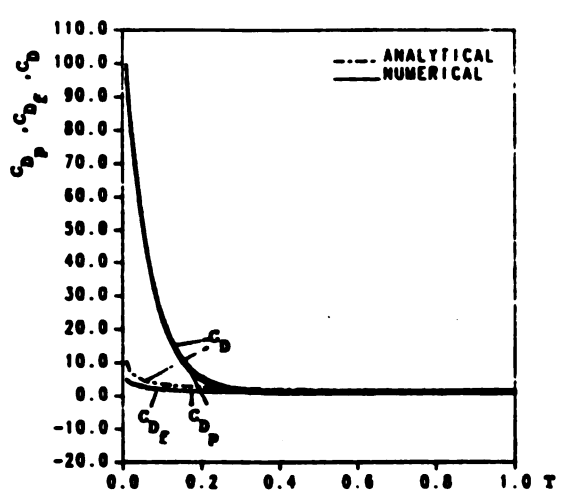


Figure V-8 Development of the Drag Coefficients C_{D_p} , C_{D_g} , C_D for Flow With $\gamma=0.05$, $\Omega=1.0$ and $R_d=100$.

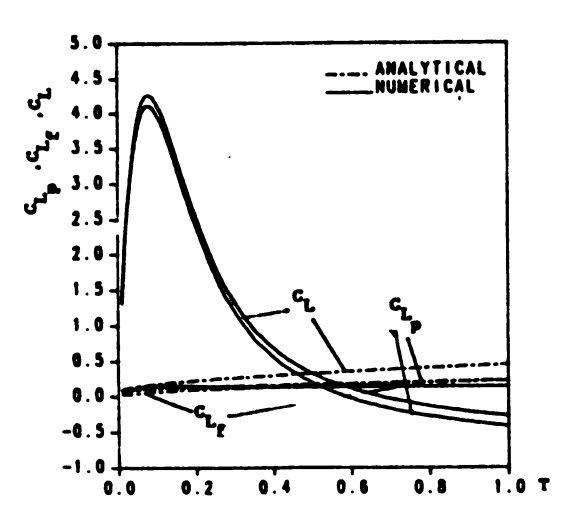


Figure V-9 Development of the lift Coefficients C_{L_p} , C_{L_f} , C_L for Flow With $\gamma=0.05$, $\Omega=1.0$ and $R_d=100$.

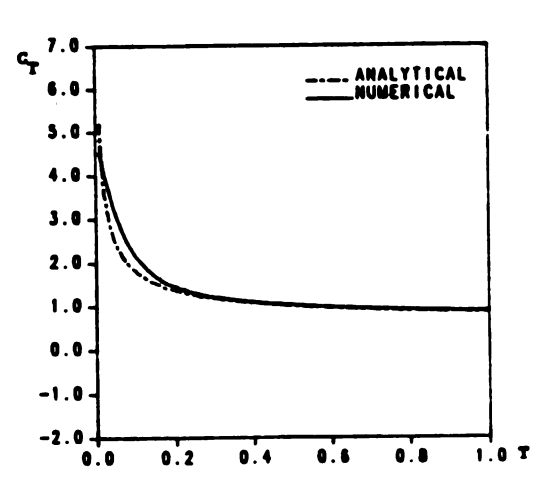


Figure V-10 Development of the Moment Coefficient C_T for Flow With γ = 0.05 , Ω = 1.0 and R_d = 100.

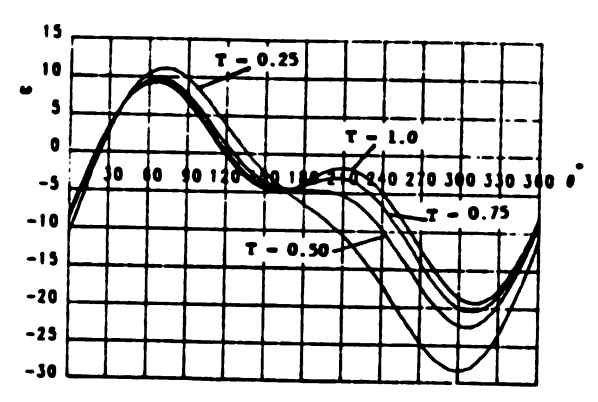


Figure V-11 Development of Surface Vorticity ω for Flow With γ = 0.05 , Ω = 1.0 and R_d = 100, Numerical.

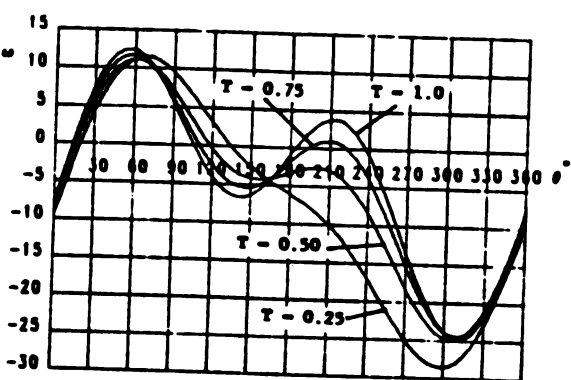


Figure V-12 Development of Surface Verticity ω for Flow With $\gamma=0.05$, $\Omega=1.0$ and $R_{\rm d}=100$, Analytical.

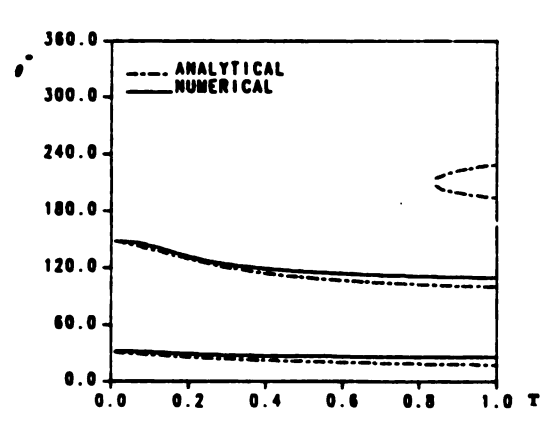


Figure V-13 Separation Points History For Flow With γ = 0.05 , Ω = 1.0 and $R_{\rm d}$ = 100.

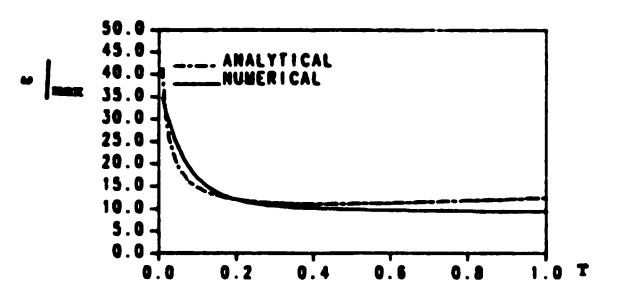


Figure V-14 Development of Maximum Surface Verticity for Flow With $\gamma = 0.05$, $\Omega = 1.0$ and $R_{\rm d} = 100$.

The main objective of the present work has been to compute and understand the nature of the forces and the moment acting on a spinning projectile at angle of attack. The Navier-Stokes equations were solved using the method of matched asymptotic expansions for the initial stage of motion, and the forward-in-time centered-space explicit numerical scheme for (the vorticity equation) and the Fast Fourier Transform (for Poisson equation) were used for the later stage of motion. From this study the following major conclusions can be drawn:

- 1- The cross-flow analogy is a powerful tool for solving complex three-dimensional problems such as the present problem one. Our results show that both solutions (Numerical and Analytical) successfully predict the flow characteristics.
- 2- The increase of the surface expansion speed γ (or equivalently, the lowering of the angle of attack, α) has a direct effect on separation. Separation is delayed when γ increased. This effect is opposite to that of the Reynolds number, which delays separation when decreased.
- 3- A pair of secondary bubbles appears at higher Reynolds numbers. The symmetry is destroyed by rotation.
- 4- The drag is nearly constant after the singular start.

Although satisfactory results have been obtained, we recommend investigating the effect of the higher-order analytic solution in the case when there is rotation. We expect that the present results for the case of the rotating cylinder can be improved when higher-order terms are added. On the other hand extending the current numerical solution to a higher order of accuracy probably will not improve the results significantly. We recommend the trial use of alternative numerical schemes to investigate this problem. We note that numerical schemes that have been adapted for moving boundaries in problems arising in fluid mechanics are few.

References

- ALLEN, H. J. and PERKINS, E. W. (1951), "A Study of the Effects of Viscosity on Flow over Slender Inclined Bodies of Revolution", Rep. Nat. Adv. Comm. Aero., Washington 1048.
- 2. THWAITES, B. (editor) (1960), "Incompressible Aerodynamics", Fluid Motion Memories, Clarendon press, Oxford.
- 3- BLASIUS, H. (1908), "Small Perturbation Solution of the Boundary Layer", NACA TM 1256, Washington, D.C.
- 4- TOLLMIEN, W. (1924), "Die Zeitliche Enwicklung der Laminaren Grenzschicht an Rotierenden Zylinder", Dissertation Gottingen.

 Also, Handbuch der Exp. Physik, IV, I, 271 (1931).
- 5- GOLDSTEIN, S. and ROSENHEAD, L. (1936), "Boundary Layer Growth ",
 Proceedings of the Cambridge Philosophical Society, Vol. 32,
 pp392-401.
- 6- GORTLER, H. (1944), " Displacement Effect of the Laminar Boundary
 Layer and the Pressure ", NACA TM 1315, Washington, D.C.
- 7- GORTLER, H. (1948), "Grenzschichtentstehung an Zylinder bei Anfahrt aus der Ruhe ", Archiv fur Mathematishe Karlsruhe, vol 1, pp 138-147.
- 8- WATSON, E. J. (1955), "Boundary Layer Growth", Proceedings of the Royal Society, vol. A231, pp 104-116.
- 9- SCHUH, H. (1953), " Calculation of Unsteady Boundary Layer in Two-Dimensional Laminar Flow ", Zeit. Flugewiss, vol. 1, pp 122-131.
- 10- WUNDT, H. (1955), "Washtum der Laminaren Grenzschich an Schrag
 Angestroemten Zylinder bei Anflahrt aus der Ruhe ", Ingen. Arch.
 vol. 23, pp 212-230.

- 11- WANG, C. Y. (1966), " The Impulsively Started Elliptic Cylinder, Origin of Lift ", Dissertation, Massachusetts Institute of Technology.
- 12- WANG, C. Y. (1967), "The Flow Past a Circular Cylinder Which is Started Impulsively from Rest ", J. Math. Phys., vol. 46, pp 195-202.
- 13- WANG, C. Y. (1968), " A Note On the Drag of an Impulsively Started Cylinder ", J. Math. Phys., vol 47, pp 451-455.
- 14- COLLINS, W. M. and DENNIS, S. C. R. (1973a), "The Initial Flow Past an Impulsively Started Circular Cylinder ", Quarterly J. Mech.

 Applied Math., vol. 26, pp 53-75.
- 15- COLLINS, W. M. and DENNIS, S. C. R. (1973b), "Flow Past an Impulsively Started Circular Cylinder ", J F M, vol. 60, part 1, pp 105-127.
- 16- BAR-LEV, M. (1974), "Impulsively Started Circular Cylinder ",

 Dissertation, Department of Aerospace Engineering, U. Southern

 California.
- 17- BAR-LEV, M. and YANG, H. T. (1975), "Initial Flow Field Over an Impulsively Started Circular Cylinder ", J F M, vol. 72, part 4, pp 625-647.
- 18- CHIEN, L. C. (1977), "Impulsively Started Viscous Flow Over a Circular Cylinder ", Dissertation, Engineering, U. Southern California.
- 19- GOURLEY, A. R. (1970), "Hopscotch: A Fast Second-Order Partial Differential Equation Solver ", J. Institute Math. Application, vol. 6, pp 375-390.
- 20- THOM, A. (1933), "The Flow Past a Circular Cylinders at Low Speeds
 ", Proceedings of the Royal Society of London, A141,

 pp 651-666.

- 21- KAWAGUTI, M. (1953), "Numerical Solution of the Navier-Stokes

 Equations for Flow Around a Circular Cylinder at Reynolds Number

 40 ", J. Phys. Society of Japan, vol. 8, pp 747-757.
- 22- PAYNE, R. B. (1958), " Calculation of Unsteady Viscous Flow Past a Circular Cylinder ", J F M, vol. 4, pp 81-86.
- 23- PROUDMAN, I. and JOHNSON, K. (1962), "Boundary Layer Growth Near a

 Rear Stagnation Point ", J F M, vol. 12, part 2, pp 161-168.
- 24- KAWAGUTI, K. and JAIN, P. C. (1966), "Numerical Study of a Viscous Fluid Past a Circular Cylinder ", J. Phys. Society of Japan, vol. 21,pp 2055-2062.
- 25- INGHAM, D. B. (1968), "Note on The Numerical Solution for Unsteady Viscous Flow Past a Circular Cylinder ", J F M, vol. 31, part 4, pp 815-818.
- 26- THOMAN, D. C. and SZEWCZYK, A. A. (1969), "Time Dependent Flow Over a Circular Cylinder", Phys. of Fluids, vol. 12,pp II-76 to II-87.
- 27- JAIN, P. C. and RAO, K. S. (1969), "Numerical Solution of Unsteady
 Viscous Incompressible Flow Past a Circular Cylinder ", Phys.
 Fluids, vol. 12, pp II-57 to II-64.
- 28- SON, J. S. and HANRATTY, T. J. (1969), "Numerical Solution of Flow Around a Cylinder at Reynold Number of 40,200and500 ", J F M, vol. 35, part 2, pp 369-386.
- 29- CHORIN, A. J. (1973), " Numerical Study of Slightly Viscous Flow ",

 J F M, vol. 57, part 4, pp 785-796.
- 30- LOC, T. P. (1980), "Numerical Analysis of Unsteady Secondary

 Vortices Generated by Impulsively Started Circular Cylinder ", J

 F M , vol. 100, part 1, pp 111-128.
- 31- ECE, E. C. and WALKER, J. D. A. (1985), "The Boundary Layer on an Impulsively Started Rotating and Translating Cylinder", Phys. of Fluids, 27, 5, pp 1077-1089.

- 32- HILL, J. A. F. (1954), "A Non-Linear Theory of the Lift on Slender Bodies of Revolution ", Proc. U. S. Navy Symposium on Aeroballistics, U. S. Naval Ordnance Test Station Rep. 5338
- 33- BRYSON, A. E. (1959), "Symmetric Vortex Separation on Circular Cylinders and Cones", J. Appl. Mech., 26,pp 643-648.
- 34- SCHWABE, M. (1935), "Uber Druckermittlung in der Instationnen Stromung ", Ing. Arch. 6, 34. Also, NACA TM 1038 (1943).
- 35- SARPKAYA, T. (1966), " Separated Flow about Lifting Bodies and Impulsive Flow about Cylinders ", AIAA J., vol. 4, No. 3., pp 414-420.
- 36- HANJI, H. and TANEDA, S. (1969), "Unsteady Flow Past a Circular Cylinder", J. Phys. Society of Japan, vol. 27, pp 1668-1677.
- 37- LAMANT, P. J. and HUNT, B. L., "Pressure and Force Distribution on a Sharp Nosed Circular Cylinder at Large Angles of Inclination to a Uniform Subsonic Stream ", J. F. M., vol. 76, part 3, pp 519-559.
- 38- VAN-DYKE, M. (1975), "Perturbation Methods in Fluid Mechanics ",
 Parabolic press, Stanford, California.
- 39- SCHLICHTING, H. (1979), "Boundary Layer Theory ", Seventh edition, McGraw-Hill Co., New York.
- 40- MURPHY, G. M. (1960), "Ordinary Differential Equations and Their Solutions ", Van Nostrand Co., New York.
- 41- CARSLAW, H. S. and JAGER, J. C. (1959), " Conduction of Heat in Solids ", Oxford University Press, Oxford.
- 42-GOLDSTEIN, S. (editor), (1965), "Modern Development in Fluids

 Dynamics ", Dover, New York.
- 43- CHENG, S. I. (1970), "Numerical Integration of the Navier-Stokes

 Equations ", AIAA J., vol. 8, No. 12.

- 44- RICTYMER, R. D. and MORTON, K. W. (1967), "Difference Methods for Initial Value Problems", Interscience Publishers, New York.
- 45- MARCUS, M. (1957), "Basic Theorems in Matrix Theory ", National Bureau of Standards, Applied Mathematics Series, 57.
- 46- COOLY, J. W. and TUKEY, J. W. (1965), " An Algorithm for the Machine Calculations of Complex Fourier Series ", Math. of Comp., vol. 19, no. 90, pp 297-301.
- 47- ROACH, P. J. (1982), "Computational Fluid Dynamics ", Hermosa Publishers, New Mexico.
- 48- ORSZAG, S. A. and ISRAELI, M. (1974), "Numerical Simulation of Viscous Incompressible Flows", Ann. Rev. Fluid Mech., 6.
- 49- ISAACSON, E. and KELLER, H. B. (1966), " Analysis of Numerical Methods ", John Wiley, New York.